JAERI-Review
2004-025

TIARA Annual Report 2003

November 2004

Advanced Radiation Technology Center

日本原子力研究所
Japan Atomic Energy Research Institute

本レポートは，日本原子力研究所が不定期に公刊している研究報告書です。
入手の問合わせは，日本原子力研究所研究情報部研究情報課（〒319-1195　茨城県那珂郡東海村）あて，お申し越しください。なお，このほかに財団法人原子力弘済会資料センター（〒319-1195　茨城県那珂郡東海村日本原子力研究所内）で複写による実費頒布をおこなっております。

This report is issued irregularly.
Inquiries about availability of the reports should be addressed to Research Information Division, Department of Intellectual Resources, Japan Atomic Energy Research Institute, Tokai-mura, Naka-gun, Ibaraki-ken, 319-1195, Japan.

編集兼発行　　日本原子力研究所

JAERI-Review 2004-025

TIARA Annual Report 2003

Advanced Radiation Technology Center

Takasaki Radiation Chemistry Research Establishment
Japan Atomic Energy Research Institute
Watanuki-machi, Takasaki-shi, Gunma-ken

(Received October 4, 2004)

This annual report describes research and development activities which have been performed with the JAERI TIARA (Takasaki Ion Accelerators for Advanced Radiation Application) facilities from April 1, 2003 to March 31, 2004. Summary reports of 115 papers and brief descriptions on the status of TIARA in the period are contained. A list of publications, the type of research collaborations and organization of TIARA are also given as appendices.

Keywords: JAERI TIARA, Ion Accelerators, Solid State Physics, Radiation Effects in Materials, Materials for Space, Semiconductors, Organic Materials, Inorganic Materials, Nuclear Fusion Reactor, Functional Materials, Radiation Chemistry, Radiation Biology, Nuclear Medicine, Biotechnology, Radioisotope Production, Nuclear Chemistry, Radiation Shielding, Materials Analysis, Microbeam Technology, Accelerator Technology, Safety Control

---

(Eds.) Yoshiro OHARA, Kazuo ARAKAWA, Shigeru TANAKA, Hiroshi NARAMOTO, Masaru YOSHIDA, Hisayosi ITOH, Masato YOSHIKAWA, Atsushi TANAKA, Yasuhiko KOBAYASHI, Mitsuhiro FUKUDA, Michiaki OTSUBO, Satoshi TAJIMA and Susumu TANAKA

原研イオン照射研究施設（ＴＩＡＲＡ）平成１５年度年次報告

日本原子力研究所高崎研究所
放射線高度利用センター

（2004年10月4日受理）

本年次報告は、原研イオン照射研究施設で、2003年4月1日から2004年3月31日までの間に行われた研究活動の概要をまとめたものである。1）宇宙用半導体、2）バイオテクノロジー、3）放射線化学および有機材料、4）無機材料、5）材料解析、6）核科学およびラジオアイソトープ製造、7）マイクロビーム応用、8）加速器施設の放射線遮蔽、9）加速器技術の9部門にわたる１１５編の研究報告に加えて、施設の運転保守・利用状況、公表された文献、企業・大学等との研究協力関係、研究開発・施設運営組織を収録する。

高崎研究所：〒370-1292 群馬県高崎市綿貫町 1233

PREFACE

This report covers research and development activities which have been conducted with TIARA(Takasaki Ion accelerators for Advanced Radiation Application) during the period from April 2003 to March 2004, and also gives an outline of the operation of TIARA in the same period.

All accelerators in TIARA, the AVF cyclotron, the 3MV tandem accelerator, the 3MV single-ended accelerator and the 400kV ion implanter, have been operated steadily since the start of operation in 1993. The beam-time has been allocated to the research programs as evaluated in advance by the Subcommittee of TIARA of Advisory Council for JAERI's Research Facilities. In the meantime, available ion species and their energy ranges have been widened to meet the requirements from users, and the quality of ion beams have been improved intensively.

In the research on semiconductors used in space, radiation degradation of solar cells, single event phenomena (SEP) in integrated circuits, and development of radiation resistant devices have been investigated using TIARA. In radiation effects in solar cells, it was found from proton irradiation at around 200K that the radiation hardness of $Cu(In,Ga)Se_2$ and InGaP solar cells were attributable mainly to annealing of radiation damage at room temperature. Regarding SEP, transient currents observed in MOS capacitors irradiated with high energy heavy ions like 322MeV-Kr were interpreted as displacement currents generated in the oxide film. In order to examine SEP caused in terrestrial LSIs by cosmic-rays (high energy neutrons), the measurement technique of transient currents induced in diodes by quasi-monoenergetic neutrons has been developed. In the R&D of radiation resistant devices, SiC-based n-channel MOS field effect transistors (MOSFETs) exhibiting the electron channel mobility of $230cm^2/Vs$ have been successfully fabricated using hot-implantation and pyrogenic oxidation.

In the field of biotechnology, the biological effects of track structure were investigated for different swift ions with the same LETs by visualizing DNA damage around ion tracks in the hit cells. A number of bystander effect studies are in progress using heavy-ion microbeams. The formations of foci of γH2AX were found in the unirradiated cells in the bystander colonies. For the positron emitting tracer imaging system (PETIS), mathematical analysis method of the PETIS data was developed to understand the photoassimilates transportation and partitioning in a broad bean plant quantitatively. The rate of photoassimilates transportation in the stem increased with recede from $^{11}CO_2$ feeding leaf. For the mutation induction of plants, novel phenotypes such as late bolting in bunching onion, different alkaloid contents in ipecac, and others have been generated. As increased dose of ion beams easily induce the decrease of the nuclear DNA contents, many investigators prefer to use low dose irradiation for the mutation induction.

In the field of radiation chemistry and organic materials, the following results should pay attention in these studies. γ-irradiation to polyethylene terephthalate films bombarded with ^{129}Xe ions (3.5 MeV/n) effectively promoted the formation of crosslinked structures in the latent tracks, thereby increasing the thickness of the gel layer swollen by absorbed etchant. It was newly found that the current-voltage analysis of the crosslinked Si-based polymer nanowires with the length of 10 – 1000 nm and the thickness of 4.0 – 19.4 nm obtained by the high-energy single ion hitting method is clearly indicated intrinsic semiconductive features. In cluster ion bombardment experiments, the mass spectroscopy is a very useful tool for chemical analysis of materials with lower electric conductivities.

In the field of nuclear fusion and advanced fission reactor materials, various kinds of

experimental studies were performed. In order to simulate the effects of He and/or H produced through transmutation reactions, dual or triple ion-beams were irradiated onto the candidate fusion/fission reactor materials (reduced activation ferritic/martensitic steels, austenitic stainless steels, SiC/SiC composites). Effects of implanted helium and/or hydrogen atoms on physical, chemical properties and thermo-mechanical properties (thermal diffusivity, radiation hardening, corrosion) as well as microstructure evolution (change in composition, voids) by irradiation damage were investigated.

In the field of inorganic materials, the changes of the electronic structures induced by nitride-implantation to pure Titanium were examined by in-situ TEM observation and the formation processes of Titanium nitride during ion-irradiation were clarified. The growth condition of TiO_2 films on highly oriented ZnO buffer layer with nanometer sizes grain on a quartz glass was determined by using X-ray diffraction and Rutherford backscattering (RBS) analysis and photo-catalytic films with a high efficiency was realized for the decomposition reaction. As for the study of fast cluster ions, the dependence of energy spectra of cluster-induced electrons on the number of cluster atoms was observed and the energy spectra in the range from 0 to 10 eV was found to reflect the interaction of the cluster with the target electrons up to a depth of about 100 Å. .

The activities in materials analysis have been extended from the classical field into the new and interdisciplinary ones, and the solid-state reaction process between defects and implants has been employed in a positive manner to realize novel materials phases. The ion beam treated surfaces have been reasonably analyzed by employing complementary directional beams including ion beam. Intensive effort to generate the cluster ions with the broad range of energies and ion-species has made possible to study about the non-linear effect of radiation effects by structured ions with possible applications of the massive momentum transfer process.

In the nuclear science and radioisotope production, the study on the production method of positron emitting nuclei was continued. In particular, the excitation functions of ^{73}Se and ^{75}Se were determined by the stacked foil method. For the therapy of bone cancer, production procedure of endohedral ^{133}Xe-fullerrenol was modified to obtain high yield. Further, preliminary experiments were performed to develop a mathematical analysis technique for PETIS data.

In the field of microbeam applications, in-air micro-PIXE and micro-PIGE(Proton Induced Gamma-ray Emission) techniques have been widely used for investigation of elemental distribution in microscopic area and for quantitative analysis with high spatial resolution. X-ray detection efficiency of the in-air micro-PIXE analysis system has been drastically improved. Low concentration of Cs in the yeast *S. cerevisae* has been detected by the in-air micro-PIXE analysis, while the Cs peak was not observed by SEM-EDS(scanning electron microscopy energy dispersive spectroscopy). New information on fluorine concentration at carious and sound fissures of teeth has been obtained by the in-air micro-PIXE analysis. Application of monochromatic X-rays produced by MeV protons to high contrast X-ray imaging of biological samples has been demonstrated. Development of a 260 MeV $^{20}Ne^{7+}$ microbeam is steadily in progress at the AVF cyclotron facility.

In the field of radiation shielding for accelerator facilities, three experiments have been conducted aiming to contribute to the radiation safety of the accelerator facilities. The first one is on the measurement of G-value for nitric acid production by high energy (50MeV) proton irradiation to atmospheric air, and the G-value was calculated to be 1.2. The second one is on a successful

measurement of absorbed dose distributions in phantoms irradiated by 40MeV and 75MeV quasi-monoenergetic neutrons. It was found that the calculated absorbed dose by MCNPX and PHIS agreed well with the measured ones. The third one is on a development of track detector type personal dosimeter for high-energy neutrons. The increase in the sensitivity has been obtained experimentally for a thick radiator of the order of a few g/cm^2.

In the field of accelerator technology, a positron source using the nuclear reaction with proton accelerated by the cyclotron was designed and installed in order to generate an intense positron beam. In the cluster ion beam research, the secondary ion emissions from a highly oriented HOPG target bombarded by carbon cluster ions were measured by the TOF mass spectrometer, and a non-linear effect was observed clearly. Coulomb explosion images and average charge states of carbon cluster ions after passing through a thin foil were measured. In the development of a flat-top acceleration system for the cyclotron, the turn-separation, which indicated a lower energy spread of the beam, was clearly observed using the beam of 260MeV $^{20}Ne^{7+}$. A beam current stabilization system using beam attenuator was designed and installed on a beam-line connected to the ion implanter, and the beam stability of less than $\pm 3\%$ was achieved.

The TIARA accelerators have been utilized smoothly in 2003 fiscal year and the operation time of each accelerator was 3382 hours, 1988 hours, 2286 hours and 1773 hours for the AVF cyclotron, the tandem accelerator, the single-ended accelerator and the ion implanter, respectively. The radiation safety controls and radioactive waste managements were also steadily carried out.

The reception of the users, the supports on utilizations of the experimental apparatus, and safety management of the radiation controlled area have been conducted smoothly.

The Thirteenth TIARA Research Review Meeting was held on June 28 and 29, 2004 in Takasaki, of which subjects were reported in this issue. Thirteen oral and ninety five poster papers, and one invited lecture were presented. Three hundred and twenty one persons participated in the meeting.

We owe the progress mentioned above to the advice of the Consultative Committee for Joint Research Project and the Subcommittee of TIARA of Advisory Council for JAERI's Research Facilities.

Yoshihiro Ohara, Director
Advanced Radiation Technology Center
Takasaki Radiation Chemistry Research Establishment

This is a blank page.

Contents

1. Semiconductor for Space

This is a blank page.

1.1 Radiation Response of $Cu(In,Ga)Se_2$ Thin Film Solar Cells

S. Kawakita*, K. Shimazaki *, T. Sumita*, M. Imaizumi*, S. Kuwajima*,
T. Ohshima** and T. Kamiya**
Japan Aerospace Exploration Agency (JAXA)*
Department of Material Development ,JAERI **

1. Introduction

A copper indium gallium di-selenide (CIGS) thin-film solar cell is a promising candidate for future thin-film solar cells used in space since the cells have demonstrated conversion efficiencies exceeding 19%, which is significantly higher than other thin-film solar cells[1]. CIGS solar thin film solar cells exhibit excellent radiation tolerance[2]. In addition, CIGS solar cells perform better than conventional Si and GaAs space solar cells, because they are low cost and light weight, and because the cells can be formed on either polyimide[3] or stainless steel sheet[4] substrates.

Radiation damage studies for CIGS thin-film solar cells show that high energy electron irradiation does not degrade the electrical properties of the cells, but high energy proton irradiation degrades those properties in much the same way as in other types of solar cells[2]. These studies also show that in radiation damage to the cells by proton irradiation, the irradiated cells were gradually recovered when kept at room temperature[5]. This recovery implies that the annealing rate of radiation damage in CIGS thin-film solar cells is faster than that in other types of solar cells[6]. Therefore, radiation damage in the CIGS cells is supposed to be recovering during proton and electron irradiations. To clarify the recovery phenomenon of radiation damage in CIGS thin-film solar cells, we must study annealing effects of radiation damage in the CIGS cells in detail.

In this paper, we report on the results of irradiation experiments with various energies of protons and 1MeV electrons. The annealing rates of proton degraded electrical properties are derived from our results.

2. Experimental

CIGS thin-film solar cell samples (total area of 0.6 cm^2) were cut out from a 30cm×30cm CIGS thin-film circuit (integrated mini-module) and fabricated by a selenization/sulfurization method[7]. The structure of the cells was $ZnO/Zn(O,S,OH)x/Cu(In,Ga)Se_2/Mo/Glass$[7]. The solar cells had an average efficiency of 10.0%, open-circuit voltage (Voc) of 570 mV, short-circuit current density (Isc) of 40 mA/cm^2, and a fill factor (FF) of 60%, which were measured under AM0, one-sun condition. The cells had a lower FF than typically reported for CIGS thin-film solar cells, because the cells had relatively high series resistance due to their contact structure.

3. Results and Discussion

3.1 Relative Damage Coefficient(RDC) of CIGS Solar Cells

We performed proton irradiation using the ion implanter, the tandem accelerator and the AVF cyclotron at the Japan Atomic Energy Research Institute, Takasaki. We irradiated the cells with protons of 0.05, 0.10, 0.20, 0.38, 1.00, 3.00 and 10.00 MeV to study the dependence of radiation damage on proton energy. Figure 1 shows the degradation of the cells by proton irradiation. The cell performance did not

degrade below the level of 0.20 MeV in proton energy, because the protons may stop at the ZnO window layer on the CIGS absorption layer. We derived the RDC of the performance on the cells as shown in Fig. 1. The RDCs of the short-circuit current (Isc)

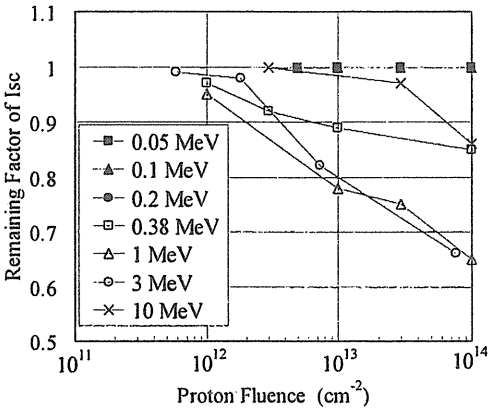

(a) Short-Circuit

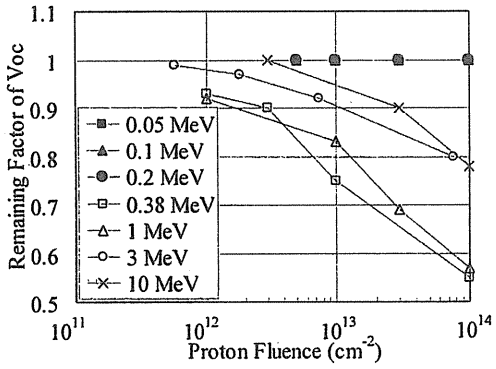

(b) Open-Circuit Voltage

Fig. 1 Remaining factors of (a) Isc and (b) Voc on the CIGS solar cells irradiated with 0.05, 0.1, 0.2, 0.38, 1, 3 and 10 MeV protons.

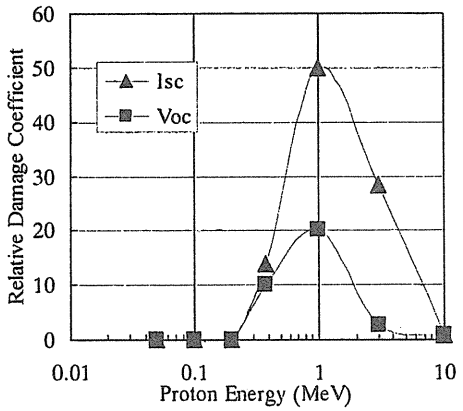

Fig. 2 Relative damage coefficients for Isc and Voc of the CIGS solar cells irradiated with protons.

and the open circuit-voltage (Voc) are derived from the proton fluence of 10 % degradation compared with that in the case of 10 MeV proton. The RDC value at each proton energy is shown in Fig.2.

3.2 Annealing Rates of Voc and Isc of Proton-Irradiated CIGS Solar Cells

The following equation expresses the annealing rate of irradiated CIGS solar cells:

$$B = B_d \exp(-At) \quad , \qquad (1)$$

where B is the degradation after annealing, B_d is the degradation before annealing, A is the annealing rate and t is time.

We conducted the thermal annealing experiments in darkness for the CIGS solar cells irradiated with 3MeV protons. The proton fluence was 1×10^{14} cm^{-2}. The remaining factors of Isc and Voc were 85 % and 55 %, respectively. The relations of the annealing rates of Isc and Voc in the cells to temperature are shown in Fig. 3 (a) and (b), respectively.

3.3 Intrinsic Degradation of CIGS Solar Cells by Protons at Low Temperatures

We performed the proton irradiation tests for CIGS solar cells at low temperatures to verify the intrinsic degradation rate without thermal annealing. The cells were cooled using a cryo generator system in order to avoid the thermal annealing effect. The lowest temperature of the sample without proton and light irradiation was below 200 K. Figure 4 illustrates the changes of the remaining factors of Voc and Isc after irradiation of 10 MeV protons. We measured the performance of the cells irradiated with 10MeV protons for each fluence level. The temperature of the cells was 250K to 270K during the irradiation test. The data in Fig. 3 demonstrates that the recovery rate of the cell performance was less than 1×10^{-8} s^{-1} and the experiment lasted 5 hours. Therefore, the

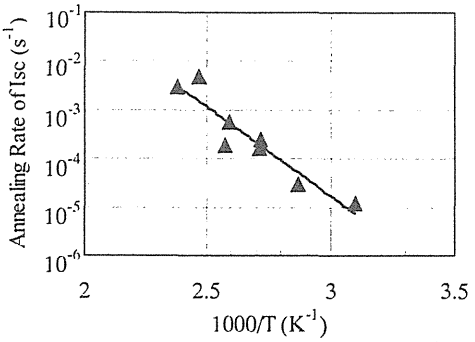

(a) Short-Circuit Current

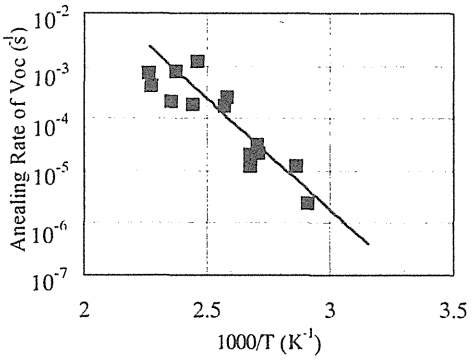

(b) Open-Circuit Voltage

Fig.3 Annealing rates of (a) Isc and (b) Voc on the cells irradiated with 3 MeV protons.

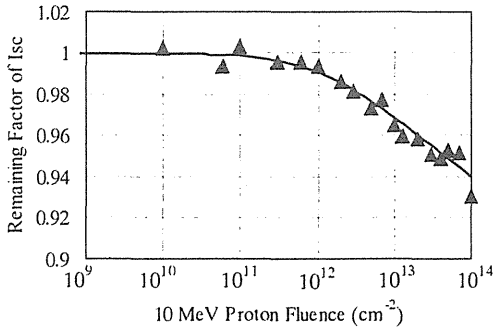

(a) Short-Circuit Current

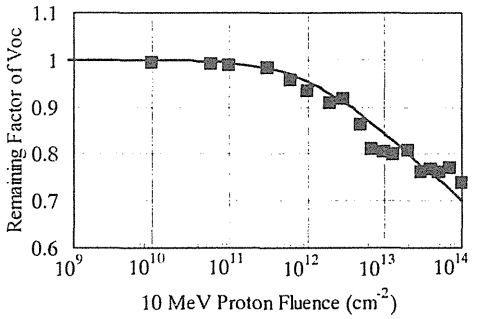

(b) Open-Circuit

Fig. 4 Remaining factors of (a) Isc and (b) Voc obtained at low temperatures for the CIGS solar cells irradiated with 10MeV protons. The solid lines are derived from Eq. (2).

recovery from proton induced-damage in the solar cells was less than 1% and therefore negligible.

We express the degradation of the solar cells electrical performance as follows:

$$D = D_0 - C\log\left(1+\frac{\phi}{\phi_0}\right), \qquad (2)$$

where D is the performance after irradiation, D_0 is the initial performance, C is the constant value, ϕ_0 is the fitting parameter and ϕ is the radiation fluence. The value of C and ϕ_0 of the cells were derived from the fitting to the experimental result using equation (2) and are shown in Table 1.

Table 1. Degradation rate of CIGS solar cells irradiated with 10 MeV protons.

	X	ϕ_0 (cm^{-2})
Isc	0.03	1×10^{12}
Voc	0.15	1×10^{12}

References

1) K. Ramanathan, M.A. Contreras, C. L. Perkins, S. Asher, F. S. Hasoon, J. Keane, D. Young, M. Romeo, W. Metzger, R. Noufi. J. Ward and A, Duda: Prog. Photovolt. **11** (2003) 225

2) T. Aburaya , T. Hisamatsu and S. Matsuda, *Second WCPEC*, (1998) 3568

3) S. Wideman, M. E. Beck, R. Butcher, I. Repins, N. Gomez, B. Joshi, R. G. Wendt and J. S. Britt, Twenty-ninth *IEEE PVSC*, (2002) 575

4) J. R. Tuttle, A. Szalaj and J. Keane, Twenty-eighth *IEEE PVSC*, (2000) 1042

5) A. Bohen, D. Bräunig, J. Klaser, F. H. Kang, B. Hösselbarth and G. La Roche, Twenty-eighth *IEEE PVSC*, (2000) 1038

6) S. Kawakita, M. Imaizumi, M. Yamaguchi, K. Kushiya, T. Ohshima, H. Ito, and S. Matsuda, Jpn. J. Appl. Phys., **41** (2002) L797

7) K. Kushiya, M. Tachiyuki, T. Kase, Y. Nagoya, I. Sugiyama, O. Yamase and H. Takeshita: Sol. Energy. Mater. Sol. Cells **49**(1997) 277.

1.2 Recovery of Electrical Properties of InGaP Solar Cells after Proton Irradiation at Low Temperatures

A. Ohi*, T. Ohshima*, T. Kamiya*, M. Imaizumi**, T. Sumita**, S. Kawakita**
And K. Shimazaki**
Department of Material Development, JAERI*
Japan Aerospace Exploration Agency (JAXA)**

1. Introduction

Solar cells are used as the primary energy source of artificial satellites in space. Since the electrical performance of solar cells is degraded in space radiation environment, the prediction of their lifetime is very important to design power system of artificial satellites with high reliability. For this purpose, it is necessary to understand the degradation behavior of electrical characteristics of solar cells. Recently, with increasing electric requirements of satellites, solar cells with high efficiency are needed to develop. Since multi-junction solar cells based on III-V compounds show high efficiency, these solar cells are regarded as promising candidate for space application. InGaP n-p junction solar cells are used as the top subcells of InGaP/GaAs/Ge triple junction solar cells, and it was reported that the electrical performance of InGaP cells irradiated with 1MeV-electrons was recovered by the injection of minority carriers[1]. For the accurate prediction of lifetime of these solar cells, it is necessary to understand details of recovery behavior as well as that of degradation behavior. Because both the degradation of electrical characteristics due to irradiation and the recovery due to carrier injection affect the power generation by solar cells, we need to propose degradation models including recovery effects. Thermal annealing effects are also thought to affect the recovery of the electrical characteristics of solar cells. Therefore, for understanding the recovery effects by carrier injection, the measurement should be carried out at low temperatures.

In this study, we report *in situ* technique for the measurement of solar cell properties combined with proton irradiation at low temperatures.

2. Experimental procedure

The sample used in this study was a InGaP single n-p junction solar cell on GaAs/Ge substrate. Figure 1 shows a schematic diagram of experimental setup. The sample was set on the stage of which temperature can be controlled. The electrical properties of the solar cell were characterized under light illumination. A single lamp solar simulator was used as the light source in this study. The electrical characteristics such as short circuit current (Isc), open circuit voltage (Voc) and maximum power (Pmax) were

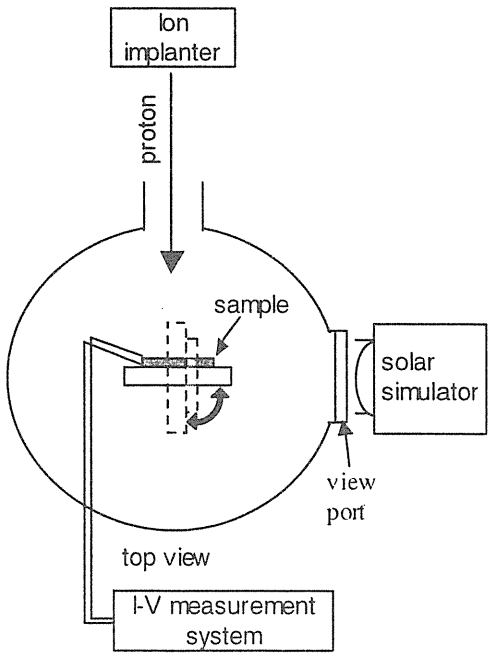

Fig.1 Schematic diagram of experimental setup

derived from current-voltage (I-V) curves. The cell was kept in dark condition except under I-V measurements.

After evacuation and cooling, the sample was irradiated with 40 keV-protons. Protons at energy of 40 keV penetrate to the p-type InGaP base layer. The sample temperature was kept around 140 K and the total proton fluence was $1.2\times10^{12}/cm^2$. To check the recovery of cell characteristics by carrier injection, I-V measurements under light illumination were repeatedly performed at 140 K after proton irradiation. Then, thermal annealing behavior of cell characteristics was observed.

3. Results and discussion

The Isc, Voc and Pmax values measured at low temperatures after proton irradiation are shown in Fig.2. No significant change in both Isc and Voc are observed due to current injection by light illumination. On the other hand, Pmax recovered and saturated after 600min. This result indicates that the recovery of curve fill factor (FF) occurs by current

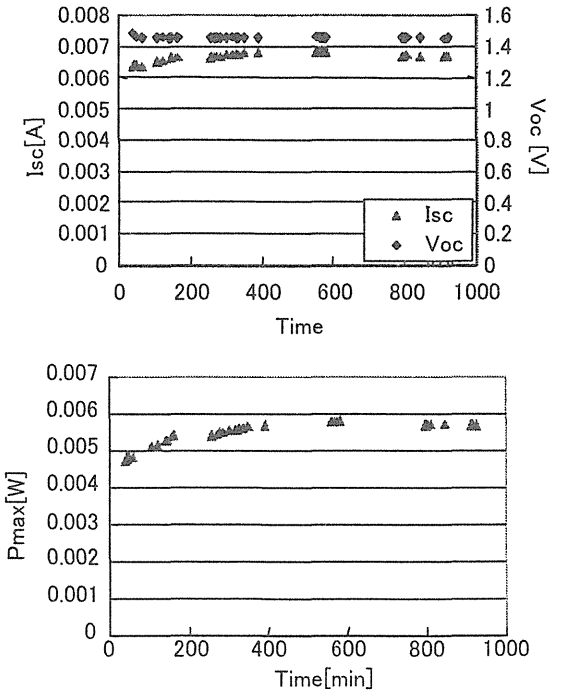

Fig.2 Solar cell characteristics at a low temperature (~130K) after proton irradiation

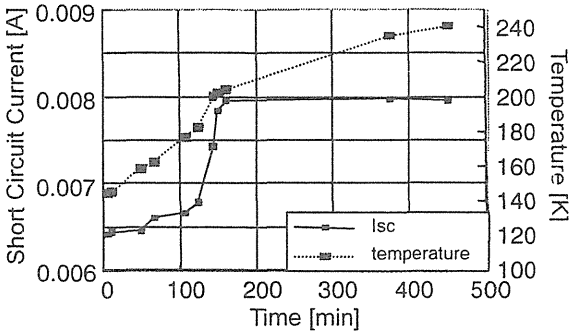

Fig.3 Isc recovery by sample annealing

injection. Since FF relates to p-n junction properties such as leakage currents, the result obtained in this study suggests that defects near junction decrease by carrier injection.

The values of Isc and measurement temperature obtained from the annealing procedure are plotted as a function of time in Fig. 3. A remarkable increase of Isc is observed at temperatures around 150-200 K and no significant increase of Isc is observed above 200 K. This means that defects which act as carrier traps decrease around 150-200 K. Therefore, the results obtained in this study suggest that two type of the recovery (carrier injection and thermal annealing) occurs in InGaP solar cells irradiated with protons. To clarify the structure of these defects, further investigations are necessary.

4. Summary

The electrical properties of InGaP solar cells irradiated with 40keV protons were evaluated using low temperature proton irradiation and *in situ* I-V measurement technique. Recovery of cell performances is found in annealing after proton irradiation. These results indicate that this technique can provide us new information about radiation response of solar cell properties.

References

1) M. Yamaguchi *et al.*, Appl.Phys.Lett. **70** (12), 1566 (1997)

1.3 Bulk Damage Caused by Protons and Heavy Ions in SDRAMs

H.Shindou*, Y.Iide*, N.Ikeda*, S.Kuboyama*, S.Matsuda*,
T.Hirao** and T.Kamiya**
Japan Aerospace Exploration Agency (JAXA) *
Depertment of Materials Development, JAERI**

1. Introduction

In the design rule for integrated circuits, the circuit size is becoming smaller year-by-year. Along with the design rule, the signal level handled in the circuits is also becoming smaller. In extremely fine devices, the bulk damage introduced by single proton or heavy ion is expected to affect their performance while single ion induced malfunctions called single event upsets (SEUs), multiple bit upsets (MBUs)[1] and single event functional interrupts (SEFIs)[2] are well known. In a previous study[3] it was confirmed that most of the bulk damage caused by protons and heavy ions was defect clusters formed by the recoiled atom cascade in X-ray observation Charge Coupled Devices (CCDs). This type of damage is a serious problem for CCD imagers because in the pixel involving such defects, a large dark current is generated without any optical input.

It is most likely that displacement damage degrades the electrical performance of memory devices like dynamic random access memories (DRAMs), which are also very susceptible to single event effect (SEE) and total ionizing dose (TID) effects[4, 5]. This study is concerned with a new failure mode that is attributable to the bulk damage caused by single proton hit in commercial 256Mbit SDRAMs.

2. Possibility of device malfunction caused by bulk damage

At first, we describe the possible mechanism of the new error mode caused by the radiation induced bulk damage in DRAMs. The representative cross-sectional structure of the DRAM memory cell is shown in Fig.1. In DRAMs, the data is physically memorized as charged or discharged state of the storage capacitor. It is necessary to refresh the data repetitively to maintain the charged state because the storage capacitor discharges gradually. In the charged state, electrons are swept out from the diffusion layer and the depletion layer is formed around the diffusion layer- substrate junction. If some stable defects are introduced in the depletion layer, electron-hole pairs are generated and electrons are collected to the diffusion layer by the electric field. As the result, the defects in the depletion layer accelerate the discharge of the capacitor, and the refresh rate required to retain memorized data becomes shorter. Thus the refresh rate is considered as the key parameter to examine the damage effect on the memory storage.

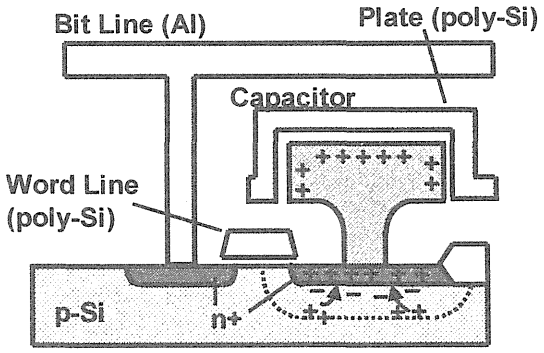

Fig.1. Representative cross-section structure of DRAM cell (Stack type)

3. Experimental

Two types of commercial 256Mbit SDRAM were used in this experiment. A summary of these devices is shown in Table 1. Both memory devices are organized as 8Mword x 8bit x 4bank. The change in the refresh rate to retain memorized data was measured as a typical parameter to detect the effect of bulk damage. For ion irradiation to the sample devices, we used 70MeV protons and 322MeV Xe ions accelerated with the azimuthally varying frequency (AVF) cyclotron at the Takasaki Radiation Chemistry Research Establishment of Japan Atomic Energy Research Institute (JAERI). The irradiation was performed at room temperature with all the terminals grounded to prevent the influence of other phenomena such as single event latch-up (SEL). The pre- and post- irradiation refresh rate was measured using an LSI tester.

Table 1 Description of Sample Devices

Device type	Manufacturer	Cell
TC59SM808BFT-80	Toshiba	Trench
HM5225805BTT-A6	Hitachi	Stack

4. Result and discussion

Three sample devices of each device type were tested. Fig.2 shows the number of failed words in the virgin devices as a function of the refresh rate. The maximum specification limit of refresh rate for both test samples is defined as 64ms. In the HM5225805BTT-A6, no error was observed when the refresh rate was prolonged to 200ms. In the TC59SM808BFT-80, the error was not observed until the refresh rate reached to 400ms. It is confirmed that the shortest refresh rate at which the error is observed is longer than the specification limit for both test samples.

In order to evaluate the damage level introduced by the irradiation, we defined and used an error cross-section, which was defined as the number of failed words increased by irradiation divided by the total fluence at each refresh rate. Fig.3 shows the cross-section as a function of the refresh cycle for the sample devices irradiated with protons or Xe ions. Total fluence of protons was about 3.3×10^9 particles/cm^2 and that of Xe ions was about 3.0×10^7 particles/cm^2. These correspond to the absorption dose of about 3.6Gy(Si) for proton and about 55 Gy(Si) for Xe ion irradiation.

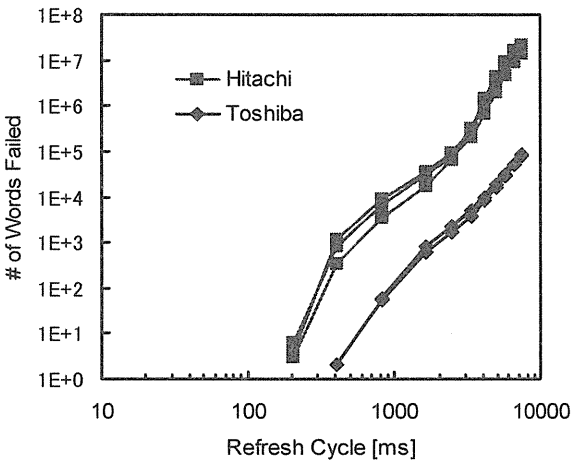

Fig. 2. Initial characteristics for SDRAMs

As shown in Fig.3, several words failed even if the refresh rate is shorter than the specification limit after irradiation. No significant difference was observed in the results obtained for two device types. The electrical characteristic such as the retention time in DRAMs is significantly sensitive to TID[5]. Thus to distinguish the influences of the TID and bulk damage, we performed the γ–ray irradiation test for the same samples using Co-60 γ–ray irradiation facility at Takasaki Radiation Chemistry Research Establishment of JAERI. The absorbed dose of γ–ray irradiation was set to about 30Gy(Si). The number of failed words as a function of the refresh rate before and after irradiation is shown in Fig.4. No increase of power supply current was observed in this

irradiation level. For the comparison between proton and γ–ray irradiations, the data shown in Fig.3 is re-plotted and shown in Fig.5. The effect of annealing was hardly seen even if 100 hours have passed after the irradiation test. Whereas TID causes the degradation in the refresh rate of devices, significant difference is observed between proton and γ-ray irradiation test results. In the γ–ray irradiation, no failure word was observed in the refresh cycle range shorter than the specification limit (64ms). On the other hand, in the proton irradiation, the number of failure is increased in a low refresh cycle below 200ms although the absorbed dose is an order of magnitude smaller. This difference suggests strongly that the failure caused by proton irradiation is not attributable to the TID effect. Therefore, the bulk damage introduced by protons probably affects the performance of test memory devices. Further investigations are necessary to confirm the effect of bulk damage on malfunction in memory devices.

References

1) A. Makihara, H. Shindou, N. Nemoto, S. Kuboyama, S. Matsuda, T. Oshima, T. Hirao, H. Ito, S. Buchner, and A. B. Campbell, IEEE Trans. Nucl. Sci., NS-47 (2000) 2400-2404.
2) R. Koga, P. Yu, K. B. Crawford, S. H. Crain, and V. T. Tram, IEEE Radiation Effects Data workshop Record (2001) 6-13.
3) S. Kuboyama, H. Shindou, T. Hirao, and S. Matsuda, IEEE Trans. Nucl. Sci., NS-49(2002) 2684-2689.
4) L. D. Edmonds, S. M. Guertin, L. Z. Scheick, D. Nguyen and G. M. Swift, IEEE Trans. Nucl, Sci., NS-48 (2001) 1925-1930.
5) T. R. Oldham, K. W. Bennett, IEEE Trans. Nucl. Sci., NS-40 (2001) 1820-1830

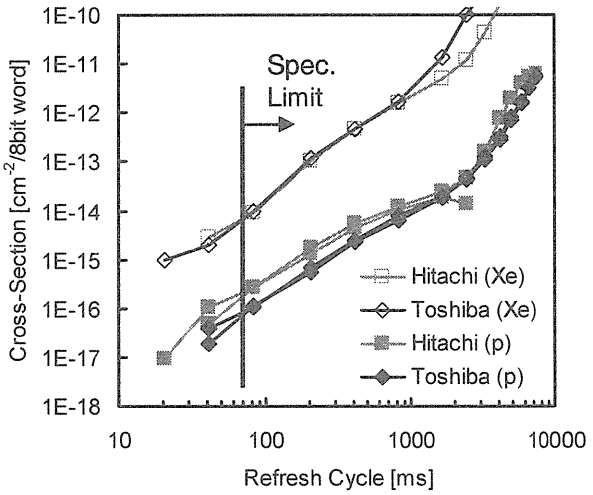

Fig. 3. Error cross-section for SDRAMs irradiated with protons and Xe ions.

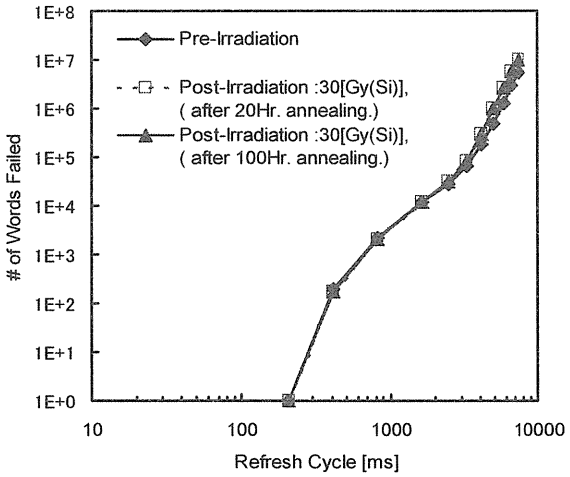

Fig. 4. γ–ray irradiation test result for Hitachi: HM5225805BTT-A6

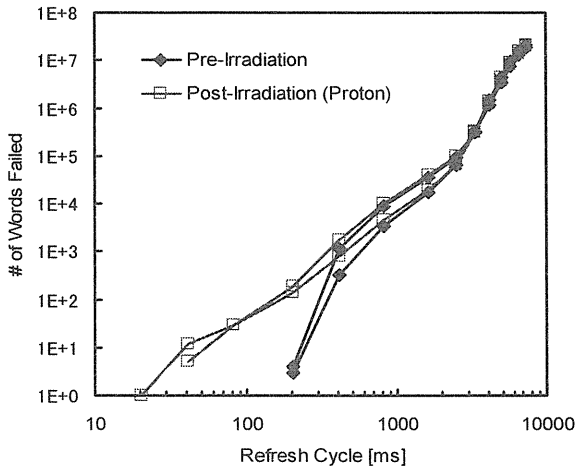

Fig. 5. Proton irradiation test result for Hitachi: HM5225805BTT-A6

1.4 Study on Proton-induced Single Event Upset in CMOS Circuit Fabricated using 65nm Technology

H. Fukui*, M. Hamaguchi*, H. Yoshimura*, H. Oyamatsu*, F. Matsuoka*,
T. Noguchi*, T. Hirao**, H. Abe**, S. Onoda**, T. Yamakawa**,
T. Wakasa** and T. Kamiya**
TOSHIBA CORPORATION Semiconductor Company*
Department of Materials Development, JAERI**

1. Introduction

CMOS LSIs are widely used in various fields and become one of the most important elements constructing the infrastructure because both their characteristics and cost can be improved by shrinking the dimensions of CMOS devices. However, scaling of devices involves many serious problems. Increasing Single Event Upset (SEU) is one of the most serious problems, because it causes the operational errors of the system. It has been reported that when the gate length of MOSFETs becomes smaller than 50 nm, SEU caused by cosmic rays will affect the system operation even at the ground level[1]. Therefore, for mass production utilizing them, it is required to develop the method to suppress SEU induced by cosmic rays.

Our objective in this work is to develop the guideline to design the soft-error immune circuits utilizing CMOSFETs with the gate length below 50nm. We have developed the measurement system of SEU and verified that the measurement has been completed successfully. We have also measured the SEU cross section caused by proton irradiation and found the radiation energy dependency of the SEU cross section.

2. Experiment

We have prepared the shift register with 40,000 flip-flop stages for SEU measurements as shown in Figure 1. Each flip-flop cell is connected in series. After 40,000 cycles of clock

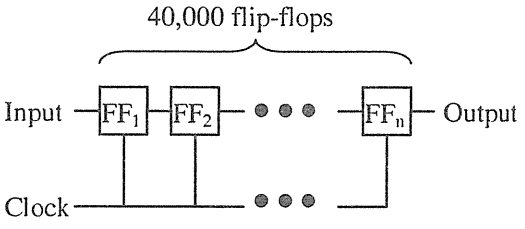

Figure 1. Schematic diagram of the test circuit used in SEU measurements.

signal, data is output. Test circuit was fabricated by 65nm CMOS process. It consists of CMOSFETs with the gate length of 90 nm.

Figure 2 shows the measurement procedure. At first, the experimental conditions are input into the system and the circuit is initialized. Next proton beam irradiation starts. During irradiation, the data pattern is sequentially written into the circuit. In the experiment, we write the same data into each stage. Next, the

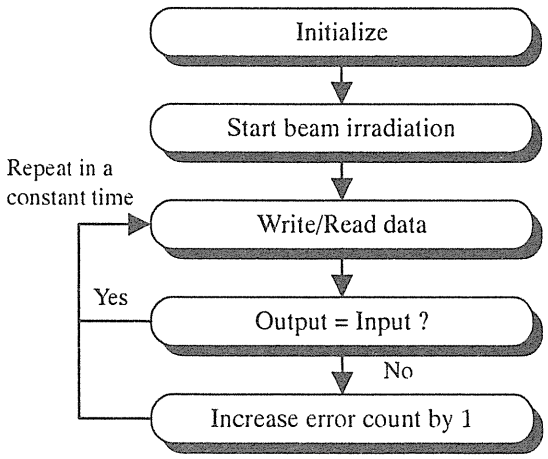

Figure 2. Measurement procedures.

output is compared the input. When the output is different from the input, we consider that SEU occurs and increase the error count by one. The above procedures are repeated in a constant time and errors are summed up.

Accelerated soft error testing was performed utilizing Cycrotron at JAERI Takasaki. The test circuits were irradiated directly by a scanning proton beam in 5 minutes. The scanning frequency was 50Hz (X-axis) and 2.5Hz (Y-axis). The proton flux was measured by Faraday cup. The SEU measurement was done at the energies of 20, 50 and 80 MeV. The SEU cross section can be calculated by the total error counts, proton fluence and the area of the test chip.

3. Results and Discussion

Figure 3 shows the relationship between the SEU cross section and the supply voltage V_{dd} at the radiation energy of 80 MeV. In Figure 3, "All High" or "All Low" means that high or low level is written into all cells, respectively. As shown in Figure 3, the SEU cross section of "All High" is the same as that of "All Low" for each V_{dd}. This tendency is observed at the other radiation energies. Test chip is composed of 40,000 flip-flop cells as shown in Figure 1. Each

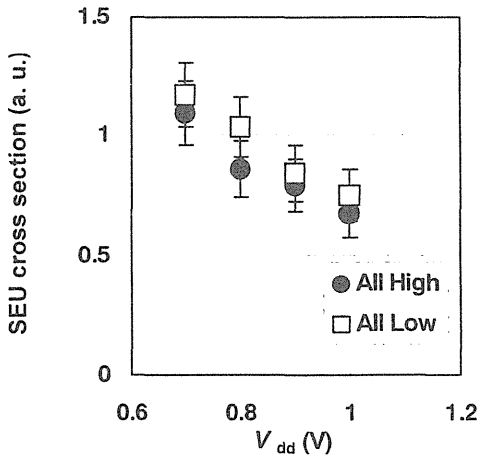

Figure 3. Relationship between the SEU cross section and the supply voltage V_{dd}. The proton energy is 80 MeV.

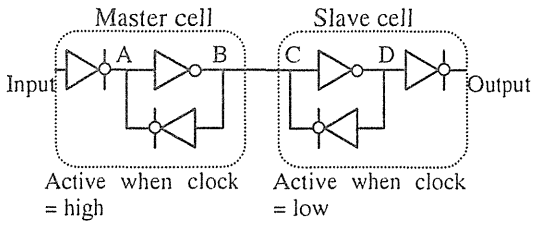

Figure 4. Circuit configuration of flip-flop cell, which is composed of master- and slave cells. Master cell is active when clock = high, while slave cell is active when clock = low.

Table 1. Voltage at the nodes shown in Figure 4. H and L mean high (V_{dd}) and low (Ground) levels, respectively. Node voltage of master cell at input = H is the same as that of slave cell at input = L.

	Master		Slave		
Input	A	B	C	D	Output
H	L	H	H	L	H
L	H	L	L	H	L

flip-flop cell is composed by master- and slave cells as shown in Figure 4. Since both cells have the same structure, their SEU cross section are the same. Table 1 shows the input and the voltage at the nodes shown in Figure 4. From Table 1, it is found that the node voltage in master cell at input = High is the same as that in slave cell at input = Low. As a result, the SEU cross section is independent of the input. It is also found from Figure 3 that the SEU cross section increases linearly with decreasing V_{dd}. This is explained by the fact that the charge Q_{crit} required for SEU decreases with decreasing V_{dd} as shown in Figure 5. Since Q_{crit} decreases linearly with decreasing V_{dd}, the SEU cross section is the linear function of Q_{crit}.

Figure 6 shows the dependence of the SEU cross section on radiation energy, indicating that the SEU cross section exhibits the maximum value around 50MeV. This result is in good agreement with the previous report[2].

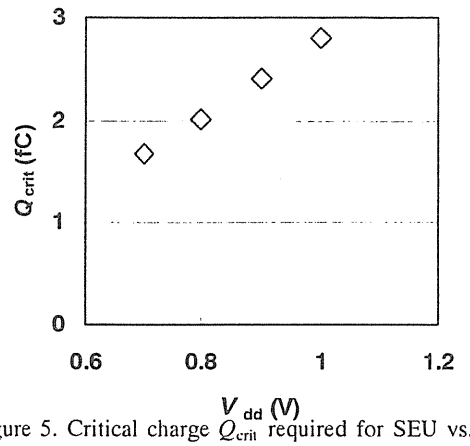

Figure 5. Critical charge Q_{crit} required for SEU vs. V_{dd}. Q_{crit} is obtained by SPICE simulation. Q_{crit} increases linearly with increasing V_{dd}.

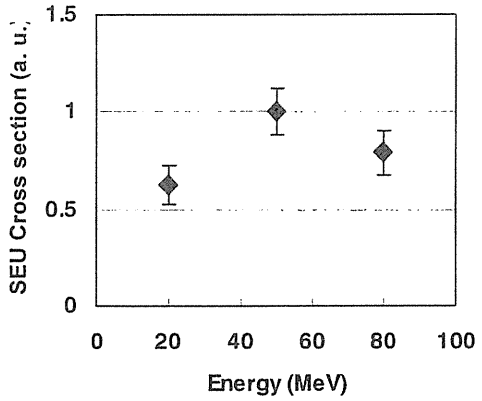

Figure 6. Dependence of SEU cross section on proton energy. The SEU cross section has the maximum value around 50 MeV.

4. Summary

We have developed the measurement system of the SEU and verified that the measurement has been completed successfully. We have measured the SEU cross section caused by proton irradiation. As a result, it is found that the SEU cross section is independent of the input data and increases linearly with decreasing V_{dd}. We have investigated the dependence of the SEU cross section on proton energy. Experimental data show that the SEU cross section has the maximum value around 50 MeV.

References

1) R. Baumann, Technical Digest of IEDM (2002) 329-332.
2) P. E. Dodd, M. R. Shaneyfelt, J. R. Schwank, and G. L. Hash, Technical Digest of IEDM (2002) 333-336.

1.5 Anomalous Gain Mechanisms during Single Ion Hit in Avalanche Photodiodes

J. S. Laird[*], T. Hirao[*], S. Onoda[*,**], T. Wakasa[*,**], T. Yamakawa[*,**], H. Abe[*], H. Ohyama[***] and T. Kamiya[*]
Department of Materials Development, JAERI[*]
Graduate School of Engineering, Tokai University[**]
Department of Electronic Engineering, Kumamoto National College of Technology[***]

1. Introduction

With the reduction in typical operational bias and improved temperature stabilization, the Avalanche Photodiode (APD) is becoming the device of choice for high-speed low light level applications where they exhibit sensitivities of 5 to 10 dB better than *p-i-n* structures (provided both the gain-bandwidth product is high and the multiplication noise is low). However, the intrinsic gain mechanism makes them susceptible to high energy heavy ions generated by proton induced nuclear reactions[1]. Heavy ion strikes result in large Single Event Transients (SET) which degrades the Bit Error rate (BER) of an optical link[2]. To more fully understand mechanisms which lead to BER degradation we have examined the spatial charge collection characteristics of a high-speed commercial APD for 6MeV N and 7MeV O to ascertain the existence or not of any non-linear charge collection/gain mechanisms.

2. Experimental Results

2.1 Device Specifications

The device under test (DUT) was a 2.5GHz InP-InGaAsP-InGaAs communications APD with cross-sectional structure as given in the top of Fig.1. The InGaAsP increases the bandgap discontinuity between the InGaAs and InP reducing the large dark current from narrow gap InGaAs. The top p^+n-InP region was 0.92μm; the InGaAsP thickness was 0.1μm and the *n*-InGaAs layer was 1.23μm[1]. Dark current and photocurrent characteristics of the device were measured using a 1.5μm laser at room temperature.

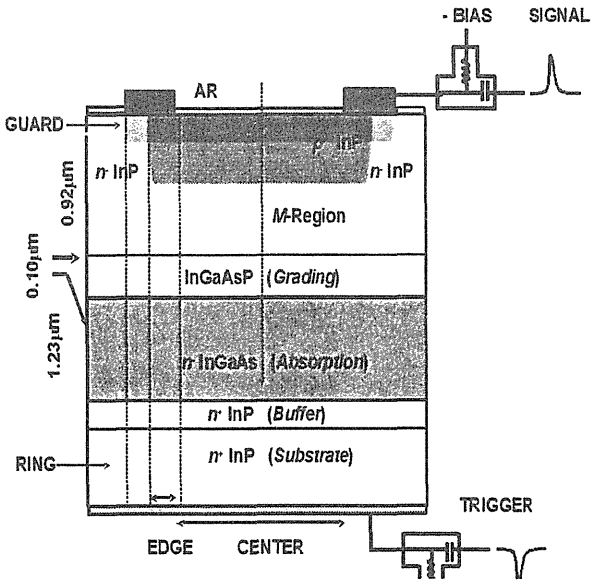

Fig.1: APD device cross-section. Charge generated in the absorption region is multiplied in the M-region resulting in gain. Both 6MeV N and 7MeV O have a range of approximately 4.5μm.

As shown in Fig.2, the photocurrent curve undergoes several discrete steps when the bias reaches that required for punchthrough into the InGaAs region. The main step occurs for hole transport over the CENTER region at V_{center} = 35V.

2.2 Transient IBIC Measurements

For these experiments focused 6MeV N and 7MeV N beams were scanned over the APD and SET data collected using the JAERI TIBIC system[2] in conjunction with a 3GHz Tektronix TDS694C. These ions and energies were chosen to have the same range of 4.5μm.

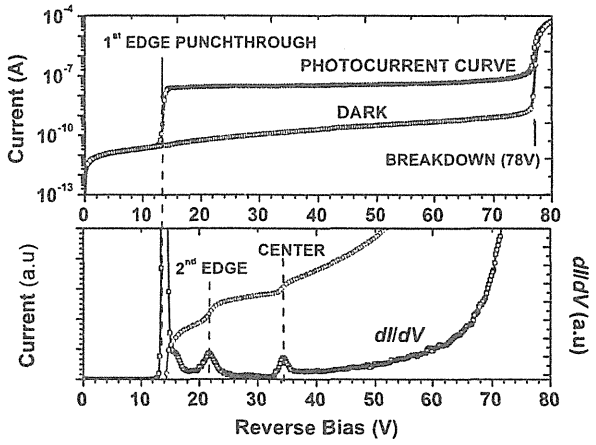

Fig. 2: Photocurrent and dark current IV curve taken at room temperature. The main punchthrough into the CENTER region occurs at around 35V. The device breaks down at close to 78V.

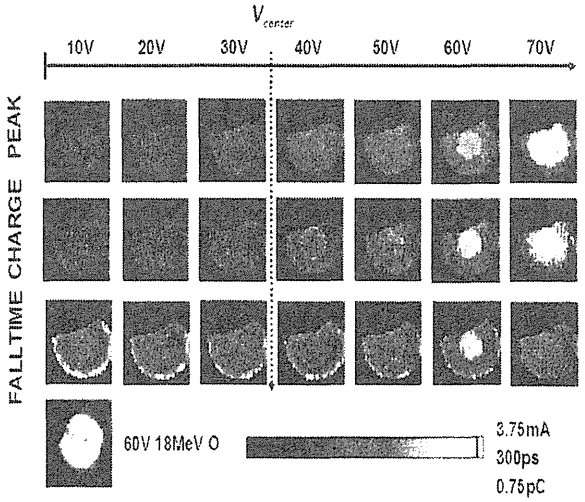

Fig. 3: TIBIC Peak, Charge and Falltime images of the APD under test. For V>V center, the peak and charge increase dramatically due to impact ionization. For analysis average SET data was extracted from the circular mask shown.

Any marked differences in the SET amplitudes and characteristics can therefore be ascribed to the non-linear charge collection/gain mechanism described earlier. Post-data collection TIBIC peak current, charge and falltime images were generated as shown for the case of 6MeV N in Fig.3. Also shown for comparison is data from a previous 18MeV O experiment on the same device where the EDGE region generated large SET amplitudes[1]. As we are examining gain mechanisms prevalent during an ion strike the device CENTER region was chosen for all further analyses.

3. Results and Discussion

Shown in Fig.4 below are the bias dependencies for both the average peak current and total charge as extracted from the area of the average SET in the CENTER. The peak current is seen to increase exponentially due to field induced impact ionization in the M-region. Interestingly, the charge collected for biases below all punchthrough points is greater than that expected (0.06pC was predicted by SRIM combined with known energies required to generated an electron-hole pair in InP[3] and InGaAs[4]). This suggests an additional collection mechanism is at play; drawing charge from below the InGaAs InP heterointerface. This charge is likely due to the influence of funneling fields.

For biases $V > V_{center}$, the situation is more complicated and comparisons are necessary. After normalizing to the beam energy, we can see that both data sets lie clearly within error of one another suggesting the absence of any strong electron-hole plasma density dependent non-linear charge collection mechanism for these low LET ions. We are currently analyzing this data in more detail

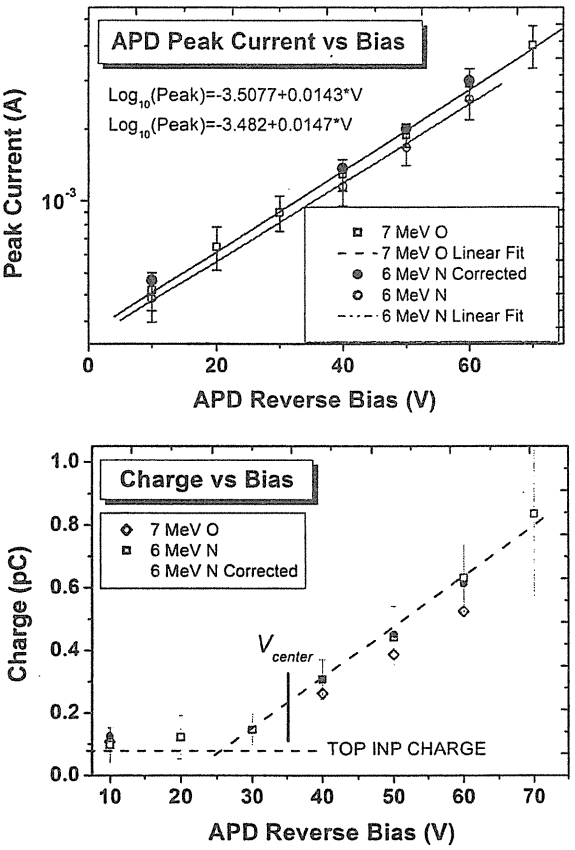

Fig. 4: TIBIC peak current and charge versus bias for both 7MeV O and 6 MeV N ions extracted from the CENTER region.

and comparing these low LET results to data collected with higher LET ions, where additional charge collection mechanisms were found to contribute to an anomalous gain.

References

1)J. S. Laird, T. Hirao, S. Onoda, H. Ohyama, and T. Kamiya, IEEE Transaction on Nuclear Science **50**, 2225-2232 (2003).

2)J. S. Laird, T. Hirao, H. Mori, S. Onoda, T. Kamiya, and H. Itoh, Nuclear Instruments and Methods in Physics Research Section B: Beam Interactions with Materials and Atoms **181**, 87-94 (2001).

3)P. G. Pelfer, F. Dubecký, R. Fornari, M. Pikna, E. Gombia, J. Darmo, M. Krempaský, and M. Sekácová, Nuclear Instruments & Methods in Physics Research A **458**, 400-405 (2001).

4)S. Belogurov, G. Bressi, G. Carugno, E. Conti, D. Iannuzzi, and A. T. Meneguzzo, Nuclear Instruments and Methods in Physics Research Section A: Accelerators, Spectrometers, Detectors and Associated Equipment **452**, 377-380 (2000).

1.6 Transient Current Induced by Heavy Ions in MOS Devices

T. Shibata*, **, T. Hirao*, S. Onoda*, ***, H. Abe*, T. Yamakawa*, ***, T. Wakasa*, *** and T. Kamiya*
Department of Material Development, JAERI*
College of Science and Technology, Nihon University**
Graduate School of Engineering, Tokai University***

1. Introduction

Silicon on insulator (SOI) devices, which are structured by placing an oxide layer between a thin top silicon layer and a silicon substrate, exhibit high performance and need low power in comparison with conventional bulk silicon devices because the amount of electrical charge during device operations can be reduced due to a low parasitic capacitance of SOI devices. An additional advantage of SOI devices is their high resistance to radiations. Thus SOI devices are expected to be applied in space. In recent years, an anomalous charge collection in SOI device has been observed when high-energy charged particles traverse their active regions[2, 3]. This fact suggests that dense charges generated under a buried oxide contribute to the charge collection. To investigate the charge collection mechanisms in SOI devices, we have measured transient currents induced in Metal Oxide Semiconductor (MOS) capacitors by high-energy heavy ions.

2. Experimental Procedure

The samples used were MOS capacitors fabricated at Nihon University[4]. An oxide layer was grown on an n-type Si wafer with the carrier concentration of 2×10^{15} cm^{-3}. The thickness of the grown oxide layer was about 50 nm. The Al contact with the diameter of 50 μm was deposited on the oxide layer. The depth of inversion layer at an applied bias of –10 V was about 0.6 μm.

In heavy ion irradiation, we used cocktail ion beams which consist of N, Ne, Ar and Kr ions accelerated by an AVF cyclotron at JAERI Takasaki. The beam flux were controlled to be ~100 $cm^{-2}s^{-1}$ to minimize the displacement damage effects. The value of the Linear Energy Transfer (LET) and the project range of each ion were calculated by SRIM code[4] and listed in Table 1. Transient currents were recorded with a 3 GHz Tektronix oscilloscope (model TDS694C).

Table 1. LET and range of ions used in this study.

Ions & Energy	LET (MeV cm^2/mg)	Range (. m)
$^{15}N^{3+}$ 56 MeV	3.31	53.9
$^{20}Ne^{4+}$ 75 MeV	6.33	42.5
$^{40}Ar^{8+}$ 150 MeV	15.3	39.6
$^{84}Kr^{17+}$ 322 MeV	39.9	40.9

3. Results and Discussion

Typical transient current waveforms induced by different ions are shown in Fig. 1. The peak currents obtained for N, Ne, Ar and Kr ion irradiations were 22.9, 43.0, 59.9 and 66.6 μA, respectively. After reaching the peak, the current was reduced with elapsed time, and finally became negative. In order to estimate the intersection of the waveforms and the ground level, the amount of charges were derived by integrating transient currents. The results are shown in Fig. 2. The time when the transient charge reaches the maximum means the intersection. The periods to the intersection for N, Ne, Ar and Kr ion irradiations are 325.6,

266.4, 179.2 and 132.8 ns, respectively. The maximum charges of them are 333.1, 586.2, 1181.3 and 1693.6 fC, respectively. Such behavior has not been observed for pn junctions, in which the charge collection was dominated by conduction currents[5].

Now we discuss what the nature of observed transient current is. Recently, several researchers reported that the current collected in SOI devices is caused by the displacement current[6, 7]. For general definition, the displacement current is proportional to the capacitance and the time dependence of potential variation across the gate dielectrics. When the generated carriers drift toward Si/SiO_2 interface by electric field, the potential at the interface increases with elapsed time. As a result the current is induced on the terminal of electrode as shown in Figs. 1 and 2. After collected charge reaches maximum, the charge reduces because the excited potential relaxes and the induced current flow to the opposite direction. Regarding observed transient current as displacement current, the experimental results are successfully explained.

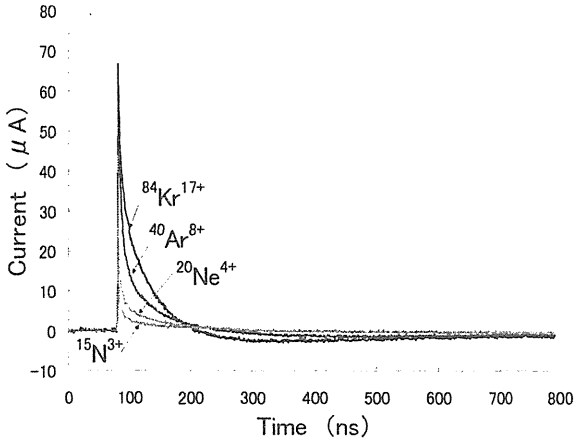

Fig. 1 Transient currents observed in MOS capacitor irradiated with heavy ions.

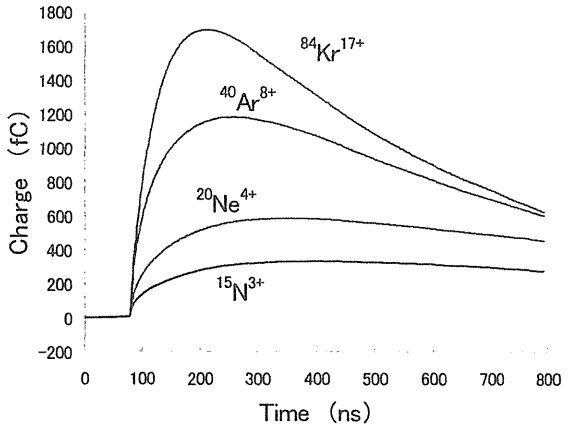

Fig. 2 Transient charges derived using the data shown in Fig. 1.

4. Summary

Transient currents induced by high-energy heavy ions in MOS capacitors were measured and analyzed. We found that the displacement currents play an important role in the charge collection of MOS capacitors. Since a typical SOI structure contains capacitors, the displacement currents have to be considered in the charge collection of SOI devices.

Acknowledgment

We would like to acknowledge Prof. K. Ohnishi and Dr. Y. Takahashi of Nihon University for their corporation in fabricating samples and simulating the displacement current.

References

1) T. Hirao, et al., Nucl. Instr. and Meth., B 158 (1999) 260.
2) T. Hirao, et al., Nucl. Instr. and Meth., B 206 (2003) 457.
3) J. R. Schwank, et al., IEEE Trans. Nucl. Sci., NS-49, No.6 (2002) 2937.
4) J. F. Ziegler, *Stopping and Range of Ions in Solids*, Pergamon, 1985.
5) I. Nashiyama, et al., IEEE Trans. Nucl. Sci., NS-40, No.6 (1993) 1935.
6) M. A. Xapsos, et al., IEEE Trans. Nucl. Sci., NS-34, No.6 (1987) 1214.
7) O. Musseau, et al., IEEE Trans. Nucl. Sci., NS-38, No.6 (1991) 1226.

1.7 Transient Currents Induced in MOS Capacitors by Ion Irradiation: Influence of Incident Angle of Ions and Device Temperature

T. Yamakawa*,**, T. Hirao*, H. Abe*, S. Onoda*, **, T. Wakasa*, **
T. Shibata*, *** and T. Kamiya*
Department of Material Development, JAERI*
Graduate School of Engineering, Tokai University**
College of Science and Technology, Nihon University ***

1. Introduction

It is well known that the SOI (silicon on insulator) structure is suitable for high speed operation and power saving. SOI devices are also of great interest due to their radiation hardness. Concerning the tolerance of single event phenomena, they are thought to be highly resistant because the buried oxide layer is expected to prevent the transport of charges generated in the substrate to the top silicon (Si) layer. On the other hand, recent investigations of high energy ion irradiation to SOI devices showed that the amount of charges collected exceeded that generated in the top layer.[1] In order to clarify the influence of buried oxides on the charge transportation, detailed investigations of the charge transportation in SOI devices using high energy ions are necessary. In this work, we have performed the measurements of transient currents induced in metal-oxide-semiconductor (MOS) capacitors, which were used instead of complicated SOI devices, by irradiation of high energy heavy ions under the conditions of different ion incident angle and device temperature. Theoretical investigations based on electromagnetics have also been made to explain the experimental data.

2. Experiments

The structure of the device sample used in this study is schematically shown in Fig. 1. The oxide layer with the thickness of 50nm was grown on the n-type silicon (Si) substrate with the doping density of

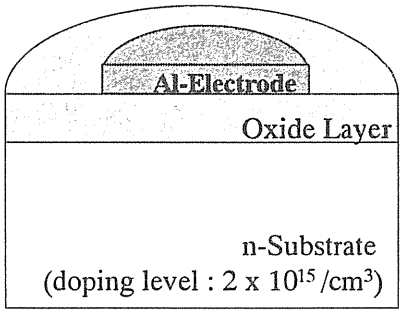

Fig. 1. Schematics illustration of the MOS capacitor sample

$2x10^{15}/cm^3$. Aluminum (Al) was deposited on the oxide to make an electrode with the diameter of 100μm and thickness of 50nm. Irradiation of carbon ions with the acceleration energy of 15MeV was performed using the ion microbeam system connected to a 3MV Tandem accelerator at JAERI Takasaki. The transient current induced in the sample by a single ion was measured with the TIBIC (Transient Ion Beam Induced Current) system developed at JAERI. During the measurements, a reverse bias of –10V was applied to the sample. The incident angle of ions to the sample was set at 0 (normal to the sample), 30 or 60 degree. The sample temperature was also changed from room temperature (RT: approximately 25°C) to 180°C.

3. Results and Discussion

Fig. 2 shows the waveforms of the transient current obtained at RT at the ion incident angles of 0, 30 and 60 degree. As reported in the reference 1, charges were collected at the Al electrode even though it

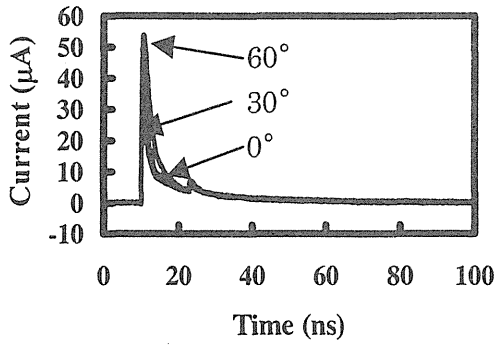

Fig. 2. Transient currents obtained at RT at the ion incident angles of 0, 30 and 60 degrees.

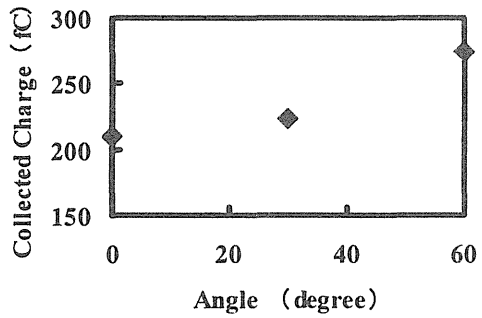

Fig. 3. Dependence of the amount of collected charge on the incident angle of ions.

was separated from the semiconductor substrate by the oxide. The result can be explained in terms of the displacement current induced by a change in the electric potential in an insulator.[2] The total amount of collected charge at the electrode is plotted in Fig. 3 as a function of the incident angle of ions. The collected charge was found to increase with increasing in the ion incident angle. Then the charge generated in the substrate is estimated to increase as the ion incident angle increases. It is likely that a large amount of generated charge in the substrate causes large displacement current, accounting for the result obtained.

Fig. 4 indicates the waveforms of the transient current obtained at the normal incidence of ions at RT, 75, 125 and 180°C. Apparently the peak value of the transient current decreases with increasing

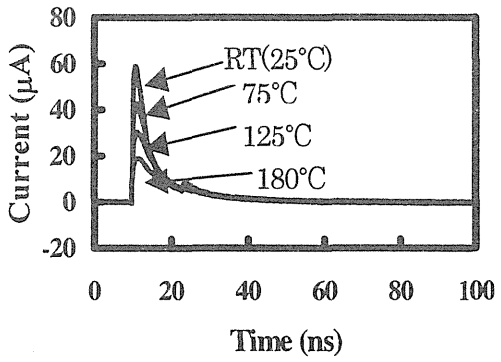

Fig. 4 Transient currents obtained at the normal incidence of ions at temperatures of 25°C, 75°C, 125°C and 180°C.

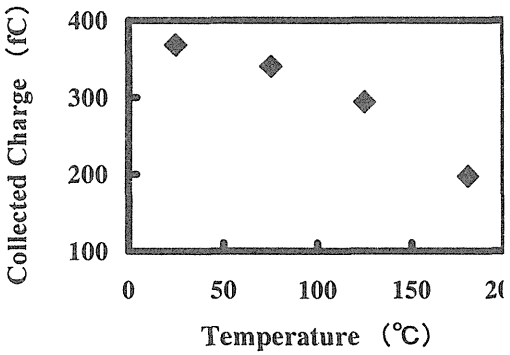

Fig.5. Dependence of the amount of collected charge on the device temperature.

temperature. The amount of collected charge also decreased by raising temperature, as shown in Fig. 5. Theoretical investigations leaded to no significant change in the capacitance of the oxide by raising temperature from RT to 180°C. It was also estimated that similar amount of charge was generated in the substrate at each temperature. Further investigations are necessary to clarify the mechanism behind the temperature dependence of the collected charge in MOS capacitors.

References

1) T. Hirao, et al., Nucl. Instr. and Meth., B 158 (1999) 260.
2) T. Hirao, et al., RADECS 2003 Proceedings, in press.

1.8 Observation of Single -event Transient Currents Induced by Neutron Irradiation in Si pin Photodiodes

T. Wakasa*, ***, T. Hirao*, H. Abe*, T.Sanami****, S.Onoda*, ***,
J.S.Laird*, T.Yamakawa*, ***, S.Tanaka**, H.Hirayama**** and T. Kamiya*
Department of Mat erials Development, JAER I*
Advanced Radiation Technology Center, JAERI **
Graduate School of Engineering, Tokai University ***
Radiation Science Center, KEK ****

1. Introduction

It is well known that when an energetic ion passes through semiconductor devices used in space, a dense electron-hole plasma is generated along the ion track, leading to an assortment of single event phenomena (SEP) [1]. In recent years, SEP have been reported to be also induced by neutrons in terrestrial devices [2]. Such SEP are regarded as a serious problem. For fabricating reliable electronic system, it is necessary to clarify mechanisms behind neutron induced SEP. For this purpose, it is important to measure the charge collection characteristics in semiconductor devices. In this study, we have developed the measurement system of single event transient (SET) currents in silicon pin photodiodes subjected to irradiation of quasi-monoenergetic neutrons, and acquired the data using the system.

2. Experiments

The samples investigated were Si pin photodiodes with a junction diameter of 450 μm. A 65MeV quasi-monoenergetic neutron beam used in this study was generated by using the ^{7}Li(p,n) quasi-monoenergetic neutron source facility which is schematically shown in Fig.1.

A proton beam accelerated with the AVF cyclotron was transported to a ^{7}Li (99.8% purity) target. Neutrons produced via a ^{7}Li(p,n) reaction traveled directly into the experimental hall and irradiated to the samples. The neutron flux at the sample position was about 10^{4} cm^{-2} s^{-1}. Protons transmitted through the Li target are mass separated by a magnet and dumped into a faraday cup for flux monitor.

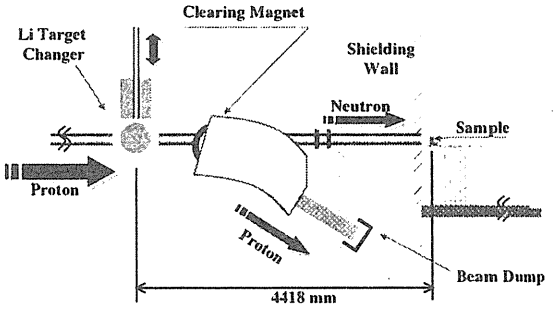

Fig. 1: Schematic view of ^{7}Li(p,n) quasi-monoenergetic neutron source facility

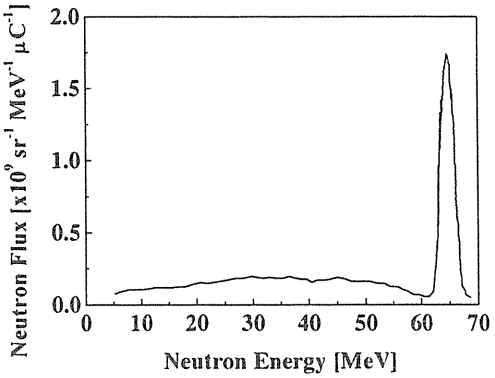

Fig. 2: Energy spectrum of the quasi-monoenergetic neutron beam generated by 68 MeV protons [3]

Fig. 2 shows the energy spectrum of a quasi-monoenergetic neutron beam measured by time of flight (TOF) when proton energy of 68 MeV was used. The TOF measurement was carried out in the neutron beam axis using a scintillation detector [3]. As shown, the neutron peak energy was approximately 65 MeV. Coincident TOF and SET currents were measured using the system displayed in Fig. 3. The signal from the top contact of the sample (SET current) was recorded with a 3 GHz Tektronix 694C DSO, while the bottom contact was connected to a time to amplitude converter (TAC). The TAC was used to perform the TOF measurement by recording the time difference between an RF signal provided by the AVF Cyclotron and the SET current observed. A minimum value of the TAC amplitude was used to determine whether neutrons of a peak energy had in fact hit the device. This procedure allowed us to discriminate peak neutrons (65 MeV neutrons) from scattered or lower energy ones.

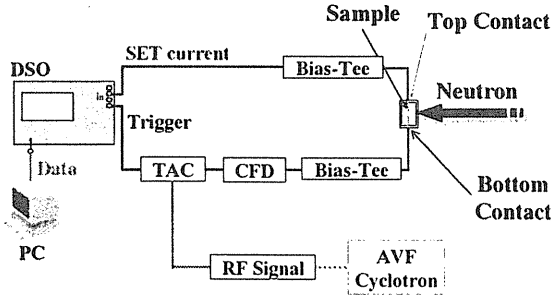

Fig. 3: Schematic diagram of the SET current measurement system.

3. Results and Discussion

Fig. 4 shows the normalized TAC output spectrum. The initial peak at approximately 700 mV corresponds to 65 MeV neutrons. SET current measured with the TAC output, which has a 400 to 1000 mV

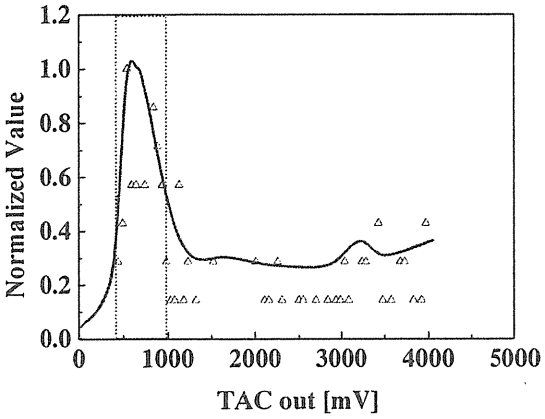

Fig. 4: Normalized TAC output spectrum

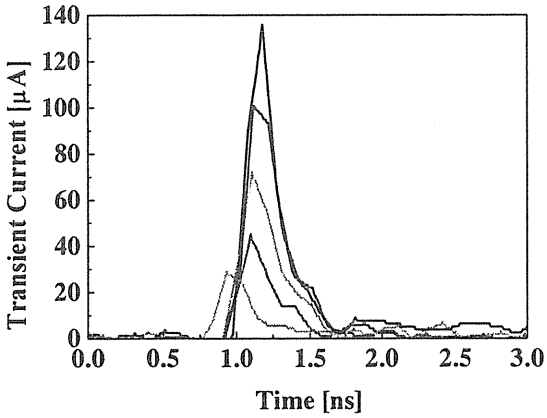

Fig. 5: SET current waveforms induced by 65 MeV neutrons

amplitude, was chosen as 65 MeV neutron induces. Fig. 5 shows typical SET current waveforms measured using the above energy discrimination system. A variety of SET current waveform shapes were observed. This variation is caused by the generation of several kinds of nuclides due to nuclear reactions. Fig. 6 shows the normalized collected charge distribution obtained by integrating SET currents. The peak of collected charge is seen around 200 fC. Fig. 7 shows the secondary nuclides production cross section distributions derived from the ENDF database (ENDF/B-VI) [4]. Hear, the production cross section of heavy particles than α particles is negligibly small.

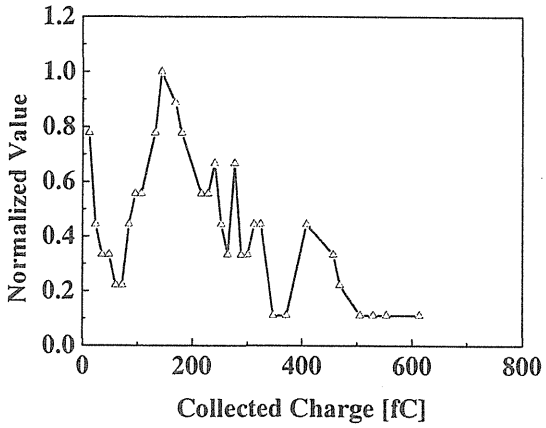

Fig. 6: Normalized collected charge distributions

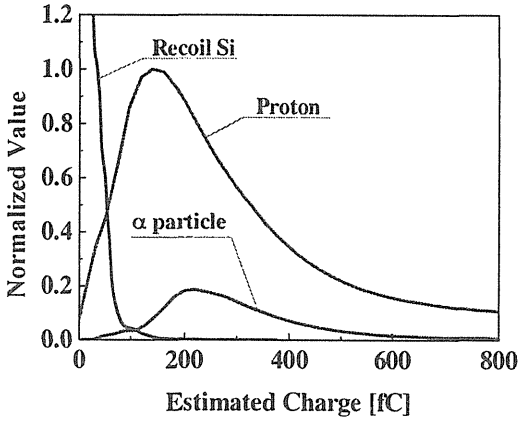

Fig. 7: Secondary nuclides production cross section distributions from the ENDF database

The cross section in the ordinate is normalized by the peak value of proton production cross section. We can convert the secondary nuclides energy E (MeV) to the generated charge Q (fC) by using the simple equation (1),

$$Q = \frac{E}{W} q, \qquad (1)$$

where, q is the electronic charge and W (3.6 eV in Si) is the energy required to generate an e-h pair.

From the comparison of data between Fig. 6 and Fig. 7, the shape of the collected charge distribution is quite similar to the sum of the secondary nuclides production cross section distributions. Therefore, we can conclude that the SET current observed in Si pin diodes by irradiation of 65 MeV neutrons are ascribed to the currents generated mainly by secondary induced protons and recoil Si nuclei.

4. Summary

In this study, we has succeed in the measurement of neutron induced SET currents in Si pin photodiodes using the neutron energy discrimination system. It can be concluded from the comparison between the collected charge distribution and the secondary nuclide production cross section distribution that secondary protons and recoil Si nuclei mainly induce the SET currents.

References

1) T.Hirao et al., Nucl. Instrum. and Methods, B210 (2003) , 227-231.
2) H.Ibe et al., OYO BUTURI, Vol.70, No.1,(2001), 92-93.
3) M.Baba et al., Nucl. Instrum. and Methods, A428 (1999) , 454.
4) P. G. Younget al., Proc. IAEA Workshop Nucl. Reaction Data and Nucl. reactor -Physics, Design, and Safety, Triest (1996) , 227.

1.9 Electrical Characteristics of Metal-oxide-semiconductor Field Effect Transistor Fabricated on Cubic-SiC

T. Ohshima, K. K. Lee and T. Kamiya
Department of Material Development, JAERI

1. Introduction

Silicon carbide (SiC) is regarded as a promising candidate for high-power and high-frequency devices because of its excellent physical properties. Although the device performance expected from bulk properties is superior, the channel mobility for Metal-Oxide-Semiconductor Field Effect Transistors (MOSFETs) fabricated on hexagonal SiC (4H- and 6H-SiC) epitaxial layers has not yet reached enough values for commercial applications. The origin of such a low channel mobility is interpreted in terms of the interaction between carriers (electrons) and interface traps near the conduction band of hexagonal SiCs[1]. Because the bandgap of cubic SiC (3C-SiC) is smaller than that of hexagonal SiCs, the effect of the interface traps on the channel mobility for 3C-SiC MOSFETs is expected to be smaller than that for hexagonal SiC MOSFETs[2]. In previous studies, it was reported that the transconductance of 3C-MOSFETs was 0.46 mS/mm (the channel mobility ≈ 100 cm^2/Vs) at RT and the MOSFETs could operate up to 823K[3]. Furthermore, Wan *et al.*[4] reported 3C-SiC MOSFETs with a channel mobility of 165 cm^2/Vs and breakdown voltage of gate oxide of 3.5 MV/cm. These reports suggest that 3C-SiC has an enough potential for MOS applications. However, since the crystal growth technique for bulk 3C-SiC has not been fully developed, the electrical characteristics of 3C-SiC MOSFETs are not yet clarified well. Recently, Nagasawa *et al.*[5] developed a growth method for thick 3C-SiC epitaxial layers using silicon (Si) (001) substrates with undulation oriented to [-110] direction. In addition, Ishida *et al.*[6] reported that high quality 3C-SiC layers were homo-epitaxially grown on the thick 3C-SiC. This indicates that MOSFETs can be fabricated on homo-epitaxial 3C-SiC layers.

In this article, the electrical characteristics of 3C-SiC MOSFETs are studied.

2. Experimental details

N-channel MOSFETs were fabricated on p-type 3C-SiC homo-epitaxial layers grown on 3C-SiC substrates. The 3C-SiC substrates grown on undulant-Si substrates were supplied by HOYA Advanced Semiconductor Technologies Corporation. The 3C-SiC substrates were polished to remove roughness of the surface prior to the homo-epitaxial growth. After sacrificial oxidation, homo-epitaxial 3C-SiC layers were grown at 1600 °C using silane and propane gases as precursors, and hydrogen as a carrier gas. Tri-methyl-aluminum (TMA) was used as Al-dopant. The net acceptor concentration of the homo-epitaxial layers is $1x10^{16}$ /cm^3. For source and drain region, three-fold phosphorus (P) implantation (140, 90 and 60 keV) was performed at 800 °C. The mean P concentration of implanted regions is $5x10^{19}$ /cm^3. The samples were annealed at 1650 °C for 3 min in Ar after implantation. The gate oxide (27 nm thick) of the MOSFETs was formed using pyrogenic oxidation (H_2:O_2 = 1:1) at 1100 °C for 20 min. No post-oxidation annealing to gate oxide was carried out in this study. Al electrodes (70 nm) were formed using lift-off technique. The gate length and width of MOSFETs are 10 μm and

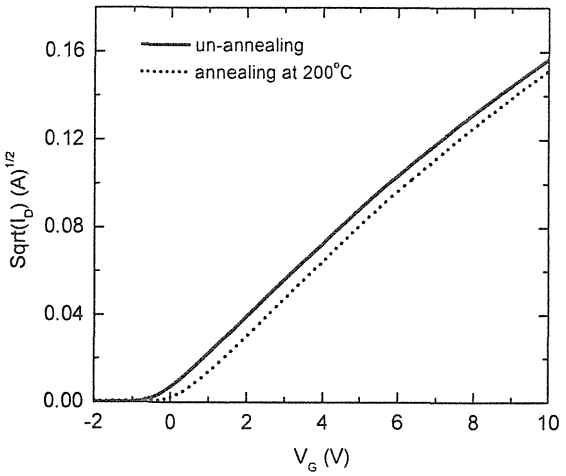

Fig. 1 Drain current (I_D) - gate voltage (V_G) characteristics at a drain voltage (V_D) of 10V for un-annealed (solid line) and annealed (broken line) 3C-SiC MOSFETs.

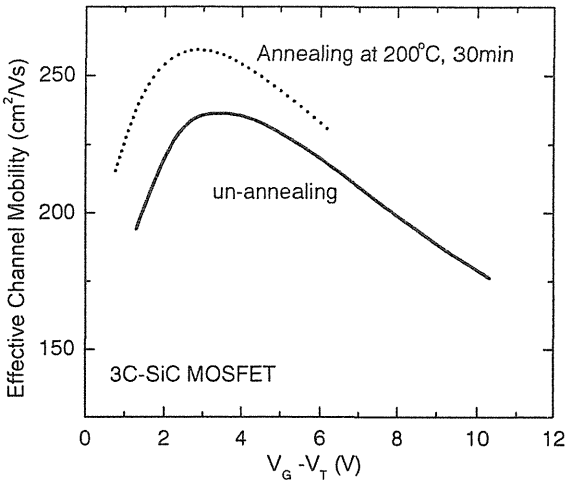

Fig. 2 Effective channel mobility (μ) for un-annealed (solid line) and annealed (broken line) 3C-SiC MOSFET as a function of V_G-V_T.

200 μm, respectively. The direction of current in inversion layer is designed to be perpendicular to [-110] direction. Some samples were annealed at 200 °C in Ar for 30 min. The electrical characteristics were measured at RT in a shielded box.

3. Results and discussion

Figure 1 shows the drain current (I_D) - gate voltage (V_G) characteristics at a drain voltage (V_D) of 10V for un-annealed (solid line) and annealed (broken line) 3C-SiC MOSFETs. The value of I_D for 3C-SiC MOSFETs is of the order of 10^{-8} A at a gate voltage (V_G) of –2 V. For the threshold volatge (V_T), the value for un-annealed 3C-SiC MOSFETs is –0.5 V despite the fabrication design was for enhancement type. By annealing at 200 °C in Ar, V_T for becomes 0.23 V, which indicates that the MOSFETs exhibit the enhancement-type behavior. Because positive oxide-trapped-charge and/or acceptor-like interface traps shift V_T to negative voltages, the result obtained in this study suggests that oxide-trapped -charge or/and interface traps decrease by the annealing.

Figure 2 shows the effective channel mobility (μ), which was estimated from the linear region of I_D–V_D curves, for un-annealed (solid line) and annealed (broken line) 3C-SiC MOSFET as a function of V_G-V_T. The value of μ increases with increasing V_G-V_T, and the μ peaks around 3 V. The peak value for MOSFETs before annealing is 230 cm^2/Vs. The values of μ obtained in this study are higher than values reported for MOSFETs fabricated on hetero-epitaxial 3C-SiC layers[3, 4]. Since the electrical characteristics of MOSFETs depend on the quality of epitaxial layers, the result obtained in this study suggests that the one of the reasons of the improvement of the channel mobility is due to high quality 3C-SiC homo-epitaxial layers grown at high temperature. By annealing at 200 °C, the peak value of channel mobility becomes 260 cm^2/Vs. This result can be attributed to the decrease in interface traps by annealing because interface traps act as scattering centers for

carriers in the inversion channel. However, some MOSFETs on the same chip do not show the improvement of the channel mobility by annealing, and as a result, the average value of effective channel mobility is 234 cm^2/Vs. From this study, we cannot conclude that annealing at 200 °C for 30 min in Ar is effective for the improvement of the channel mobility or not. Further investigations are necessary to clarify the effects of post-oxidation annealing on the channel mobility.

4. Summary

N-channel MOSFETs were fabricated on p-type 3C-SiC homo-epitaxial layers grown on 3C-SiC substrates. The drain current for 3C-SiC MOSFETs is in the order of 10^{-8} A at a drain voltage of 10V and a gate voltage of –2V. The values of channel mobility are 230 and 234 cm^2/Vs for un-annealed and annealed MOSFETs, respectively.

Acknowledgements

The authors would like to thank Dr. Nagasawa at HOYA Advanced Semiconductor Technologies Corporation for providing 3C-SiC substrates. And also, the authors are very thankful to Y. Ishida, K. Kojima, Y. Tanaka, T. Takahashi, H. Okumura and K. Arai (National Institute of Advanced Industrial Science and Technology) for the epilayer growth using chemical vapour deposition.

References

1) R. Schorner, P. Friedrichs and D. Peters: IEEE Trans. Electron Devices **46** (1999) p533.
2) F. Ciobanu, G. Pensl, H. Nagasawa, A. Schoner, S. Dimitrijev, K.–Y. Cheong, V.V. Afanas'ev and G. Wagner: Mater. Sci. Forum **433-436** (2003) p.551.
3) J. W. Palmour, H. S. Kong, and R. F. Davis: J. Appl. Phys. **64** (1988) p.2168.
4) J. Wan, M. A. Capano, M. R. Melloch and J. A. Cooper, Jr.: IEEE Electron Device Lett. **23** (2002) p.482.
5) H. Nagasawa, T. Kawahara and K. Yagi: Mater. Sci. Forum **389-393** (2002) p.319.
6) Y. Ishida, M. Kushibe, T. Takahashi, H. Okumura and S. Yoshida: Mater. Sci. Forum **389-393** (2002) p.275.

1.10 Al Composition Dependence of Luminescence Properties of Eu Implanted $Al_xGa_{1-x}N$ ($0 \leqq x \leqq 1$)

Y. Nakanishi*, A. Wakahara*, H. Okada*, A. Yoshida*, T. Ohshima** and T. Kamiya**

Department of Electrical and Electronic Engineering, Toyohashi University of Technology *

Department of Material Development, JAERI **

1. Introduction

Rare earth ions (REIs)-doped solid devices have been developed to apply for optically pumped optical sources and amplifiers in optical communication systems because 4f-4f intra-transitions of REIs in solids have sharp emission lines, and the peak positions are not affected by temperature.[1] Recently, REIs doped nitrides have been also investigated because GaN and other nitride alloys are one of the wide bandgap semiconductors, so that they can allow a transition in visible region. Visible electroluminescent devices based on nitrides have been reported,[2-4] however, to achieve high efficient light emitting devices such as light emitting diodes and laser diodes, it is necessary to study the luminescence mechanism in detail and to develop methods for the improvements of the luminescence efficiency.

Recently, we have investigated the photoluminescence (PL) properties of Eu-implanted $Al_xGa_{1-x}N$ (with x=0.0-0.1), and have found that the PL intensity of Eu^{3+}-related $^5D_0$-$^7F_2$ transition increased with increasing the Al composition.[5] This result suggests that it is possible to improve the emission efficiency by introducing the REIs into AlGaN. In this study, we investigate Eu^{3+}-related luminescence properties doped into $Al_xGa_{1-x}N$ with whole Al content by using ion implantation.

2. Experiments

$Al_xGa_{1-x}N$ ($0 \leqq x \leqq 1$) epitaxial layers were grown on sapphire (0001) substrate by organometallic vapor phase epitaxy at 1100°C in 76 Torr. The full width at half maximum (FWHM) of X-ray rocking curve at (0004) was approximately 250-400 arcsec. The ion implantation was carried out at room temperature (RT) with 200 keV using ion-implanter at TIARA. Ion dose was 10^{15} cm^{-2}. The projection range and peak concentration were calculated to be approximately 100 nm and $3x10^{20}$ cm^{-3} by TRIM, respectively. After the implantation, to remove implantation-induced damages and optically activate incorporated impurities, the implanted samples were annealed by rapid thermal annealing for 60 sec in the temperature range from 1000 to 1600°C in N_2 ambient at atmospheric pressure. The crystalline quality was evaluated by reflection high energy electron diffraction and X-ray diffraction. The luminescence properties were measured by PL and cathodeluminescence (CL) measurements. The PL measurement was done in the temperature range from 14 K to RT using He-Cd laser as the excitation light source with the power density of approximately 3 mW/cm^2. In CL measurements, the acceleration energy and electric current density of electron beam were 20 keV and 150 mA/cm^2, respectively.

3. Results and discussion

Figure 1 shows CL spectra of Eu doped $Al_{0.4}Ga_{0.6}N$ and undoped GaN at RT. The annealing temperature for Eu-doped $Al_{0.4}Ga_{0.6}N$ is 1400°C. Strong and sharp red emission peaks attributed to the 4f-4f intra transitions of Eu^{3+}

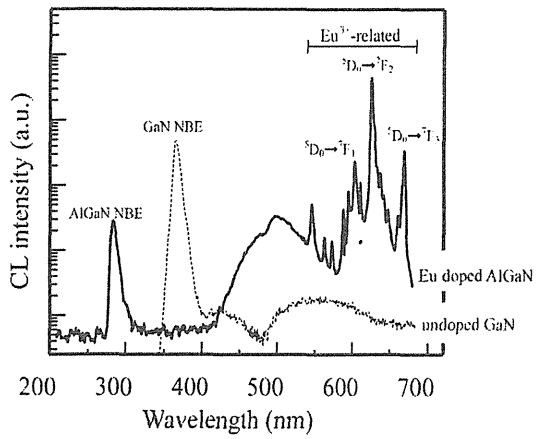

Fig.1 CL spectrum for Eu-doped $Al_{0.4}Ga_{0.6}N$ at RT. Dashed line is the spectrum for undoped GaN as a reference.

ions are observed around 600-660 nm, and the strongest emission at 621 nm is assigned as a transition from $^5D_0$ to $^7F_2$ of Eu^{3+} ion. The CL intensity of $^5D_0$-$^7F_2$ transition for Eu-doped $Al_{0.4}Ga_{0.6}N$ is several-times stronger than near-band-edge emission of undoped GaN.

The emission properties of $^5D_0$-$^7F_2$ transition of Eu-doped AlGaN depend on the Al composition. Figure 2 summarizes the dependence of CL intensity, FWHM of line width and peak energy attributed to $^5D_0$ to $^7F_2$ as a function of Al composition in AlGaN. As the Al composition increase, the CL intensity and the line width increase and wide compared with that of Eu doped GaN, respectively. The CL intensity of Eu-doped AlGaN at an Al composition of x=0.5 is 100 times stronger than that of Eu-doped GaN. The CL peak in Eu-doped AlGaN showed peak at Al composition of x=0.5. The FWHM also showed peak as a function of Al composition and showed peak around x=0.5, as shown in Fig.2 The peak energy shifts from 1.987 eV for GaN to 1.979 eV for AlN. These results indicate that the luminescence capability of Eu^{3+} can be improved by introducing AlGaN alloy.

Figure 3 shows the temperature dependence of PL intensity and decay time related $^5D_0$-$^7F_2$ transition for Eu-doped $Al_{0.1}Ga_{0.9}N$ and GaN. Both samples showed no explicit temperature quenching in the range of 14-300 K. On the other hand, the PL intensity of band-edge emission of undoped GaN at 300 K decreases to about 3% for the luminescence at 14 K.

The PL properties of Er-doped Si and/or GaAs were reported that the luminescence intensity and the decay time of 4f-4f intra transition in REIs were thermally quenched by the energy reverse transfer process from REIs to host materials.[6,7] The small thermal quenching of 4f-4f intra transition in Eu^{3+} obtained in this study indicates that the energy back transfer from Eu^{3+} to host materials (AlGaN) is negligible, and the emission from REIs in AlGaN is suitable for application.

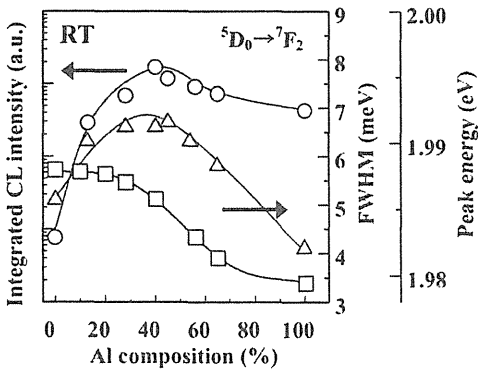

Fig.2 Dependence of CL intensity(○), FWHM of line width(△) and peak energy(□) related $^5D_0 \rightarrow {}^7F_2$ transision as a function of Al composition.

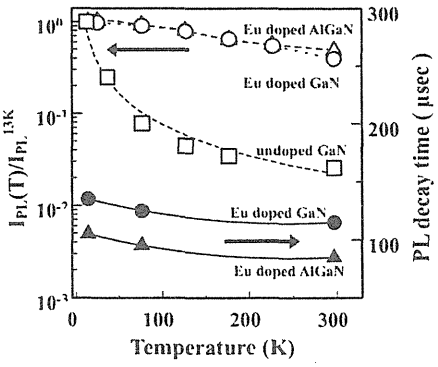

Fig.3 Temperature dependence of PL intensity and decay time related to $^5D_0 \rightarrow {}^7F_2$ transition. For comparison, temperature dependence of PL intensity of band-edge emission of undoped GaN is alsow shown.

The improvement of luminescence capability related to Eu^{3+} ions by introducing Al in GaN can be interpreted in terms of following two reasons. Firstly, the transition probability of Eu^{3+} increases by the collapse of the local symmetry around Eu^{3+} due to introducing Al in GaN. Secondly, the ion implantation-induced damage decreases with increasing Al contents. Details of the discussion on this point are given in Ref.8. Although we cannot distinguish two effects (the increase in the transition probability and the decrease in crystal damage), it can be concluded that the Eu^{3+}-related luminescence properties are improved by the combination between two effects.

Recently, we have investigated the luminescence properties of Tb doped AlGaN.[9] Sharp and strong luminescence Tb-related to 4f-4f transition of Tb^{3+} was observed, and its intensity increased with Al contents, as shown in Fig.4. The results suggest that the improvement of the luminescence capability in REIs-doped materials is expected by using AlGaN as a host material.

4. Conclusion

We investigated the effect of Al composition on luminescence properties of Eu in $Al_xGa_{1-x}N$ ($0 \leqq x \leqq 1$). Strong red emission at 621 nm, corresponding to the 4f-4f transition from $^5D_0$ to $^7F_2$ states of Eu^{3+} in AlGaN, is observed at room temperature in all Al composition. The integrated CL intensity of $^5D_0$-$^7F_2$ transition of Eu-related luminescence becomes the strongest value in the case of Al=50%. The value is 100-times stronger than that for Eu-doped GaN. Furthermore, the intensity of $^5D_0$-$^7F_2$ transition of Eu^{3+} in $Al_{0.5}Ga_{0.5}N$ is several-fold stronger than that of near-band-edge emission of undoped GaN. These results suggest that the transition capability of Eu^{3+} is improved by introducing Al in GaN as a host material.

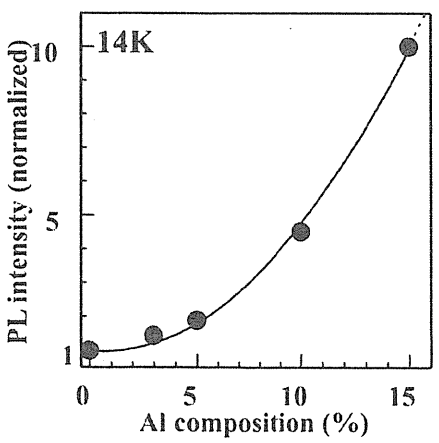

Fig.4 PL intensity related to Tb^{3+} emission as a function of Al contensts in AlGaN.

Acknowledgements

This work was partially supported in the 21st Century COE Program, "Intelligent Human Sensing" from the Ministry of Education, Culture, Sports, Science and Technology, Japan.

References

1) M.J.Weber, Phys. Rev. 171, 283 (1968).
2) A.J.Steckl, M.Garter, D.S.Lee, J.Heikenfeld, and R.Birkhahn, Appl. Phys. Lett. 75, 2184 (1999).
3) M.Garter, J.Scofield, R.Birkhahn, and A.J.Steckl, Appl. Phys. Lett. 74, 182 (1999).
4) J. Heikenfeld, M. Garter, D. S. Lee, R. Birkhahn, and A. J. Steckl, Appl. Phys. Lett. 75, 1189 (1999).
5) Y.Nakanishi, A.Wakahara, H.Okada, A.Yoshida, T.Ohshima, and H.Itoh, phys. stat. sol. (c) 0, No. 1, 461 (2002).
6) A. Taguchi and K. Takahei, J. Appl. Phys. 83, 2800 (1998).
7) K.Takahei, A.Taguchi, and R.A.Hogg, J. Appl. Phys. 82, 3997 (1997).
8) Y.Nakanishi, A.Wakahara, H.Okada, A.Yoshida, T.Ohshima, H.Itoh, T.Shibata, and M.Tanaka, phys. stat. sol. (c) 0, 2623 (2003).
9) Y.Nakanishi, A.Wakahara, H.Okada, A.Yoshida, T.Ohshima, and H.Itoh, phys. stat. sol. (b) 0, 240 (2003).

This is a blank page.

2. Biotechnology

2.1 Ion Microbeam System for Irradiating Single Plant Cells

Y. Yokota*, S. Yamada*, T. Funayama**, Y. Kobayashi**, T. Sakashita**,
S. Wada**, Y. Hase**, A. Tanaka** and M. Inoue*
Laboratory of Plant Breeding Science, Graduate School of Agriculture,
Kyoto Prefectural University*,
Department of Ion-beam-applied Biology, JAERI**

1. Introduction

It is almost established that ion beam using the 'broad field' irradiation-system can induce a novel mutation in plants at higher rate than other mutagens [1), 2)]. However, the 'broad field' irradiation-system distributes ions to targets at random, and thus, the interpretation of results obtained at low dose is unclear. Ion microbeam irradiation is considered as an ideal approach to settle this problem [3)]. In this paper, we reported the ion microbeam system developed for irradiating tobacco BY-2 protoplasts as a model of single plant cells and demonstrated some data on the survival of protoplasts irradiated with the system.

2. Experimental procedure

Sample preparation

An irradiation vessel was designed to irradiate single plant cells (Fig. 1). A hole with a diameter of 12 mm was opened at the center of a 35-mmϕ plastic dish (IWAKI 3911-035), since the ions must pass through the sample and reach a scintillator-photomultiplier assembly (PMT) on the bottom. To distinguish whether the ions hit the protoplasts or not, a sheet of Harzlas TNF-1 ion track detector (100 μm thick) was stuck over the hole. Since the Harzlas TNF-1 was highly toxic to tobacco protoplasts, a sheet of sterilized Kapton film (30 μm thick) was put on the dish to separate protoplasts from the detector sheet. Then, a sterilized polycarbonate ring was pushed into the dish over the Kapton film. As a result, protoplasts could proliferate in the vessel.

Protoplasts were isolated from the tobacco BY-2 cell line as previously reported [4)]. Since protoplasts must be fixed at their positions for the irradiation and subsequent observation, isolated protoplasts were suspended in the LS-modified medium containing 0.8% Seaplaque agarose. A total of 32.4 μl of the suspension was immediately dropped on the Kapton film of the irradiation vessel, and spread out under a sheet of cover glass (324 mm^2 area and 150 μm thick) (Fig. 1). By this procedure, protoplasts were fixed at their positions in the solid medium with a thickness of 100 μm. The mean LET of the carbon ion microbeam in the protoplast position was calculated to be 121 keV/μm using the ELOSS M computer program (Tanaka et al. 1997).

Ion microbeam irradiation

The main properties of the ion microbeam-irradiation system in JAERI were previously described [5), 6)]. For the irradiation and subsequent observation of

tobacco protoplasts, the x-y position of individual protoplast plated on the dish was recorded using an 'auto stage system' on an inverted optical microscope. Carbon ions with energy of 220 MeV were collimated by a tantalum micro-aperture with a 20-μmϕ and irradiated vertically downward to the protoplast positions (Fig. 1). Carbon ions passed through the sample were counted by PMT. When a programmed number of carbon ions were counted, carbon ion microbeam was shut off using a beam chopper.

Determination of ion hit positions

Just prior to the irradiation, images of protoplasts (Fig. 2A) and landmarks (Fig. 2B) on the rear surface of the Harzlas TNF-1 sheet, that were made by pre-irradiation and alkali etching, were recorded, and both images were superimposed on a computer (Fig. 2C). After the irradiation, the rear surface of the Harzlas TNF-1 sheet was etched by 13.4M KOH solution at 27°C for 9 h. Images of protoplasts (Fig. 2C) and etch pits (Fig. 2D) were superimposed on a computer based on the landmarks (Fig. 2E), and the ion hit positions in the protoplasts were determined on the basis of the superimposed images obtained finally.

3. Results and Discussion

The hit rate of the ions was defined as the number of ions that hit the protoplast / the number of ions counted by PMT. Fig. 3 shows the hit rates in four experiments, using auto stages made by Auto Scan Systems Pty. Ltd. (Experiments 1 and 2) and Sigma Koki Co. Ltd. (Experiments 3 and 4). Mean hit rates in Experiment 1, 2, 3 and 4 were 56.5, 61.9, 64.2 and 55.6%, respectively. There was no significant differece in the mean hit rate between the Experiments 1 and 2 and 3 and 4.

A preliminary result on the colony formation rate in tobacco protoplasts irradiated with carbon ion microbeam was shown in Fig. 4. Irradiation of 1 to 7 carbon ions per protoplast seems to have no effect on the colony formation of tobacco protoplasts.

Conclusively, the maximum hit rate obtained under the present situations was about 60%. It is necessary to increase the hit rate for analyzing exact biological effects of ion microbeam.

References

1) Shikazono, N., A. Tanaka, H. Watanabe and S. Tano (2001) Genetics **157**, 379-387
2) Shikazono, N., Y. Yokota, S. Kitamura, C. Suzuki, H. Watanabe, S. Tano and A. Tanaka (2003) Genetics **163**, 1449-1455
3) Michael, B. D., M. Folkard and K. M. Prise (1994) Int. J. Radiat. Biol. **65**, 503-508
4) Yokota, Y., Y. Hase, N. Shikazono, A. Tanaka and M. Inoue (2003) Int. J. Radiat. Biol. **79**, 681-685
5) Kobayashi, Y., T. Funayama, S. Wada, M. Taguchi and H. Watanabe (2003) Nucl. Instr. and Meth. in Phys. Res. B **210**, 308-311
6) Sakashita, T., Y. Yokota, S. Wada, T. Funayama and Y. Kobayashi (2004) JAERI-Tech **2004-007**
7) Tanaka, S., M. Fukuda, K. Nishimura, H. Watanabe and N. Yamano (1997) JAERI-Data/Code, **97-019**

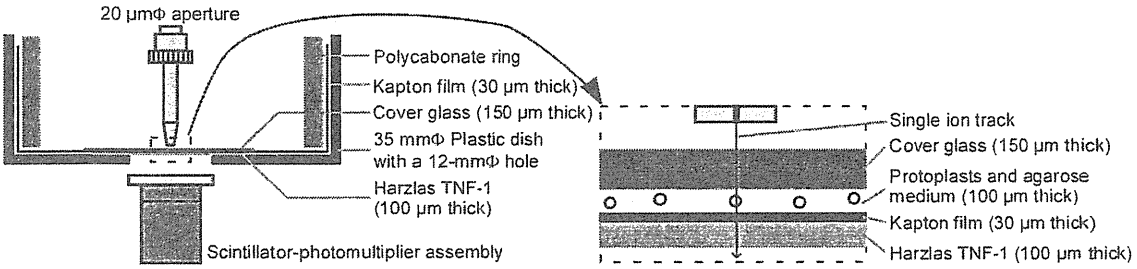

Fig. 1 Ion microbeam system for irradiating tobacco protoplasts.

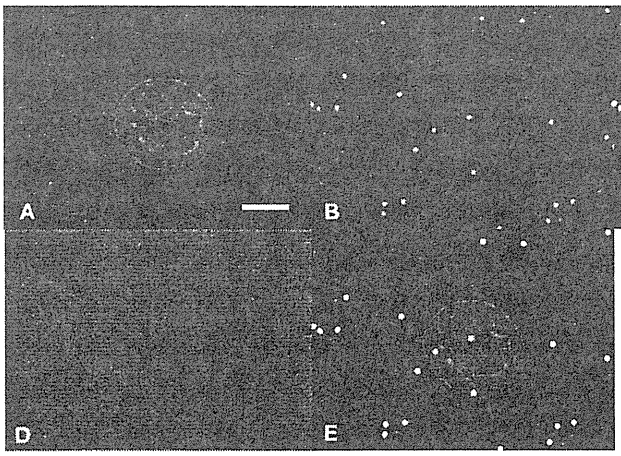

Fig. 2 Determination of ion hit positions.
A; Protoplast to be irradiated
B; Landmarks on the rear surface of HarzlasTNF-1
C; Superimposition of protoplast and landmarks (○)
D; Etch pits of ion microbeam
E; Superimposition of protoplast and etch pits (●)

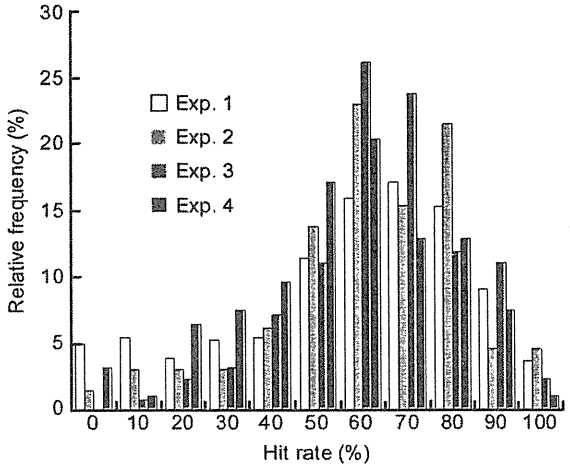

Fig. 3 Distribution of hit rates of carbon ion microbeam to tobacco protoplasts.

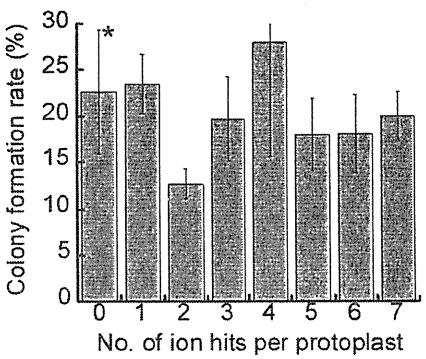

Fig. 4 Colony formation rates of tobacco protoplasts. *Mean ± SE of 3 different experiments.

2.2 Effects of Ion Beams Irradiation on Two Cultivars of Chrysanthemum(*Dendranthema grandiflorum* R.)

H. Ikegami*, K. Hirashima*, T. Suyama*, T. Kunitake*, Y. Sakai*, T. Nakahara*
Y. Hase**, N. Shikazono** and A. Tanaka**
Fukuoka Agricultural Research Center*,
Department of Ion-beam-applied Biology, JAERI**

1. Introduction

Radiation mutagenesis is one of the most useful methods for plant breeding. The ion beams have been widely used and proved to be effective to induce various mutations, especially in flowers, such as chrysanthemum[1,2], carnation[3] and verbena.[4] We succeeded to produce various types of mutants by ion-beam irradiation to chrysanthemum protoplast cells[5,6]. We also reported that the radiation sensitivity was greatly different between multicellular tissue (leaf and petal) and single cell (leaf protoplast)[7].

Here, we report the character of regenerated plants from leaf cultures exposed to ion beams in two chrysanthemum cultivars.

2. Materials and methods

Chrysanthemum variety, 'Jimba' and 'Kyokushin' (white flower) were used. Leaves were collected and cultured by the method by Ueno et al[2]. Four days after preparation, the samples were exposed to $^{4}He^{2+}$ with the dose of 1 Gy (50 MeV) for Jimba and to $^{12}C^{6+}$ with the dose of 2 Gy (320 MeV) for Kyokushin. The regenerated plants were grown in the glass house at Fukuoka Prefectural Agricultural Research Center. The cultivation phenotypes were investigated after flowering.

3. Results and Discussion

One hundred fifty plants of Jimba-Ion line and 159 plants of Kyokushin-Ion line were investigated. Table. 1 shows the means of five traits of regenerated plants. In Jimba, there were significant differences between control and irradiated lines on three traits, height, the number of leaves and the date of flowering. In Kyokushin, significant differences were observed on date of flowering (DF) and flower diameter.

Jimba-Ion line had shorter plant height, but the height of Kyokushin-Ion line unchanged. However, deviations in height were increased in

Table 1. The characteristics of regenerated plants

Line	Radiation	Dose (Gy)	No. of plants	Height (cm)	No. of leaves	No. of axillary buds	Date of flowering	Flower diameter (mm)
Jimba(control)	-	0	10	131.8± 1.2	64.8±3.8	52.0± 5.7	11/ 5±0.8	14.8±0.3
Jimba-Ion	$^{4}He^{2+}$	1	150	111.5± 6.5**	58.7±5.6**	46.8± 8.8	11/ 9±7.5**	15.1±1.3
Kyokushin(control)	-	0	6	110.0± 4.2	50.7±5.0	31.7±13.6	11/ 6±3.4	14.7±0.5
Kyokushin-Ion	$^{12}C^{6+}$	2	159	110.1±10.5	54.2±5.8	25.4±14.3	11/15±3.9**	13.6±0.9**

Jimba-Ion :Ion beams irradiated'Jimba'line
Kyokushin-Ion :Ion beams irradiated 'Kyokushin'line
Planting date :July29
*and **:the difference from the control line was significant at P<0.05 and P<0.01,respectively

both lines.

Number of axillary buds widely varied in irradiated lines. We selected several mutants with lesser number of axillary buds for further screening.

The DF distributed from November 2nd to December 10th in Jimba-Ion line, while it was from November 4th to 7th for Jimba. In Kyokushin-Ion line, it distributed from November 7th to November 25th, while it was from November 4th to 13th for Kyokushin (data not shown). Generally, irradiated plants had delayed flowering time from 4 to 9 days. However, in Jimba-Ion line, there were many plants with ealier DF. These facts indicate that ion-beam irradiation is effective in expanding DF. It is interesting that the deviation of DF in Jimba-Ion line was bigger than that in Kyokushin-Ion line.

In conclusion, it is likely that combination with ion-beam irradiation and tissue cultures is effective to induce various mutations in Chrysanthemum, especially in expanding the DF.

Finally we have selected ten lines having useful characters for further secreening.

References

1) S. Nagatomi, A. Tanaka, A. Kato, H. Yamaguchi, H. Watanabe and S. Tano, TIARA Annual Report 6:41-43(1998)

2) K. Ueno, S. Nagayoshi, Y. Hase, N. Shikazono, and A. Tanaka, TIARA Annual Report 2002 52-54(2003)

3) M. Okamoto, N. Yasuno, M. Takano, A. Tanaka, N. Shikazono, Y. Hase, TIARA Annual Report 2002 50-51(2003)

4) K. Suzuki, Y. Shihou, T. Abe, Y. Katumoto, K. Miyazaki, S. Yoshida, T. Hisazumi, RIKEN Accel.Prog.Rep. 35, 129 (2002)

5) H. Ikegami, H. Murakami, K. Hirashima, T. Nakahara, Y. Hase and A. Tanaka, TIARA Annual Report2001 28-30 (2002)

6) T. Nakahara, K. Hirashima, H. Murakami, A. Tanaka, N. Shikazono, Y. Hase and H. watanabe, TIARA Annual Report 1999 31-32(2000)

7) H. Ikegami, K. Takata, H. Kai, K. Hirashima, T. Nakahara, Y. Hase N. Shikazono and A. Tanaka, TIARA Annual Report2002 40-41(2003)

2.3 Effects of Ion Beams on Shoot Regeneration of Osteospermum Leaf Cultures

M.Iizuka*, Y.Kimura*, Y.Hase** and A.Tanaka**
Gumma Agricultural Technology Center*
Department of Ion-beam-applied Biology, JAERI**

Introduction

Ion beams, which have a higher linear energy transfer (LET) than X and gamma rays, are one of efficient mutagenic agents, and applicable to mutation breeding of many horticultural crops. However, there have been few studies on the effects of ion beam irradiation on induction of mutation in vegetables and ornamental crops. The lethal dose of the $^{4}He^{2+}$ and $^{12}C^{5+}$ ion beam irradiation to strawberry, hydrangea and spiraea seed became clear [1),2),3)].

In Gumma Prefecture, Osteospermam cultivation is prosperous and its quality has obtained high evaluation. We have wild out the mutation breeding of the Osteospermam that is important pot cultures. Ion beams were irradiated to Osteospermam for the purpose of getting variation of the flower color and character. Here examined effects of ion beam irradiation on germination of Osteospermam.

Materials and Methods

Osteospermam in greenhouse were used as plant materials. Young leaves were excised, and the surface was sterilized by immersing in 70% ethyl alcohol for 1 min, followed by 1%(W/V) sodium hypochlolite solution for 15 min and then rinsed three times in distilled water. The leaf segments were cultured on modified Murashige and Skoog's (MS) medium supplemented with 0.1 mg/l NAA and 1mg/l BA. The samples covered with Kapton film were irradiated with carbon ion beam (220 MeV $^{12}C^{5+}$ and 320 MeV $^{12}C^{6+}$) at various doses (2 to 150 Gy). After irradiation the leaf segments were transferred to the fresh medium and cultured at 25 °C and 16 hr-photoperiod. Rgeneration rate was investigated after 40-50 days of culture.

Results and Discussion

When the dosage of irradiation increased, the rgeneration rates of the leaf segments decreased. At the dose of more than 10Gy in $^{12}C^{5+}$ion beams, the rgeneration rate decreased rapidly(Fig.1). And at the dose of more than 20Gy in $^{12}C^{6+}$ion beams, the rgeneration rate decreased rapidly(Fig.2).

We are performing cytological studies to investigate horticultural values of the mutants and are screening mutants of flower color variation in the growing plants.

References

1) N. Kudo et al. TIARA Ann. Rep., 16:62-64. (1998)
2) M. Iizuka et al. TIARA Ann. Rep., 2.3:30-31. (1999)
3) M. Iizuka et al. TIARA Ann. Rep., 2.7:45-46. (2001)
4) M. Iizuka et al. TIARA Ann. Rep., 2.4:42-43. (2002)

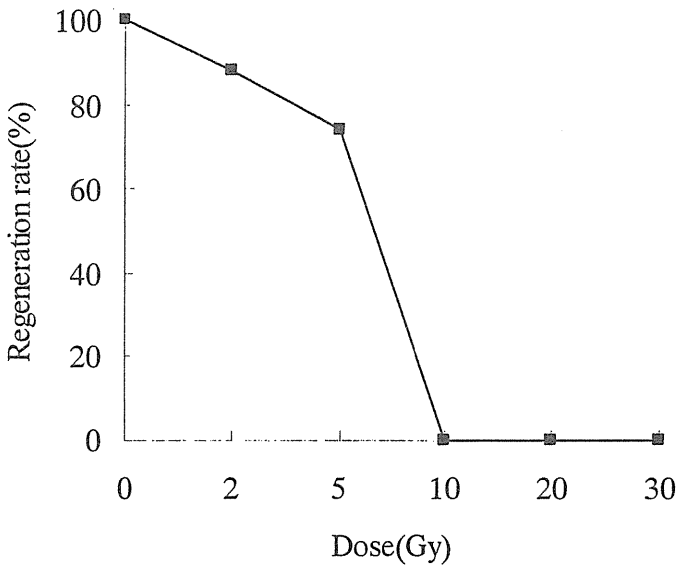

Fig.1. Effect of $^{12}C^{5+}$ ion beam on the regeneration of Osteospermam

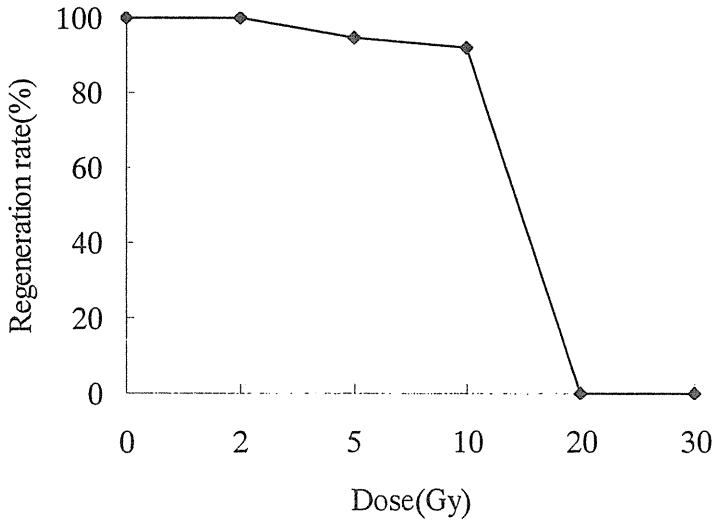

Fig.2. Effect of $^{12}C^{6+}$ ion beam on the regeneration of Osteospermam

2.4 Mutation in *FRILL1* Gene, a Sterol C24 Methyltransferase, Causes Ectopic Endoreduplication in Arabidopsis Petals

Y.Hase*, S. Fujioka**, S. Yoshida**, G. Sun*, M. Umeda*** and A. Tanaka*
Department of Ion-beam-applied Biology, JAERI*
Plant Functions Laboratory, RIKEN**
Institute of Molecular and Cellular Biosciences, Univ. of Tokyo***

1.Introduction

In a screen for mutants defective in organ development, we previously isolated and characterized the *frill1* (*frl1*) mutant that has serrated petals and sepals[1]. In the distal region of *frl1* petals, radial cell arrangement that can be seen in the wild type was disorganized. In this region, number of cells was reduced whereas both cell size and nuclei size dramatically increased. These results suggested that the *frl1* mutation affected the cell division and also caused the abnormal endoreduplication in the distal part of petals. To further investigate the function of the *FRL1* gene, we aimed to clone the gene by a map-based approach. Here, we report that the *FRL1* is identical to *STEROL METHYLTRANSFERASE 2* (*SMT2*), which is involved in phytosterol biosynthesis.

2.Experimental procedure

Mapping and complementation test. The *frl1* was mapped using CAPS markers. About 400 F_2 mutant plants that were obtained from a cross of *frl1* and the Ler ecotype were used. In order to complement the *frl1* mutant, a 6.3 kb *Bam*HI-*Eco*RI genomic fragment containing the *SMT2* gene was exciced from the insert of BAC clone F14O10. Transformation was done by the infiltration method.

Analysis of endogenous sterols. Inflorescence (400-600 mg fresh weight) were collected from *frl1* and wild-type plants that were just starting to flower. Sterols were analyzed as described by Noguchi *et al.*[2].

Flowcytometry. Petal tips were collected from several fully-opened flowers. Ploidy level was measured using a PAS flow cytometer (Partec). The lowest peak was assumed to be 2C nuclei (C is a haploid DNA content). For each run, more than 3,000 nuclei were analyzed.

Microscopy. To observe the size of nuclei, collected petals were cleared in 70% ethanol and dyed in 1 μg/ml DAPI solution.

3.Results and Discussion

The *frl1* mutant was originally isolated as a morphological mutant having serrated petals and sepals (Fig.1a). The gross morphology and size of *frl1* plants are similar to those of the wild type. The *frl1* locus was closely linked to the CAT3 marker (29.91 cM) on chromosome 1. Finally, *frl1* was mapped to the 105-kb region that spans three BAC clones. Sequencing of this region revealed a single base deletion in the F14O10.7 gene that encodes SMT2. The *frl1* mutant was completely restored by the transformation with genomic *SMT2* fragment (Fig.1b). The *frl1* gene has a single base deletion

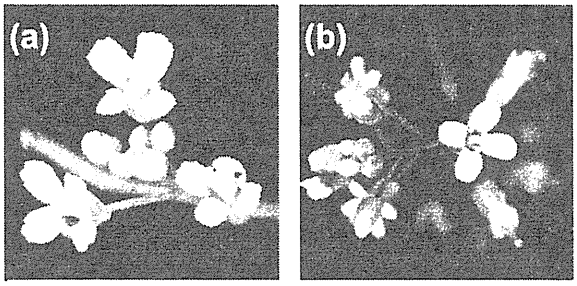

Fig.1 Serrated petals and sepals of *frl1* mutant is due to the mutation in *SMT2*. (a) Overview of inflorescence of *frl1*. (b) *frl1* plant transformed with genomic *SMT2* fragment.

in the middle of the coding region (Fig.2). This results in the aberrant translation of 44 amino acids before the new stop codon at the 218th amino acid. Three motifs conserved in SMT proteins are lost as a result of the mutation.

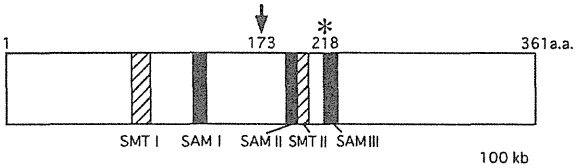

Fig.2 Mutation found in *SMT2* locus of *frl1* mutant. SMT2 has a single ORF with no intron. One base deletion (arrow) results in aberrant translation of 44 amino acids and a new stop codon (asterisk). Hatched boxes are conserved motifs for C-24 SMTs and blackened boxes are conserved motifs for S-adenosylmethionine-dependent methyltransferases.

Sterols are membrane components and have a role in regulating membrane fluidity and permeability[3]. They also serve as a precursor for brassinosteroids (BRs), which has been extensively studied as growth-promoting plant steroid hormones. The majority of sterols in higher plants are alkylated at carbon 24. This alkylation is performed by two classes of *S*-adenosyl-methionine-dependent C-24 SMTs.[3]. Arabidopsis has three SMT genes (*SMT1*, *SMT2* and *SMT3*). The protein encoded by *SMT1* catalyses the first methylation step, and SMT2 and SMT3 work together in the second methyl-addition step.

Endogenous sterol levels were measured in inflorescences of *frl1* and wild type. The sterol biosynthetic pathway in Arabidopsis divides into two branches at the position of *SMT2* activity. One branch produces C24-methyl sterols, such as campesterol as major end products. The other branch produces C24-ethyl sterols, such as sitosterol or stigmasterol. Sitosterol is the most abundant sterol in plants and is an important structural molecule that regulates membrane characteristics[3),5)]. In the *frl1* mutant, the amounts of C24-ethyl sterols were between 20% and 38% of the amounts in the wild type, whereas the amount of C24-methyl sterols were more than 4 times higher than the amounts in the wild type (Table 1). These results show that the direction of biosynthetic flow is changed by mutation of *SMT2*.

Table 1 Altered sterol composition in *smt2^{frl1}* plants

Sterol	Wild type	*smt2^{frl1}*
Cycloartenol	1.2	0.8
24-methylene cycloartenol	0.2	0.3
cycloeucalenol	0.1	0.1
24-methylene lophenol	0.2	1.5
24-methylene cholesterol	3.5	15.8
campesterol	10.4	43.3
24-ethylidene lophenol	0.5	0.1
isofucosterol	9.1	2.2
sitosterol	65.0	25.0
stigmasterol	3.3	1.0

Values are endogenous levels of each sterol shown as a percentage of total sterols. Total sterol contents were 187.7 μg g^{-1} fresh weight in the wild type and 240.0 μg g^{-1} fresh weight in *smt2^{frl1}*.

We found that the nuclei in the distal part of *frl1* petals are larger and of various sizes (Fig.3a) in contrast to nuclei of uniform size in the equivalent part of wild-type petals (Fig.3b). A similar difference was observed at the borders of sepals (data not shown). Therefore, unusual endoreduplication is suggested to be the cause of the marginal serration. We carried out flow cytometric analysis in petal tips and rosette leaves. Almost all of the nuclei were at the 2C level in the wild-type petals, indicating no evidence of endoreduplication in petal tips (Fig.4a). Whereas 4C peak was obvious in the

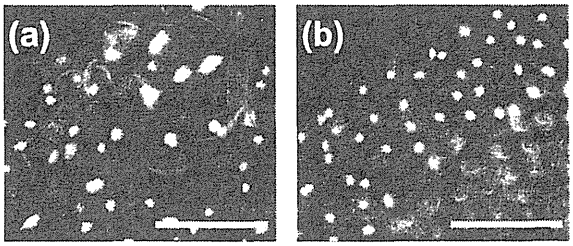

Fig.3 Comparison of nuclei size in petal margin. (a) *frl1* petals, (b) wild-type petals. Scale bars are equivalent to 50 μm.

frl1 petals. In rosette leaves, both wild type and *frl1* showed polyploidy up to 32C, but *frl1* had higher percentage of 16C and 32C nuclei (Fig.4b). These results show that the *frl1* mutation causes ectopic endoreduplication in petal tips and also enhances endoreduplication level in rosette leaves.

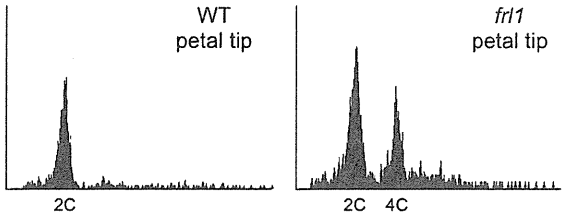

Fig.4 Flow cytometric analysis of nuclear DNA content in petal tips. Data are shown on a semilogarithmic scale. C is a haploid DNA content.

The phenotype of the *frl1* mutant suggested that the *FRL1* is a petal- and sepal-specific gene. However, to our surprise, the *FRL1* was identical to the *SMT2*, which is broadly expressed throughout the plant. The *frl1* mutation resulted in the accumulation of 24-methyl sterols at the expense of 24-ethyl sterols. This alteration of sterol profile is in good agreement with the position of SMT2 in the biosynthetic pathway. A question to be addressed is how the mutation in *SMT2* results in serrated petals and sepals. Because the sterol alteration is seen all over the *frl1* plant, petals and sepals are thought to be the most sensitive organs for the altered sterol profile found in the *frl1* mutant. The flow cytometric analysis revealed an unusual polyploidization in the distal part of petals, in which the endoreduplication does not normally occur. The rosette leaves also showed increased endoreduplication level. These results show that normal sterol profile is necessary not only to regulate the endoreduplication level but also to regulate the transition from mitotic cycle to endocycle. The rosette leaves of *frl1* do not show apparent morphological changes. This suggests that the rosette leaves have plasticity that can adaptively regulate morphogenesis in response to the enhanced endoreduplication level. However, the petals of *frl1* can not, probably because the petal tip does not naturally endoreduplicate and it has regular cell arrangement. Suppression of endoreduplication is thought to be important for petal morphogenesis. There should be some factors that suppress endoreduplication in the distal part of petals and the border of sepals. These factors could be affected by the altered membrane properties or a shortage of some sterol-derived substances, although the mechanism is unknown. The *frl1* mutant provides a useful tissue to investigate the molecular mechanism of endoreduplication.

References

1) Y. Hase, A. Tanaka, T. Baba and H. Watanabe, Plant Journal 24 (2000) 21-32.
2) T. Noguchi, S. Fujioka, S.Choe, S. Takatsuto, F. E. Tax, S. Yoshida and K. A. Feldmann, Plant Physiology 124 (2000) 201-209.
3) M.-A. Hartmann, Trends in Plant Science 3 (1998) 170-175.
4) P. Bouvier-Náve, T. Husselstein and P. Benveniste, European Journal of Biochemistry 256 (1998) 88-96.
5) I. Schuler, A. Milon Y. Nakatani, G. Ourisson, A. M. Albrecht, P. Benveniste and M. A. Hartman, Proceedings of National Academy of Sciences of USA 88 (1991) 6926-6930.

2.5 Mutation Induction in Orchids using Ion Beam

Mohd Nazir, B.*, Sakinah, A.*, Affrida, A. H.*, Zaiton, A.*, A. Tanaka**, N. Shikazono**, Y. Oono** and Y. Hase**
Agrotechnology and Biosciences Division, Malaysian Institute for Nuclear Technology Research (MINT)*,
Department of Ion-beam-applied Biology, JAERI**

1. Introduction

Mutation induction by ionising irradiation provides an alternative for the improvement of orchids when hybridization between species or genera proved difficult. The sensitivity of orchid protocorms towards irradiation treatments was shown to be affected by the age of protocorms and differences in ploidy levels of different species or hybrids[1]. However, irradiation on protocorms of *Dendrobium* Ekapol and *Dendrobium* Sonia has resulted in changes of flower pigmentation and flower size. The colour variations were observed in the flower petals, sepals, lips and the column. In addition, morphological variations were also observed in the flower arrangement and branching of the sprays, characteristics of the flower stalks, and flower forms[2),3)].

While acute gamma irradiation has proved useful and reasonably effective for mutation induction in orchids, the use of high LET radiation such as ion beam might be more effective in producing novel and stable mutants. Ion beam results predominantly in single or double strands DNA breaks. Thus, large DNA alteration such as inversion, translocation and large deletion are produced. Studies at JAERI has shown that ion beam induces mutation at high frequency, shows broad mutation spectrum and produce novel mutants that are not produced by other mutagens including gamma rays.

In this study, experiments were carried out to determine the optimal dose for mutation induction in orchids using ion beam.

2. Experimental procedure

2.1 Plant material

Dendrobium mirbelliannum is chosen for this study. It is easy to grow, robust and produces long spray (up to 45 cm) with up to 30 flowers. It has good flowering habit and the flowers last for about 4 weeks but cannot be used for cut flower. There are many other characteristics that can be improved to make this species more commercially valuable.

This species is propagated and maintained in the shadehouses at MINT under 30% shade provided by plastic netting. Mature seeds were collected from self-pollinated flowers. The seed capsules were surface sterilized by dipping them in ethanol followed by flaming. They were cut open with sterile tools and the seeds were germinated on half-strength Murashige and Skoog (1/2x MS) medium at 26°C with 12h photoperiod until protocorms were formed.

2.2 Ion beam irradiation

Protocorms of uniform in size were transferred into sterile 6.0 cm Petri dish, covered with sterile Kapton film of 0.8 μm in thickness and sealed with Nescofilm. The protocorms were irradiated with 220 MeV $^{12}C^{5+}$ ion beam at JAERI, Takasaki at doses 0, 0.2, 0.4, 0.8, 1.0, 2.0, 4.0, 6.0, 8.0, 10, 12, 15, 20, 30 and 50 Gy.

Two to three days after irradiation clump of protocorms were transferred onto fresh 1/2x MS medium and allowed to proliferate. Subsequently the protocorm clumps were subcultured onto fresh medium every four weeks.

3. Results and Discussion

The growth of the protocorm clumps was determined by the number of protocorms and the size of the clumps. After 1.5 months the number of growing and surviving protocorm clumps were noted and grouped into clumps consisting of less than 5 protocorms, between 5 and 10 protocorms and clumps consisting of more than 10 protocorms (Table 1). There was no clear correlation trend between the increasing dose of irradiation and the protocorm growth. Growth was inhibited initially at 0.2 Gy but more clumps were observed to grow at higher doses of 0.4 to 2.0 Gy. The growth of protocorms was reduced again at doses higher than 4.0 Gy. Doses higher than 15 Gy totally inhibited growth. The difficulty in estimating the effective irradiation dose for mutation induction based on the survival or growth of the protocorms could be due to factors such as contaminations of the protocorm cultures and sensitivity of the young protocorms to tissue culture manipulations during pre and post irradiation subculturing procedures.

These protocorms were then allowed to regenerate into shoots on the same medium. The number of regenerated shoots that were more than 1.0 cm in height and have at least two leaves were recorded after two subcultures (Table 2).

In general, the percentage of the regenerated shoots per protocorm clump was decreasing at doses higher than 0.4 Gy. At doses 6.0 Gy and 10.0 Gy the percentage was 30% and 50% respectively (Table 2). However, it should be noted that the total number of regenerated shoots is small.

The data does not show any particular correlation between the number of regenerated shoots and irradiation dose. This could have been because the data was taken after two subcultures (3 months after culture initiation). Thus, the number of shoots regenerated may not have originated from the small number of initially surviving protocorms after the irradiation treatments but also from protocorms that have multiplied after two subculturing stages. Therefore, the regenerated shoots are mixed population of several vegetative generations.

The experiment was repeated using protocorms that had been precultured in the 6.0 cm Petri plates for 1 week to allow the

Dose(Gy)	% surviving clumps with number of protocorms per clump		
	<5	5 to 10	>10
0.0	0.25	0	0.75
0.2	0.6	0	0.13
0.4	3	1.43	1
0.8	1.87	1.06	0.83
1.0	1.41	0.47	0.71
2.0	3.89	1.22	3
4.0	0.89	0.33	0.22
6.0	0.66	0.26	0.66
8.0	0.31	0	0.16
10.0	0.48	0.24	1.09
12.0	0.45	0.11	0.45
15.0	0	0	0
20.0	0.14	0	0
30.0	0	0	0
50.0	0.12	0	0

Table 1: Number of growing and surviving protocorm clumps (after 1.5 months)

Doses (Gy)	Total clumps	Number of growing clumps (%)	Number of regenerated shoots (> 1 cm length)	Percentage of regenerated shoots per growing clumps
0	65	53 (81.5)	13	24.5
0.2	12	7(58.3)	0	0
0.4	76	39(51.3)	13	33.33
0.8	118	67(56.8)	16	23.9
1.0	50	36(72)	5	13.9
2.0	226	132(58.4)	20	15.2
4.0	41	5(12.2)	0	0
6.0	33	10(30.3)	3	30
8.0	8	5(62.5)	0	0
10.0	14	2(14.3)	1	50
12.0	24	11(45.8)	1	9.1

Table 2: Number of regenerated shoots (after 3 months)

protocorms to stabilize under the culture conditions. Only vigorously growing and non-contaminated cultures were irradiated. Irradiated protocorms were transferred onto pre-weighed Petri plate containing the growing medium. A total of 100 protocorm clumps of about the same size were plated in each plate. The number of shoots regenerated from the protocorm clumps after 8 weeks of culture was then taken to determine the effective irradiation dose. It was assumed that at 8th week these shoots were regenerated only from the small number of surviving protocorms after the irradiation treatments. Thus it should reflect irradiation effects on the protocorms. Figure 1 shows a decreasing percentage of regenerated shoots as irradiation dose increased, except for doses 2.0 Gy and 8.0 Gy which show 47.9% and 66.7% regeneration respectively. However, the total number of surviving protocorm clumps for dose 8.0 Gy was only 9 out of 500 cultured initially (data not shown). This indicates that only small number of the protocorms survived the irradiation but most surviving protocorms were able to regenerate shoots.

The number of regenerated shoots increased tremendously after 16 weeks of culture (after 3 subcultures) indicating that the surviving protocorms have multiplied normally and are able to regenerate shoots (data not shown). The data on the number of regenerated shoots after 8 weeks of culture shows that the optimum dose for ion beam irradiation on orchid protocorms may be estimated to be between 1.0 to 2.0 Gy. The regenerated plantlets have been transferred to the shadehouse for further growth and observation.

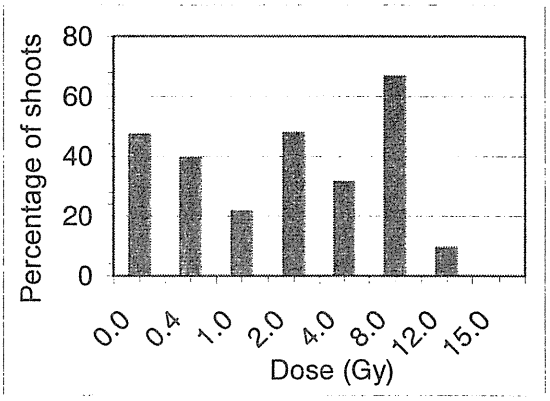

Figure 1: The number of shoots regenerated from the protocorm clumps after 8 weeks

References

1) Ling, C. H. (1998). *Effects of gamma irradiation on* in vitro *cultures of selected orchid hybrids*, MS Thesis, Universiti Putra Malaysia, Serdang, Malaysia. 113 Pages.

2) Mohd. Nazir, B., and Sakinah, A. (2001). Molecular techniques as complementary tools in orchid mutagenesis. *Proceedings of The 2001FNCA Workshop on Agriculture: Plant Mutation Breeding & Biofertilizer, August 20-24, Bangkok, Thailand,* Japan Atomic Energy Research Institute, pg 91-102.

3) Sakinah Ariffin and Mohd Nazir B. (2002). Increasing characteristic variations in Dendrobium orchid through acute irradiation. 17th World Orchid Conference and Show, Shah Alam, Malaysia, April 26-May 2, 2002.

2.6 Development of the Efficient Mutation Breeding Method using Ion Beam Irradiation

K. Degi*, T. Morishita*, H. Yamaguchi*, S. Nagatomi*, K. Miyagi**, A.Tanaka***, N. Shikazono*** and Y. Hase***
Institute of Radiation Breeding, NIAS*
Okinawa Prefectural Agricultural Experiment Station**
Department of Ion-beam-applied Biology, JAERI***

1. Introduction

In plant, a radiation induces simultaneously various levels of mutation such as genes, chromosome and genome that the most of mutation is fallen into deletion. Generally, useful mutation attributes to deletion; however, unfavorable mutation also induces at the same time[1]. Therefore, estimation of the optimum dosage in each kind of radiation is the most important to initiate an effective mutation breeding.

In sugarcane[2,4,5] and chrysanthemum[3], chromosome deletion in induced mutant can be easily estimated basing on the nuclear DNA content by flow-cytometer. A sugarcane commercial variety having around 110 chromosomes consists of basic genome eight and ten in aneuploid and allopolyploidy.

It was unveiled that in sugarcane, as the irradiation dose of gamma rays to the donor plant rose, nuclear DNA content of the mutants decreased (the deficiency increases) and the mutation rate increased so that the mutation of quantitative characters such as stalk diameter and stalk length also frequently induced[2,4,5].

Accordingly, the optimum doses on helium-ion beam was discussed basing on the relationship among the mutation rate, the nuclear DNA content and quantitative characters of mutants in sugarcane.

2. Experimental methods

Using sugarcane variety, Ni 11, individual shoots divided from multiple shoot mass derived from tissue cultured growing point were cultivated in MS medium supplemented with BA 0.2mg/l, kinetin 0.01mg/l, and sucrose 30g/l adjusted in pH5.6. These cultured shoots were irradiated with gamma rays in the Institute of Radiation Breeding and with helium-ion beam ($^4He^{2+}$,100MeV) in TIARA.

The survival rate was investigated on 40 days after the irradiation, and the lateral shoots were separated from the stock as vM_2 generation, and acclimatized in a greenhouse, then they were transplanted to the field in May 2002.

The dose responses of the radiations on stalk diameters, stalk length, stalk numbers, etc. were investigated in experimental field arranged with randomized block design consisting of 20 plants per plot in three replications. Experimental field for selection of the hairless mutants was established separately. At the beginning of October 2002, the mutants with no 57-group hair on the leaf sheath were selected.

In May 2003, five one-eyed-seedlings of hairless clones in vM_3 generation induced by the helium ion were planted by randomized block design with two replications. In the middle of October, quantitative characters and nuclear DNA content were measured in each clone. Relative nuclear DNA content of each clone was calculated comparing with the value of noble cane variety, 'Badila' (2n=80) as the internal standard. The relative nuclear DNA content of the original variety, Ni 11 was 1.42.

3. Result and discussion

As the result, it was observed that nuclear DNA content decreased in the most of the clones in the vM_2 generation. Some of the survived clone lost more than 20% of the nuclear DNA. In the helium ion, as the dose rose, nuclear DNA content decreased remarkably and its variance also increased in comparison with gamma rays. Nuclear DNA content of 10Gy irradiated clones with the helium ion was equivalent to one of 40Gy of gamma rays, and 40Gy of the helium-ion beam was equivalent to 160Gy of gamma rays, respectively (Fig. 1).

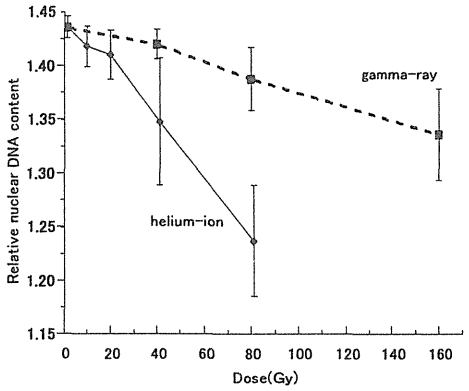

Fig.1 Effects on relative nuclear DNA contents of sugarcane with gamma rays and helium-ion beam.

Though the hairless mutation rate was 0.6% at the 20Gy of helium ion, 9.6% in 40Gy, 17.1% in 80Gy, it was rapidly increased as the dose was doubled (Table 1). The hairless mutation rate at 40Gy of helium ion was almost equal to one at 200Gy of gamma rays. Significant negative correlation (r=-0.97**) was found between average hairless mutation rate and relative nuclear DNA content in each irradiation plot of gamma rays and helium-ion beam. Both kinds of the radiations also showed the similar relationship that the increase in the dose, and nuclear DNA content decreases, and the hairless mutation rate rises (Fig. 2).

At vM_3 generation, nuclear DNA content decreased with the increase in the helium-ion beam dose, and then, the stem thinly shortened, and juice Brix of the stem tended to decrease.

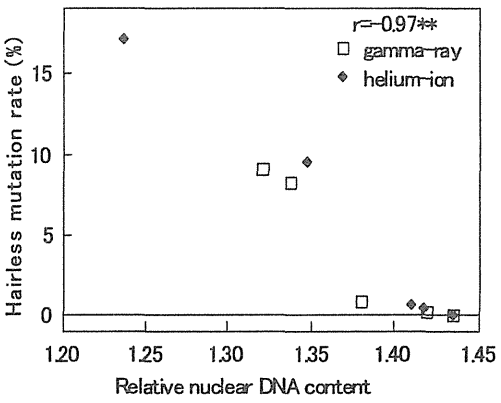

Fig.2 Relationship between relative nuclear DNA content and hairless mutation rate.

However, in the dose of 40Gy or less, the decrease of the stem length with the decrease in nuclear DNA content was gentle, and there were many clones in which the stem length did not change. And, there are many clones of high Brix in the dose of 40Gy or less. However, Brix lowered with the decrease in nuclear DNA content in 80Gy (the data omission). Estimated Brix volume per stock (a standard of the recoverable sugar quantity from the stock) tended to decrease with the decrease in nuclear DNA content. However, there were clones over original variety the estimated Brix volume in clones over 1.35 in relative nuclear DNA content (Fig. 3).

It is considered that the decrease of nuclear DNA content in this study is caused by the chromosome or/and genome deficiency. Though induction frequency of the hairless mutation is high in higher dose plots, it is guessed with that the stem thinly shortened by

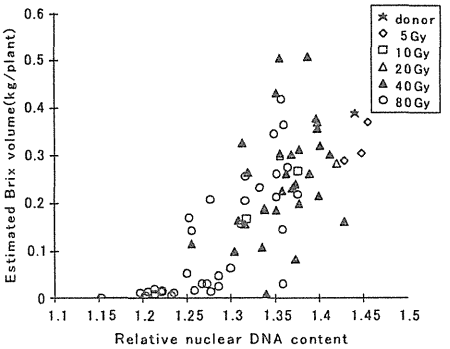

Fig.3 Relationship between relative nuclear DNA content and estimated Brix volume among hairless mutants with helium-ion irradiation.

large deficiency and that the unit crop decreased. From these result, the optimum dose on helium-ion beam seemed to be 40Gy basing on the relationship between adverse effect for quantitative characters and frequency of hairless mutation.

Table 1 Hairless mutants induced from irradiated tissue cultured multiple shoot of sugarcane with gamma rays and helium-ion

Kind of radiation	Dose(Gy)	No.of samples	No.of hairless mutant	Mutation rate(%)
He ion	10	416	2	0.48
He ion	20	505	3	0.59
He ion	40	366	35	9.56
He ion	80	310	53	17.1
Gamma rays	40	89	0	0
Gamma rays	80	84	0	0
Gamma rays	160	84	7	8.3
Gamma rays*	50	1291	3	0.23
Gamma rays*	100	1142	10	0.88
Gamma rays*	200	273	25	9.06
Not treated	0	758	0	0

* are results in 2001, others are results in 2002.

Reference

1) A. M. van Harten, Mutation Breeding, Theory and Practical Applications. (1998) Cambridge Univ. Press, pp353

2) S. Nagatomi et al., Breed.Sci.48 (Suppl.2). (1998) 334. (In Japanese)

3) H. Yamaguchi et al., TIARA Ann. Rep. 2000(JAERI-Review 2001-039) 34-35.

4) K. Degi et al., Japanese J. of Tropical Agriculture. Vol.46. (2002) 9-10 (In Japanese)

5) K. Degi et al., Breed.Sci.5 (Suppl.1). (2003) 280. (In Japanese)

2.7 Mutation Generation and the Development of New Varieties in Ornamentals by Ion Beam Breeding

M.Okamura*, N.Yasuno*, M.Takano*, A.Tanaka** and Y.Hase**
Plant Laboratory, Agribio business company, Kirin Brewery Co., Ltd.*
Department of Ion-Beam-Applied Biology, JAERI**

1. Introduction

Ion beams have much higher linear energy transfer and relative biological effectiveness (RBE) than those of gamma rays and X-rays[1] By the combined method of ion beam irradiation with cell and tissue culture, we succeeded in the development of new carnation varieties "Vital Ion series" in 2002 [2]. Ion beams proved useful as new mutagens to obtain the commercial varieties in a short time.

In this study, we investigate the efficiency of mutation generation by ion beam breeding and the development of new varieties in standard-type carnation and petunia.

2. Materials and Methods

Standard carnation variety 'Star' (orange fancy), superior variety with a long vase life and high productivity, and spreading type petunia 'EPW' were used for the experiment. In carnation small leaf segments with micro buds were placed in petri dish containing Murashige and Skoog medium supplemented with 0.1mg/l NAA and 0.1mg/l BA, 30g/l sucrose and 7g/l agar. The samples covered with Kapton film were irradiated with 220 MeV carbon ion beams from the TIARA AVF cyclotron (JAERI, Takasaki). In petunia seeds were irradiated. After irradiation, the rate of shoot growth or that of seed germination was examined in carnation or petunia, respectively. The plants derived from irradiation were cultivated in the greenhouse and their flower color and shape were investigated. The carnation plants irradiated with gamma-rays were tested as comparison.

3. Results and Discussion

The influence of ion beam irradiation on bud growth in carnation was shown in Fig.1A, and that on seed germination and plant growth in petunia in Fig.1B. The median growth dose in carnation was estimated at 17-18Gy. In petunia, the median growth dose was around 22Gy although the median lethal dose was estimated at 43Gy.

The mutants of flower color and shape in carnation derived from ion irradiation are shown in Fig 2. The mutation rates were 5 to 10% depending on the dosage. Flower color mutants such as light orange, dark orange, salmon, striped, edge-less and flower shape mutants such as round petals, cup-shaped flowers were obtained. The mutation spectrum of the flower color and shape was wider as compared with acute gamma-ray radiation (Fig.3). The irradiation dosages to obtain dark orange mutants were 5Gy, about 5 tracks per cell, and 30Gy, about 600,000 spurs per cell, in ion beams and gamma-rays, respectively.

In spreading type petunia 'EPW', flower color mutants such as pure white, rose vein, blue, salmon red and striped were obtained (Fig.4).

In this study the wide spectrum in flower-color and -shape was observed in the mutants derived from ion beam irradiated standard- type carnation and petunia. The results correspond with the reports in carnation [2] and chrysanthemum.[3] New carnation varieties "Vital Ion series" developed by ion beam breeding have been commercialized in Europe as well as in Japan. Ion beams have different effect from that of electron beams on mutation generation of crops and have great impact on plant seed and seedling business.

References

1) A. Tanaka et. al., Int. J. Radiat. Biol 72 (1997), 121-127
2) M. Okamura et. al., Nucl. Inst. and Meth. in Phys. Res. B 206 (2003), 574-578 S.
3) Nagatomi, et. al., JAERI-Review 97-015 (1998), 50-52

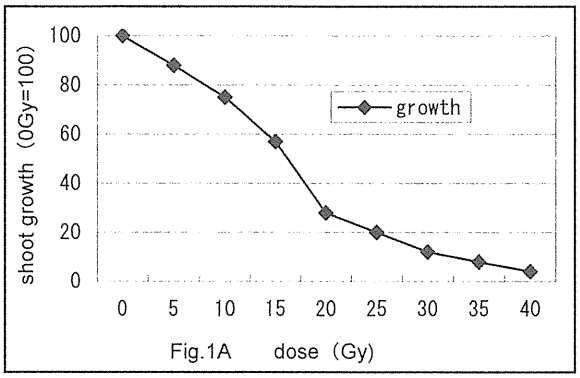

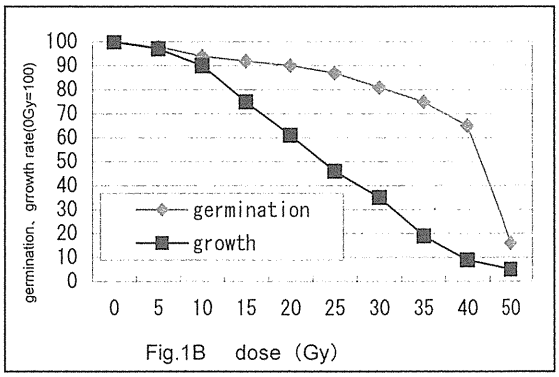

Fig.1 Influence of 220 MeV carbon ion beam irradiation on bud growth in carnation (A), and that on seed germination and plant growth in spreading petunia (B).

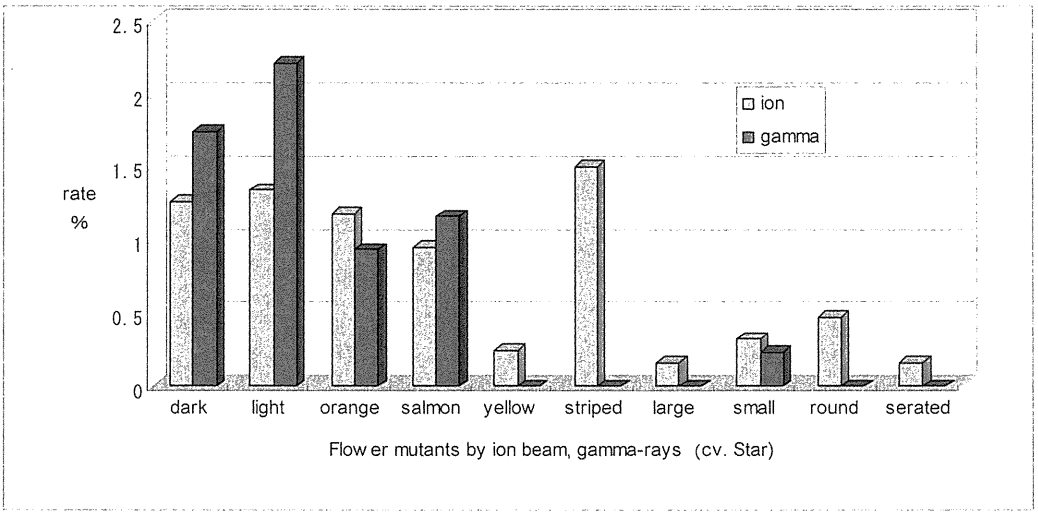

Fig.2 Rates of floral mutants in carnation obtained by the irradiation of ion beams and gamma-rays.

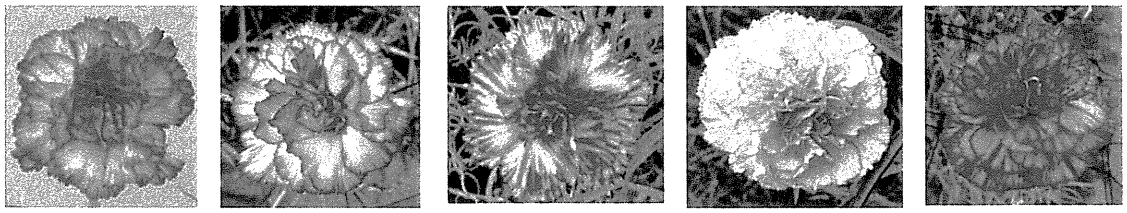

Fig.3 Floral mutants of standard carnation cv. 'Star' obtained by ion beam breeding.
(left to right): Parent cv. Star, light orange, striped, yellow, salmon.

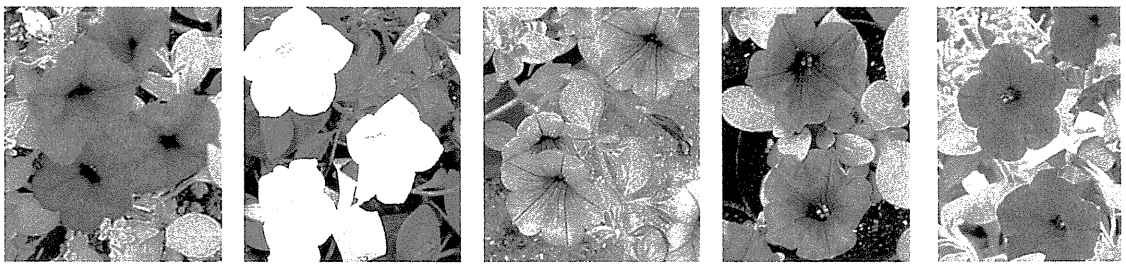

Fig.4 Floral mutants of spreading type petunia 'EPW' by ion beam breeding.
(left to right): Parent cv. EPW, pure white, rose vein, salmon red, blue.

2.8 Additional Improvement of Chrysanthemum using Ion Beam Re-irradiation

K. Ueno*, S. Nagayoshi*, Y. Hase**, N. Shikazono** and A. Tanaka**
Kagoshima Biotechnology Institute*,
Department of Ion-beam-applied Biology, JAERI**

1. Introduction

Chrysanthemums have some agronomical traits to be improved such as reducing axillary buds to save farmer's labor and lower temperature flowering to save the cost of heating. We succeeded in the introduction of two new cultivars of chrysanthemum with reducing axillary buds in 2003 using ion beam irradiation[1), 2)]. The numbers of axillary buds of these cultivars were less than half to quarter, comparing the original cv. "*Jimba*". These cultivars were named "*Imagine*" and "*Aladdin*".

We are going to prepare for selection of mutants which have both few axillary buds and low temperature flowering trait. In this paper, we describe effects of ion beam re-irradiation on the mutation induction from cultures of chrysanthemum.

2. Materials and Methods

2.1 Plant materials

Chrysanthemum (cv. *Jimba, Imagine* and *Aladdin*) leaves were cut into appropriately 4 mm × 2 mm disc and cultured on MS medium with 5 mg/l IAA and 1 mg/l BA prior to 3-6 days of irradiation. After 1 month of irradiation, leaf discs were subcultured on MS medium with 0.01 mg/l NAA and 0.05 mg/l BA for adventitious shoot development. Then after 1 month, adventitious shoots were subcultured on MS hormone free medium for plant regeneration.

2.2 Ion beam irradiation

Leaf discs were irradiated with 220 MeV or 320 MeV carbon ions, accelerated by AVF cyclotron at JAERI at doses of 1-5 Gy for chrysanthemum.

2.3 Analysis of DNA contents

DNA contents were estimated by the Proidy Analyzer (PARTEC PA)[3)]. Sugar cane was used as genome size control, then, DNA contents were determined by comparing sugar cane with chrysanthemum.

3. Results and Discussions

In 220MeV $^{12}C^{5+}$ and 320MeV $^{12}C^{6+}$ ion beams, regeneration frequency decreased rapidly with increasing dose and the 90% re-generation dose (RD90) was estimated to be 2 Gy and 3 to 4 Gy, respectively[4)]. Therefore, specimens were irradiated around RD90.

DNA contents of *Imagine, Aladdin* and M1 plants derived from the ion beam re-irradiated leaf discs were analyzed and compared with that of cv. *Jimba.* In *Imagine* it was approximately 98% of original "*Jimba*", whereas in *Aladdin* it did not show any decrease (Fig. 1). In M1 plants derived from leaf discs of *Imagine*, DNA contents decreased even 0 Gy non-irradiated controls, and in M1 plants decreasing was more than 2% when 4 Gy of ion beam were applied. These results suggest that the mutant like *Imagine* in which chromosome deficiency occurred was also lowered in its ability of DNA repair. On the other hand, in M1 plants of *Aladdin,* DNA contents remained almost the same level as in original "*Jimba*". Therefore, when we have to use the re-irradiation technique for plant

improvement, the materials or mutants use must be those with keeping original DNA amount.

In 2003, approximately 10,000 regenerated plants were obtained and grown in two different cropping systems; for selection either few axillary buds (flowering period in December) or lower temperature flowering type (flowering period in March).

From 5,173 control or M1 plants, 41 visible mutants were selected by screening of fewer axillary buds (Fig. 2, Table 1). *Jimba* #2 is early flowering type which was selected by line breeding system. However, the growth of M1 plants which are derived from *Jimba* #2 are inferior to original *Jimba* (data is not shown). On the other hand, the growth of *Aladdin* and its M1 plants are more vigorous than *Jimba*, and gave stout and higher quality cut-flowers. Among those irradiated with 320MeV $^{12}C^{6+}$, we obtained the few axillary bud mutants. These mutants showed the same or higher percentages of non-axillary buds and earlier flowering, as compared with *Aladdin*.

Under low temperature, flowering period of *Jimba* and *Aladdin* are greatly delayed. Therefore, we tried to select early flowering type which behave safely even under low temperature of 10 to 12℃. From the screening of 4,299 M1 plants derived from leaf discs of *Aladdin*, 51 visible mutants of early flowering were selected (Table 2). These mutants flowered in seven to eight weeks after lighting stop.

We hope in next season the successful selection of cultivars, in which both desirable characteristics, few axillary buds and early flowering in low temperature, are combined from the mutants we have now selected.

References

1) K. Ueno et al., TIARA Ann. Rep. 2002 (2003) 52-54.
2) S. Nagayoshi, Radiation & Industries 98 (2003) 10-16.
3) K. Mishiba and M. Mii, Cell Tech., (1988) Vol.17, No. 4: 609-615.
4) K. Ueno *et al.*, Ikushugaku Kenkyu 3 (2001) (Suppl. 2): 62.

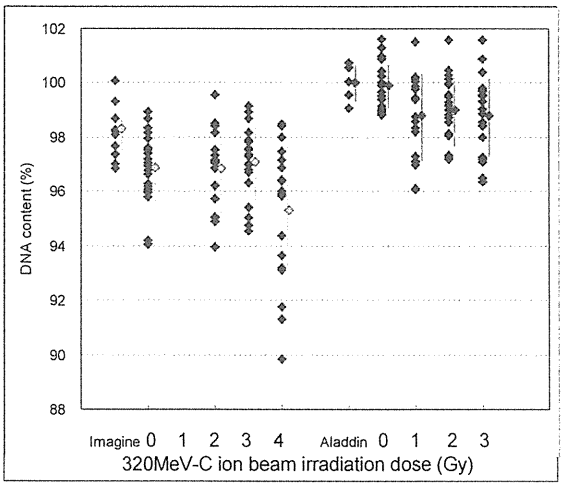

Fig. 1 DNA contents of *Imagine*, *Aladdin*, and these M1 plants compared with original *Jimba* (100%).
◆: each plant of analyzed, ◇: average, | : STD.

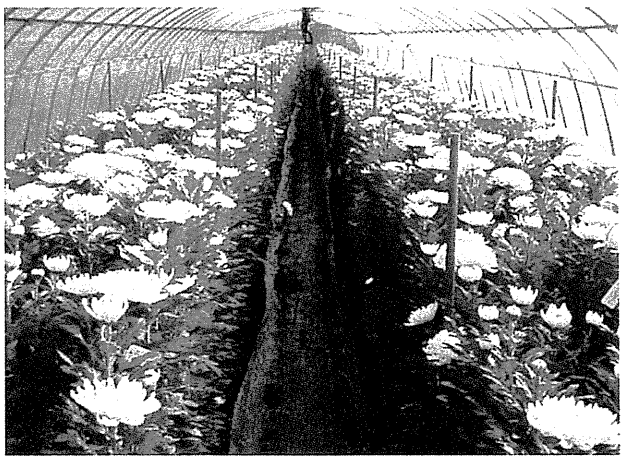

Fig. 2 Individual selection for mutant of few axillary buds.

Table 1. The number of tested and selected plants in 2003, which regenerated from leaf disc cultures irradiated by ion beam, for selection of few axillary buds.

Plant tested	Radiation	Energy MeV	Dose Gy	Flowering peoriod: December: Number of tested plants	Number of selected plants	% of selection rate	Characteristic of cultivar (*) or number of selected plants: % of nodes without axillary buds: >80	>50	>30	>10	10>	0 (%)
Aladdin	-	-		129						*	*	
Regenerated plants from re-irradiated ***Aladdin***	C	320	0	445	9	2.0	1		2	4	2	
			1	1,364	10	0.7	1		2	7	2	
			2	1,323	4	0.3			1	2	1	
			3	1,049	10	1.0				7	3	
			5	194	1	0.5				1		
		sub-total		4,375	34		2		5	21	8	
Jimba #2				44							*	*
Regenerated plants from irradiated *Jimba* #2	C	320	0	58	0	0.0						
			1	125	2	1.6			1	1		
			2	327	2	0.6			1	1		
			3	288	3	1.0			2	1		
			5	0	0	0.0						
		sub-total		798	7				4	3		
		Total		5,173	41		2		9	24	8	

Table 2. The number of tested and selected plants in 2003, which regenerated from leaf disc cultures irradiated by ion beam, for selection of early flowering type.

Plant tested	Radiation	Energy MeV	Dose Gy	Flowering peoriod: March: Number of tested plants	Number of selected plants	% of selection rate	Characteristic of cultivar (*) or number of selected plants: Number of weeks to flowering after liting stop: 7	8	9	10
Jimba A	-	-	-	14				*		
Jimba #1	-	-	-	15				*		
Jimba #2	-	-	-	27			*			
Imagine	-	-	-	33				*		
Aladdin	-	-	-	163					*	
Mutant Line H	-	-	-	107				*		
Regenerated plants from re-irradiated ***Aladdin***	C	320	0	217	3	1.4		3		
			1	109	0	0.0				
			2	705	6	0.9	4	2		
			3	428	5	1.2	2	3		
	C	220	1	569	12	2.1	1	11		
			1.5	1,519	17	1.1	3	14		
			2	752	8	1.1	2	6		
			Total	4.658	51		12	39		

2.9 Detection of Mutation in Sugi Cedar (*Cryptomeria japonica*) and Hinoki Cypress (*Chamaecyparis obtuse*) Treated with Ion Beam Irradiation

K. Ishii*, Y. Hase** and A. Tanaka**
Department of Molecular and Cell Biology, Forestry and Forest Products Research Institute*,
Department of Ion-beam-applied Biology, JAERI**

1. Introduction

Sugi cedar (*Cryptomeria japonica* D. Don) and Hinoki cypress (*Chamaecyparis obtusa* Sieb. et Zucc.) cover 44% and 24 % of the plantation area in Japan, respectively, and are the most important domestic forest conifers. They produce the highest quality wood and can be grown throughout Japan, excluding Hokkaido and the Ryukyu Island. In forest tree species with long life cycle, mutation is very promising in shortening the breeding time.

Ion beam is expected to increase the mutation frequency and wide spectrum, since it has a high LET (linear energy transfer). The combination of ion beam irradiation and tissue culture was sometimes beneficial for high frequent mutation induction[1)2)3)]. In the previous report, we have obtained the xantha and wax rich mutants in Hinoki cypress by ion beam irradiation[4)].

In this study, we tried to induce the mutants by irradiation of the in vitro cultured buds of Sugi cedar and shoot primordia of Hinoki cypress with $^{4}He^{2+}$ and $^{12}C^{6+}$ heavy ion beams. Mutants such as male-sterile, fast-growing and environmentally resistant ones are promising. We try to detect not only leaf plastid mutation by observation but also the chromosomal level mutation by flow cytometer.

2. Experimental procedure

In vitro cultured buds on half-strength LP medium[5)] of Sugi cedar originally collected from arboretum in Forestry and Forest Products Research Institute, Tsukuba, Ibaraki, were used. Shoot primordia of Hinoki cypress were also used for the experiments. They are cultured on CD medium[6)7)] supplemented with 10. M 6-benzylaminopurine and 0.03 . M naphthalene acetic acid (NAA). Fresh buds or shoot primordia were subcultured on the medium in petri dish (35 x 10 mm) which was covered with Kapton film. They were irradiated with 50 MeV $^{4}He^{2+}$ or 320 MeV $^{12}C^{6+}$ ion beam from AVF cyclotron in JAERI. After irradiation the shoot primordia were subcultured to the new media for assessing the surviving rate and detecting mutation.

For detecting mutation, not only morphological observation but also cytological method was applied. About 100 mg of plant material was chopped with a razor blade in 1 ml of 0.1 M citric acid containing 0.5 % Triton X-100[8)] . The suspension of nuclei was filtered through a 50 . m nylon net and stained with 5 . g ml^{-1} DAPI and 3. g ml^{-1} sulforhodamine in 0.4 M sodium hydrogen phosphate[9)] . Relative DNA content was measured on a Partec PA flow cytometer equipped with a 100 w high-pressure mercury lamp.

3. Results and Discussion

Surviving rate of in vitro cultured buds of Sugi cedar irradiated with 5 to 20 Gy $^{4}He^{2+}$ and 1 to 5 Gy $^{12}C^{6+}$ ion beam decreased as

the amounts of irradiation increased (Table 1,2). Shoot primordia of Hinoki cypress irradiated with 5 to 20 Gy $^{4}He^{2+}$ and 1 to 5 Gy $^{12}C^{6+}$ ion beam had similar tendency. There was no clear plastid mutation except partial light-green leaves in Sugi cedar at least until 1 year after irradiation. Wax rich shoots appeared in Hinoki cypress culture. Shoot elongation from surviving buds was suppressed with irradiation of 2 and 5 Gy $^{12}C^{6+}$ ion beam. Regenerated plantlets have been habituated and grown in a greenhouse for further assessing experiments to detect mutants. It may be possible to assess the sterile mutants by spraying gibberellic acid for inducing flowers. In the previous report, we described the albino, xantha and wax rich mutants from irradiated shoot primordium of Hinoki cypress[10]. Wax rich mutants may have some horticultural value.

Flow cytometric DNA histograms of irradiated Hinoki cypress shoot primordia contained a single G1 peak as shown in Figure 1 which was same position with that of the control shoot primordium. That indicated that the there was no ploidy level mutation occurred after irradiation. However, we cannot eliminate the possibility of chimeric partial deletion of chromosorme suggested by the broadening of the foot of the peak.

Further study is needed for detecting mutations after growing the shoots to the plantlets.

Table 1. Effect of $^{4}He^{2+}$ ion beam irradiation on rate of surviving buds, number of shoots obtained and regenerated plantlets of Sugi cedar (2 months after irradiation, 50 buds x 6 repetitions)

Dose Gy	survival rate	no. of shoots obtained	no. of plantlets
5	33.4	47	2
10	24.0	101	7
20	9.4	38	6

Table 2. Effect of $^{12}C^{6+}$ ion beam irradiation on rate of surviving buds, number of shoots obtained and regenerated plantlets of Sugi cedar (2 months after irradiation, 50 buds x 6 repetitions)

Dose Gy	survival rate	no. of shoots obtained	no. of plantlets
1	85.0	160	3
2	76.0	7	2
5	64.0	3	0

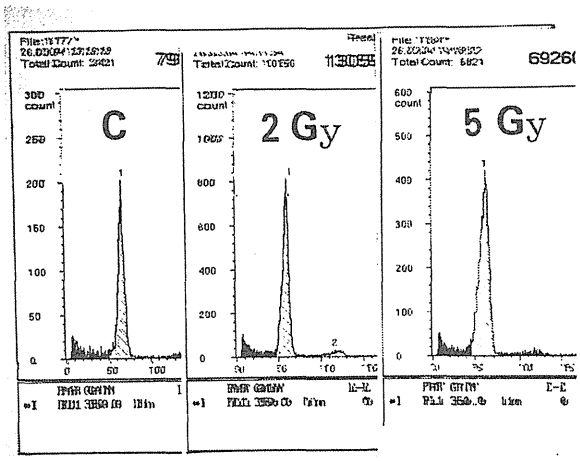

Fig. 1 Flow cytometric observation of shoot primordia of Hinoki cypress irradiated with 320 Mev $^{12}C^{6+}$ heavy ion beam.

References

1) S. Nagatomi, A. Tanaka, A. Kato, H. Watanabe and S. Tano, TIARA Annual Report 5(1996)50-52.
2) S. Nagatomi, A. Tanaka, H. Watanabe and S.Tano, TIARA Annual Report 6(1997) 48-50.
3) T. Nakahara, K.Hirashima, M. Koga, A. Tanaka, N. Shikazono and H. Watanabe, TIARA Annual Report 1998(1999)28-29.
4) K. Ishii, Y.Hase, N. Shikazono and A.Tanaka, TIARA Annual Report 2000(2001)55-56.
5) J. Aitken-Christie and T.A. Thorpe, Cell Culture and Somatic Cell Genetics of Plants 1(1984)82-95.
6) R.A. Campbell and D.J. Durzan, Can J. Bot. 53(1975)1652-1657.
7) K. Ishii, Plant Cell Tissue and Organ Culture 7(1986)247-255.
8) A.M.M. De Laat, W. Gohde and M.J.D.C. Vogelzang, Plant Breed. 99(1987) 303-307.
9) I. Ulrich and W. Ulrich, Z. Naturforsch. 40c(1986)1052-1056.

2.10 Effects of Ion Beam Irradiation on the Mutation Induction from Garlic Bulb Basal Plate Culture

T.Tashiro*, Y. Yamamoto**, A.Tanaka***, N.Shikazono*** and Y.Hase***
Faculty of Horticulture, Chiba University*
Farm Station of FSC, Faculty of Bioresources, Mie University**
Department of Ion-beam-applied Biology, JAERI***

1. Introduction

Recently, there is a great demand for garlic because garlic is one of the best-known health foods, which increase biological activities that include antibiotic, antitumor and cholesterol lowering. Garlic belongs to a group of the Allium family. Since garlic is sexual sterility and propagated by bulbs, the positive plant breeding is difficult. Therefore, the consumer and the producer could not satisfy the breeding in garlic. We established a novel system of practical micropropagation in garlic, which produced effective bulblets *in vitro*, because it is a wise method to proliferate, to select, and to plant in field[1].

The Ion beam irradiation is expected to be increase the mutation frequency and wide spectrum, since ion beam is a type of high linear energy transfer (LET) radiation and can deposit high energy on a target compared to low LET radiation such as gamma ray[2]. The combination of ion beam irradiation and tissue culture was considered to be beneficial for mutation induction of garlic. It is expected that ion beam induced novel mutation not only on morphological character but also on chemical composition in garlic.

The purpose of this study is to develop an effective method for ion beam breeding in garlic and to obtain desirable mutants, especially that of volatile sulfur compounds. In this paper, we report the effects of ion beam on shoot formation and bulblet induction from the irradiated explant of basal plate of garlic bulb.

2. Materials and Methods

Garlic (*Allium sativum* L. cv Fukuchi-howaito) was used for experiments. Bulbs were surface-sterilized with 70% ethanol and 1% sodium hypochlorite solution, and rinsed three times in sterile water. The basal plate of bulb was cut off 1~1.5mm thickness as ion beam could irradiate through them perfectly and trimmed 5x5mm in length, and then divided into 4 equal segments. 8~12 segments were placed on a 60mm diameter plastic petri dish containing 5ml LS medium supplemented with 30g/l sucrose and 3g/l gelrite for shoot differentiation[3]. The dishes were covered with Kapton film, and then irradiated with 50MeV $^{4}He^{2+}$ and 320MeV $^{12}C^{6+}$ ion beams at dosage of 0.2, 1.0 and 1.5Gy at the TIARA AVF cyclotron in JAERI. After irradiations the both samples were transferred to the fresh medium for shoot differentiation. Fresh shoots were subcultured on LS medium for bulblet formation.

The experiments were performed under 3000lux (day /night of 16/8hrs.) at 25 °C. Regeneration rate of basal plate segment and plantlet formation rate from basal plate segment were examined. And the general appearances of the plantlets were observed, comparing the morphological differences among those plantlets induced by irradiating helium and carbon ion beams.

3. Results and Discussions

1)Effect of bulb basal plate explants irradiation

on regeneration of plantlets

The dose response of plantlet regeneration with helium and carbon ion beams irradiation at 0.2, 0.5 and 1.5Gy was showed in Table 1. In helium and carbon ion beams, regenerated plantlet rate decreased gradually with increasing dosage. Regenerated plantlet rate was 77.1% at 0.2Gy, 72.7% at 0.5Gy and 46.9% at 1.5Gy for helium ion beam and 67.9% at 0.2Gy, 62.2% at 0.5Gy and 36.4% at 1.5Gy for carbon ion beam, respectively. Regenerated plantlet rate was 78.8% in non-irradiated treatment.

Various types of regenerated plantlets were observed and classified, depending on their general appearance of shoot and bulblet, into normal plantlet and variant. Generally, the normal plantlets were defined a green leaf color and more than 15cm length and 5mm width of leaf, and more than 10 mm length and 8 mm width of bulblet like the normal garlic in appearance. The variants produced by ion beam irradiation had different morphological characters such as multiple shoot (more than 5 shoots per explant[4]), variegated leaves, dwarf, delayed growth, malformed shoot, multiple-shoot bulblet (more than 2 shoots per bulblet), and shootless bulblet.

The variant rate was depended on helium and carbon ion beams with different dose. In helium and carbon ion beams, the variant rate increased with increasing dosage. The variant rate was 28.0% at 0.2Gy, 25.6% at 0.5Gy and 95.6% at 1.5Gy for helium ion beam and 21.9% at 0.2Gy, 38.1% at 0.5Gy and 43.8% at 1.5Gy for carbon ion beam, respectively. The variant rate was 8.1% in non-irradiated treatment. In the variant, the rate of complex variant which has more than 2 abnormal characters was 27.3% at 0.2 Gy, 3.1% at 0.5Gy and 18.6% at 1.5Gy for helium ion beam and 3.1% at 0.2 Gy, 9.4% at 0.5Gy and 7.1% at 1.5Gy for carbon ion beam, respectively.

These data indicated that the regenerated plantlet rate was slightly higher in carbon ion beam than in helium ion beam, and the plantlets derived from irradiated explants had higher variant rate apparently, and variant rate was slightly higher in helium ion beam than in carbon ion beam. And complex variation rate was 2 to 3 times higher in helium ion beam than in carbon ion beam. These results suggest that carbon ion beam can induce mutation at low dosage of irradiation, resulting in the effective induction of the mutants with one or a few point mutations that have no or very few undesired mutations.

2)Effect of bulb basal plate explants irradiation on morphological character of regenerated plantlets

The dose response of morphological character of regenerated plantlets irradiated with helium and carbon ion beams at 0.2, 0.5 and 1.5Gy was showed in Table 2. Regenerated plantlets irradiated at dosage of 1.5Gy in both helium and carbon ion beams showed severe morphological abnormality and abortive growth. The variant of malformed shoot and shootless bulblet were tended to obtain at the dosage of 1.5Gy in both helium and carbon ion beam irradiation. However, regenerated plantlets which irradiated at dosage of 0.2 and 0.5Gy in both helium and carbon ion beams showed less morphological abnormality and slow growth. The variant of variegated leaves and dwarf had a tendency to get from irradiated at dosage of 0.2 and 0.5Gy in both helium and carbon ion beams. The variant of multiple shoots and delayed growth were tended to produce not only at the dose of 0.2 and 0.5Gy but also at the dose of 1.5Gy in both helium and carbon ion beams. The variant of multiple-shoot bulblet were attained by helium ion beams irradiation at dosage of 0.2Gy. There was no difference in the tendency of variant type rate between helium ion beam and

carbon ion beam except for the multiple shoots rate.

The regenerated bulblets were placed on soil for sprouting, and now they are well grown in experimental field of Farm Station in Mie University. They will be harvested in June 2004 and estimated agricultural characters in details. The differences among ion beams in the effect of mutant and in the spectrum of induced mutants are investigated in detail.

References

1) Y.Yamamoto and T.Tashiro, International Plant Propagatorrs'Society 7:17-18(2000).
2) A.Tanaka, N.Shikazono, Y.Yokota, H.Watanabe and S.Tano, Int. J. Radiat. Biol. 72:121-127 (1997).
3) M.Maybe and S.Sumi, Plant Cell Reports 17:773-779(1998)
4) T.Tashiro, Y.Yamamoto, A.Tanaka, N.Shikazono, and Y.Hase, TIARA Annual Report 2002, JAERI-Review 2003-033:60-62 (2003).

Table 1 Effects of helium and carbon ion beams irradiation on regeneration of plantlets from basal plate of garlic bulb

	$^{4}He^{2+}$(Gy)			$^{12}C^{6+}$(Gy)			control
	0.2	0.5	1.5	0.2	0.5	1.5	
No. of irradiated explants(A)	153	172	96	215	135	176	189
No. of regenerated explants(B)	118	125	45	146	84	64	149
No. of explants with normal shoots and bulblets(C)	85	93	2	114	52	36	137
No. of explants with abnormal shoots and bulblets(D)	33	32	43	32	32	28	12
No. of explants with double abnormal characters (E)	9	1	8	1	3	2	0
B/A(%):Regeneration rate	77.1	72.7	46.9	67.9	62.2	36.4	78.8
C/B(%):Normal shoots and bulblets	72.0	74.4	4.4	78.1	61.9	56.3	91.9
D/B(%):Abnormal shoots and bulblets	28.0	25.6	95.6	21.9	38.1	43.8	8.1
E/D(%):Double abnormal characters	27.3	3.1	18.6	3.1	9.4	7.1	0.0

Table 2 Effects of helium and carbon ion beams irradiation on morphological character of regenerated plantlets

	$^{4}He^{2+}$(Gy)			$^{12}C^{6+}$(Gy)			control
	0.2	0.5	1.5	0.2	0.5	1.5	
No. of explants with abnormal shoots and bulblets(A)	33	32	43	32	32	28	12
No. of explants with multiple shoots (B)	5	9	0	25	12	2	12
No. of explants with variegated leaves(C)	3	7	0	1	0	0	0
No. of explants with dwarf shoots(D)	16	7	0	2	14	0	0
No. of explants with delayed growth shoots(E)	4	9	0	2	3	4	0
No. of explants with malformed shoot(F)	0	0	26	2	3	10	0
No. of explants with multiple-shoot bulblets(G)	4	0	0	0	0	0	0
No. of explants with shootless bulblets(H)	1	0	17	0	0	12	0
B/A(%):multiple shoots rate	15.2	28.1	0.0	78.1	37.5	7.1	100.0
D/C(%):variegated leaves rate	9.1	21.9	0.0	3.1	0.0	0.0	0.0
E/C(%):dwarf shoots rate	48.5	21.9	0.0	6.3	43.8	0.0	0.0
F/C(%):delayed growth shoots rate	12.1	28.1	0.0	6.3	9.4	14.3	0.0
G/C(%):malformed shoots rate	0.0	0.0	60.5	6.3	9.4	35.7	0.0
I/C(%):multiple-shoot bulblets rate	12.1	0.0	0.0	0.0	0.0	0.0	0.0
J/C(%):shootless bulblets rate	3.0	0.0	39.5	0.0	0.0	42.9	0.0

2.11 Biological Effect of Ion Beam by Seed Irradiation in Spinach

N. Hata*, K. Murakami**, Y. Yoshida**, M. Masuda**, A. Tanaka***,
N. Shikazono*** and Y. Hase***
Department of Applied Plant Science, Faculty of Agriculture,, Okayama University*
Faculty of Agriculture, Okayama University**
Department of Ion-Beam-Applied, JAERI***

1. Introduction

In spinach (*Spinacia oleracea* L.) production, the reduction of oxalate content is one of the most important issues, because oxalate causes the inhibition of calcium absorption and contributes to the formation of urinary stones in human[1]. Although several attempts to reduce oxalate have been made by cultivation techniques, they have not succeeded in drastic reduction. Furthermore, there has not been any cultivar or line whose oxalate content is significantly low[2]. A new approach through mutation breeding could provide an effectual alternative solution.

In mutation breeding of self-fertilized species, recessive mutant genes are induced in M_1 plants, and identified in homozygous status in M_2 progeny. In cross fertilized species, however, mutant genes induced in M_1 plants remain heterozygous in M_2 progeny, making phenotypic detection of mutants difficult. Thus, mutation breeding programs in these species have been limited[3].

Spinach is a typical dioecious crop, but there are spontaneously a few gynomonoecious plants with the ability of self-fertilization. Gynomonoecious lines can be established by their successive self-fertilization[4),5]. Mutation breeding may be conducted effectively by employing such a line.

Prior to mutation breeding, a mutagen should be chosen and its optimum dose determined. Gamma-ray has been utilized as a common mutagen, but other effective mutagens have been also explored. Recently, ion beam is rising as one of the effective mutagens with a wide range of mutations and high biological effects. Although Komai et al.[6] reported the effect of ion beam irradiation to spinach seeds on its sex expression, its biological effects are not investigated completely.

In this study, the biological effects of ion beam in spinach and its optimum dose in seed irradiation were examined. The possibility of mutation breeding in spinach by employing gynomonoecious plants is also discussed.

2. Experimental procedure

In the present study, *Spinacia oleracea* L. cv. Shin-Nippon (Atariya Seed, Chiba) was used because relatively higher percentages of gynomonoecious plants had been observed in this cultivar. In July 2002, self-fertilized seeds were harvested separately in three gynomonoecious plants. Pericarps were removed after soaking in tap water for 1.5 hr, and then seeds were dried back and stored. These seeds were mixed and divided randomly in lots of 100 seeds. Each seed lot was irradiated with gamma-ray, 220 MeV $^{12}C^{5+}$ and 50 MeV $^{4}He^{2+}$ ion beams were irradiated at various dosage (see Table 1). These M_1 seed lots were sown on cell flat (288 cells per tray, 30×60 cm) filled with vermiculite on 7 February 2003. Survived seedlings were transplanted to plastic pots (10 cm diam.) containing a 1:1 mixture of vermiculite and commercial soil on 18-25 March, and then planted out to open-sided plastic house

with spacing of 20 cm between and 15 cm within row on 16-23 April. Bolted plants before anthesis were covered with transparent bags to prevent cross-pollination. Self-fertilized M_2 seeds were harvested individually in each M_1 plants from July to August. On 15 September 2003, 16 M_2 seeds per M_1 plant were sown to investigate chlorophyll mutation.

Table 1 Irradiation dose of gamma-ray and ion beam in this study.

. -ray	100, 200, 250, 300 (Gy)
$^{12}C^{5+}$	5, 10, 15, 20, 25, 30 (Gy)
$^{4}He^{2+}$	50, 100, 150, 200, 250, 300 (Gy)

3. Results and Discussion

The percentage of survived M_1 seedling was observed on 18 May 2003. There were no significant survived rate deviations in treatments below gamma-ray 100 Gy, $^{12}C^{5+}$ 15 Gy and $^{4}He^{2+}$ 200 Gy (Fig. 1). It began to reduce dramatically over 100, 20 and 200 Gy in gamma-ray, $^{12}C^{5+}$ and $^{4}He^{2+}$ irradiation, respectively. Based on this result, relative biological effect is approximately 5-fold higher in $^{12}C^{5+}$ and 2-fold lower in $^{4}He^{2+}$ than in gamma-ray.

It was reported that gynoecious and gynomonoecious plants were segregated with various ratio in the progeny of selfed-gynomonoecious plants, depending on parent genotype[7]. Considering the results of 100 Gy in gamma-ray and 50-150 Gy in $^{4}He^{2+}$, approximately 60% of the plants were considered to be gynomonoecious (Fig. 2). In the case of $^{12}C^{5+}$ irradiation, the frequency of gynomonoecious plants was slightly lower at 5 Gy, and it reduced remarkably over 15 Gy. It was also lower at 200 Gy $^{4}He^{2+}$ irradiation although survival rate did not decrease. No gynomonoecious plants were observed at 200 or 300 Gy gamma-ray irradiation. Instead each of the surviving 3 plants was gynoecious.

The percentage of fertile plants was related to seedling survival percentage and the frequency of gynomonoecious plant, being about 40% as its highest value (Fig. 3). It was lower above 25 Gy and 250 Gy in $^{12}C^{5+}$ and $^{4}He^{2+}$ irradiation, respectively. No self-fertilized seeds were harvested at 200 or 300 Gy gamma-ray irradiation. In order to obtain mutants effectively, optimum dosage is considered to be about 100 Gy, 15-20 Gy and 150-200 Gy in gamma-ray, $^{12}C^{5+}$ and $^{4}He^{2+}$ irradiation, respectively, balancing on the highest possible dose with a wide mutation spectrum and without compromising the number of fertile plants.

M_2 seeds derived from self-fertilization of 337 M_1 gynomonoecious plants were sown, resulting in segregation of one albino from 10 Gy $^{12}C^{5+}$, one xanta from 250 Gy $^{4}He^{2+}$, and two viridis plants from 10 Gy $^{12}C^{5+}$ and 50 Gy $^{4}He^{2+}$ per M_1 mother plant (Table 2). This indicates that recessive mutants could be obtained in M_2 generation through self-fertilization of gynomonoecious plants in spinach. Based on a relatively higher biological effect of 15-20 Gy $^{12}C^{5+}$, it seems to be an especially good mutagen.

References

1) B. Libert and V. R. Franceschi, J. Agric. Food Chem. 35 (1987) 926-938.
2) Y. Kawazu, M. Okimura, T. Ishii and S. Yui, Scientia Hortic. 97 (2003) 203-210.
3) Y. Ukai, Gamma Field Symposia 29 (1990) 55-68.
4) S. Sugiyama and C. Suto, Bull. Nat. Inst. Agr. Sci. D6 (1964) 211-329 (In Japanese with English summary).
5) T. Nishi and T. Hiraoka, Bull. Hort. Res. Sta. A4 (1965) 153-179 (In Japanese with English summary).
6) Komai, N. Shikazono and A. Tanaka, Plant Cell Rep. 21 (2003) 713-717.
7) N. Hata, , K. Murakami, Y. Yoshida and M. Masuda, J. Japan. Soc. Hort. Sci. 72 (Suppl. 2) (2003) 405 (In Japanese).

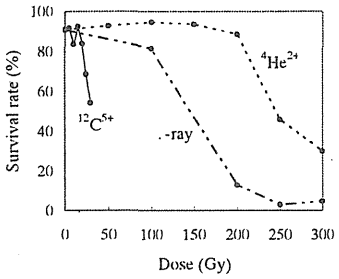

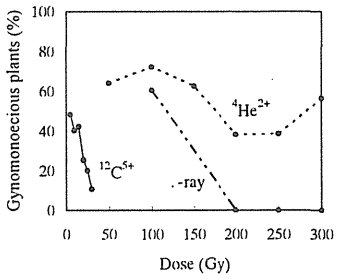

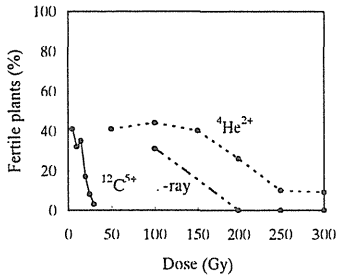

Fig. 1 Percentage of survived M_1 seedlings. **Fig. 2** Percentage of gynomonoecious plants. **Fig. 3** Percentage of fertile plants.

Table 2 Mutation spectrum of M_2 progenies.

Dose	No. of M_1 seeds used for M_2 progeny	No. of M_1 seeds with chlorophyll mutation in M_2 progeny		
		Albino	Xanta	Viridis
.-100	31	0	0	0
C- 5	41	0	0	0
C-10	32	1	0	1
C-15	35	0	0	0
C-20	17	0	0	0
C-25	8	0	0	0
C-30	3	0	0	0
He- 50	41	0	0	1
He-100	44	0	0	0
He-150	40	0	0	0
He-200	26	0	0	0
He-250	10	0	1	0
He-300	9	0	0	0

2.12 Mutation Breeding of *Solanum* Plants by Ion Beam Irradiation

N. Matsuzoe*, T. Umeda*, Y. Hase** and A. Tanaka**
Faculty of Environmental and Symbiotic Sciences, Prefectural University of Kumamoto*,
Department of Ion-beam-applied Biology, JAERI **

1.Introduction

We have carried out mutation breeding of *Solanum toxicarium* to obtain the individual without prickles because it has highly resistance to the soil-born disease and the rootknot nematode[1,2]. However, we were faced with a serious problem. It was made clear that *S. toxicarium* was a self -incompatibility by our experiment. Therefore, the purpose of this experiment had to be changed. We have been studying on the coloring and the anthocyanin biosynthesis of fruit skin of *Solanum* plants. The anthocyanin composition in fruit skin of *S. melongena* is not complex. Two kinds are known as the main anthocyanin at present. They are delphinidin 3-*p*-coumaroylrhamnosylglucoside-5-glucoside (Nasunin) and delphinidin 3-rhamnosylglucoside[3]. Thus, we decided to try to obtain the individual with anthocyanin other than these as main anthocyanin. In this paper, we describe effects of the ion beam irradiation on germination rate and survival rate.

2.Materials and Methods

Solanum melongena cvs. 'Kitta', 'Black Beauty' and 'Kumamotonaga' were used in this experiment. Those dry seeds were irradiated with ion beam (220 MeV $^{12}C^{5+}$) at various doses (25 and 50 Gy) at TIARA. After the irradiation, those seeds were germinated in the vermiculite in the plastic tray in greenhouse. Those seedlings were planted in the field to obtain the seed. The germinating rate and the survival rate were investigated every five days.

3.Results and Discussion

The influences of ion beam irradiation on germination were shown on Fig 1. The germination of all cultivars started in 10 day after seeding. The rates increased, but remained less than 100 %.

The survival rates depended on the cultivars, were 50-100% (Fig.2). The survival rates were about 100% in all cultivars with 25Gy and in 'Kumamotonaga' with 50Gy. The survival rate was the lowest in 'Kitta' with 50Gy, and was 60% or less.

From these results and our previous report[4], It is assumed that the appropriate dose of irradiation for regeneration of *S. melongena* is about 25Gy.

References

1) N. Matsuzoe, H. Okubo and K. Fujieda, J. Japan. Soc. Hort. Sci. 61, 865-872 (1993)
2) M. Ali, N. Matsuzoe, H. Okubo and K. Fujieda, J. Japan. Soc. Hort. Sci. 60, 921-926 (1992)
3) N. Matsuzoe, M. Yamaguchi, S. Kawanobu, U. Watanabe, H. Higashi and Y. Sakata, J.Japan. Soc. Hort. Sci.68, 138-145 (1999)
4) N. Matsuzoe, T. Umeda, Y. Hase and A. Tanaka, TIARA Annual Report 10, 62-63(2002)

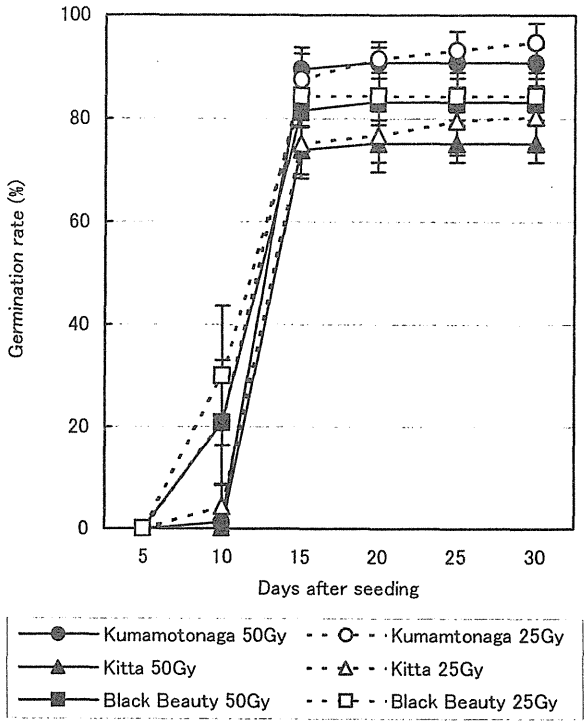

Fig.1 Effect of carbon ion beam on the germination rate of *Solanum melongena*

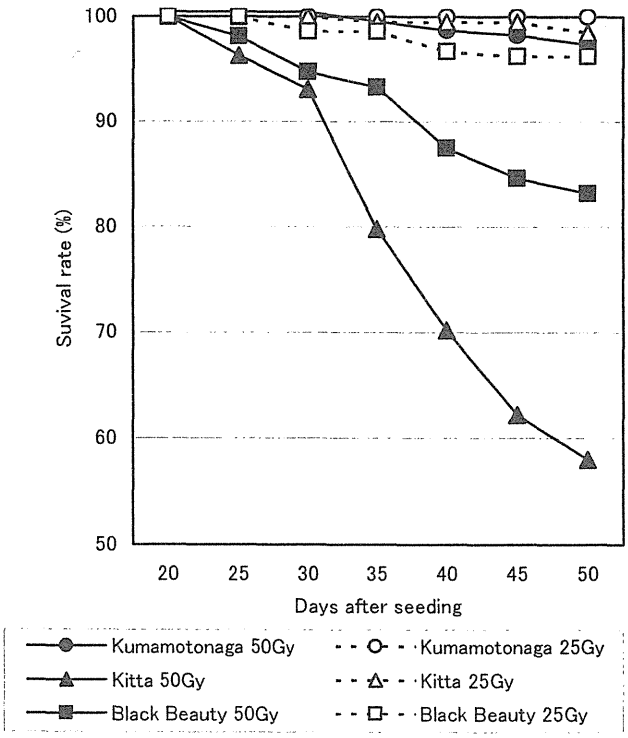

Fig.2 Effect of carbon ion beam on the survival rate of *Solanum melongena*

2.13 Studies on Flower Color and Morphological Mutations from Chrysanthemum In Vitro Explants Irradiated with Ion Beams

T.Sato*, Y.Torigoe*, Y.Hase** and A.Tanaka**
Akita prefecture Agricultural experiment station.*
Department of Ion-beam-applied Biology, JAERI**

1. Introduction

Chrysanthemum is important flower in Akita prefecture. Especially chrysanthemum cultivar "Natsuyasumi" (purpulish red flower) is suited for the climate of Akita prefecture. However, producer, market and consumer were demanded for yellow or white color cultivar.

Ion beam is expected as a new and efficient mutagen for plant mutation breeding. In flower color of chrysanthemum, it has been reported that mutants were regenerated from in vitro explants irradiated with ion beam[1].

By the last year, we examined an adequate dose for "Natsuyasumi" flower culture materials[2]. As a result, white flower color mutants were obtained with 20Gy $^{12}C^{6+}$ ion beam or 50Gy soft X ray irradiation[3](Fig.1).

However, some red remained at the center and the edge of a flower. Therefore, these white flower color mutants are not character of a purpose.

In this paper, we re-irradiated ion beam or soft X ray to node culture of a selected white flower color mutant.

2. Materials and Methods

We used the explants of node of the intact white flower color mutant on medium in petri dish, which selected from irradiated a 50Gy soft X ray or 20Gy $^{12}C5^{+}$ ion beam. In these, re-irradiated a 50Gy soft X ray or 20Gy $^{12}C^{5+}$ ion beam from the TIARA AVF cyclotron in JAERI. The energy of $^{12}C^{5+}$ was 220MeV.

In order to compared these treatments, "Natsuyasumi" node or petal irradiated with ion beams, soft X rays and gamma rays.

After the re-irradiation or irradiation, the cultured materials were transferred to a new medium and obtained regeneration plants. After acclimation, we transplantated regeneration plants to field. In flowering time, we selected flower color mutants.

3. Results and Discussion

3.1 Re-irradiation to a white flower color mutant by soft X ray irradiation.

In case of soft X ray, low plant length mutant was obtained. And in case of ion beam, light leaf color mutant was obtained.

3.2 Re-irradiation to a white flower color mutant by ion beam irradiation.

In case of both soft X ray and ion beam , low plant length or light leaf color mutants were obtained. In them, one mutant had both characters.

3.3 Irradiation to a "Natsuyasumi".

In case of both soft X ray and gamma ray, low plant length mutants were obtained. In gamma ray, light leaf color mutant was also obtained.

In case of both soft X ray and ion beam,

flower color mutants were obtained. But, the color was darker or lighter than a "Natsuyasumi", and it is not white or yellow.

In this paper, we were not able to get useful mutants. However, irradiation of ion beam or soft X ray is effective for induction of flower color mutant in chrysanthemum. Therefore, we continue soft X ray and ion beam irradiation to selected white flower color mutant.

References

1)S.Nagatomi, A.Tanaka, A.Kato, H.Watanabe and S.Tano, TIARA Annual Report (1995) 50-52.

2)T.Sato, H.Naganoma, Y.Hase and A.Tanaka, JAERI-Review 2002-035 (2002) 68-69..

3)T.Sato, Y.Torigoe, Y.Hase and A.Tanaka, JAERI-Review 2003-033 (2003) 81-82.

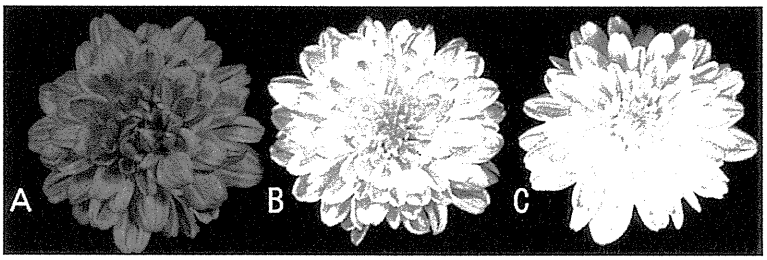

Fig.1 Selected white flower color mutants.
A : "Natsuyasumi" (Control) B : Soft X ray, 50Gy (regenerated from node)
C : $^{12}C^{6+}$ ion beam, 20Gy (regenerated from petal)

Tab.1 Mutant obtained in X ray or ion beam irradiated or re-irradiated chrysanthemum materials.

material	treatment	part	No. of plant	Flower color				No. of low Plant length	No. of light leaf color
				dark	light	white	yellow		
Natsuyasumi	Soft X ray	Node	400		1			2	
		Petal	23		2				
	Gamma ray	Node	100					8	1
	Ion beam	Node	640						
		Petal	36	2	4				
X-ray induced Mutant	Soft X ray	Node	150					1	
	Ion beam	Node	125						1
Ion beam induced Mutant	Soft X ray	Node	150					3	2
	Ion beam	Node	125					5	2

2.14 Induction of Mutations Affecting Bolting Time by Ion Beam Irradiation to Calluses of Japanese Bunching Onion (*Allium fistulosum L.*)

M. Kondo*, N. Hamato**, Y. Hoshi*, H. Kobayashi*, Y. Hase***, N. Shikazono*** and A. Tanaka***

Department of Biotechnology, Niigata Agricultural Research Institute *

Horticultural Research Center, Niigata Agricultural Research Institute **

Department of Ion-beam-applied Biology, JAERI***

1. Introduction

Japanese bunching onion (*Allium fistulosum L.*) is main vegetable alliums in Japan as well as garlic, onion, etc. In recent years, import of too cheap Japanese bunching onion from China increased rapidly. That has been interfering with Japanese bunching onion market in Japan, and we are forced to take prompt measures to deal with the problem. The flower-bud formation of Japanese bunching onion is induced by encountering low temperature and short-day in winter. And, the bolting and the blooming are induced by encountering high temperature during spring. The bolting lowers the market value of Japanese bunching onion, because the flower stalk is not only hard to eat but also ruin the appearance. Therefore, a mutant variety of Japanese bunching onion that bolts at late time or does not bolt is profitable for the producers.

Ion beam irradiation is suitable for improving only one property like the bolting-time of Japanese bunching onion because ion beams have higher Linear Energy Transfer (LET), compared to that of X-rays and gamma-rays. And, it has been reported that chimeric plants hardly regenerated from calluses after induction of mutation[1]. Therefore, we adopted the calluses of Japanese bunching onion as the material for the ion-beam irradiation. We determined that the dose of 0.5 Gy of $^{12}C^{6+}$ was appropriate for obtaining mutants, which changed a single property[2].

In this study, we regenerated the plants from the irradiated calluses and investigated the bolting time.

2. Materials and Methods

2.1 Plant material

The calluses were induced from the seed of Japanese bunching onion cultivar "Tokyo natsuguro nigou".

2.2 Ion beam irradiation

The calluses were crushed to about 1.0 mm diameter by squashing on stainless steel sieves of 0.98 mm mesh (the mesh size of 20 or less). The crushed calluses were covered with sterilized Kapton film (7.5 μm in thickness, Toray-Dupon, Japan), and exposed to 320 MeV $^{12}C^{6+}$ beam with the dose of 0.5 Gy.

2.3 Regeneration and investigation

The ion beam-exposed calluses were cultured in the liquid callus proliferation medium for 3-6 weeks and then on the regeneration medium for 2 months under 16 hr light/8 hr dark at 25°C. The regenerated shoots were acclimated in a greenhouse and planted in a field during from June to July 2003.

For the control, seedlings of Japanese bunching onion cultivars "Tokyo natsuguro nigou" which had not been exposed to ion beam, were planted in the field in June 2003.

In spring of 2004, we investigated the bolting time of those Japanese bunching onions every 7 days.

3. Results and Discussion

About 5,000 M1 plants exposed to $^{12}C^{6+}$ were planted and grown in a field (Fig. 1A). Three M1 plants bolted in autumn of the year of planting, although the control plants never bolt in this period (Fig. 1B).

The control plants bolted during from March to April but the M1 plants bolted during from March to May (Fig.1C, Table 1). We selected 31 M1 plants, which showed delayed bolting time and had normal appearance. These plants will be self pollinated and resulting M2 plants will be tested again for bolting time.

These results suggest that the ion beam can induce mutations affecting the bolting time of Japanese bunching onion without causing undesirable changes.

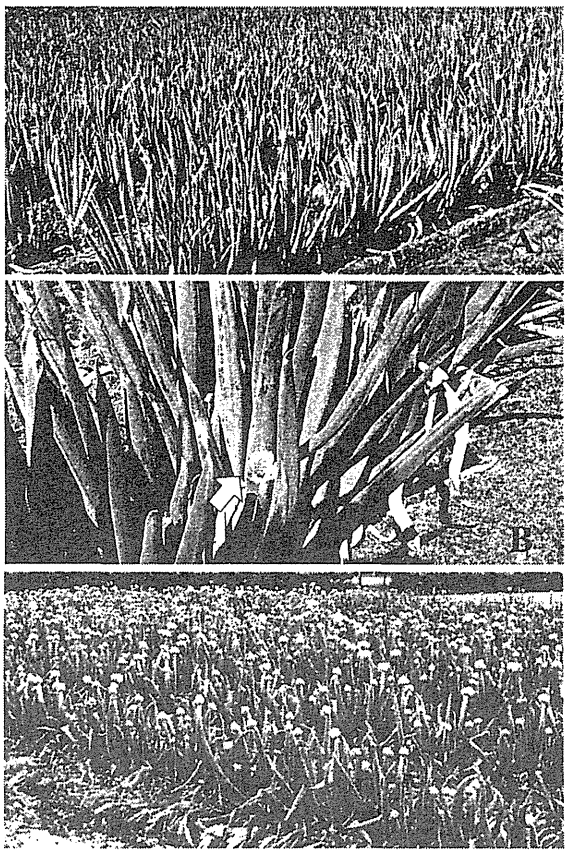

Fig. 1 Ion beam-irradiated M1 plants of "Tokyo natsuguro nigou" were planted and grown in a field in order to investigate the bolting time.
A: The M1 plants grown for 3 months on October 7, 2003.
B: The M1 plants, which bolted in autumn of the year of planting (arrow).
C: The M1 plants in spring after one year from planting.

References
1) S. Nagatomi, E. Miyahira and K. Degi, Gamma Field Symposia 35 (1996) 51-69.
2) M. Kondo, Y. Hoshi, H. Kobayashi, Y.Hase, N. Shikazono, A. Tanaka, TIARA Annual Report 2002 (2003) 83-85.

Table 1 Bolting time of ion beam-irradiated M1 plants and non-irradiated plants.

Bolting time	Irradiated "Tokyo natsuguro nigou"		Non-irradiated "Tokyo natsuguro nigou"
3/13～ 3/19	22		1
3/20～ 3/26	121		1
3/27～ 4/ 2	733		13
4/ 3～ 4/ 9	587		5
4/10～ 4/16	1020		9
4/17～ 4/23	842		10
4/24～ 4/30	488		1
5/ 1～ 5/ 7	356		0
5/ 8～ 5/14	114	(13)	0
5/15～ 5/21	40	(15)	0
5/22～ 5/28	5	(3)	0
5/29～ 6/ 4	0		0
Total	4328	(31)	40

( ) = Number of selected plants for self-pollination in order to obtain late- or non-bolting M2 mutants

2.15 Isolation of UV-sensitive or Resistant Rice (*Oryza sativa*) Mutants

J. Hidema*, Y. Takahashi*, M. Yamamoto*, Y. Hase**, A. Sakamoto**,
A. Tanaka** and T. Kumagai*
Graduate School of Life Sciences, Tohoku University*,
Department of Ion-beam-applied Biology, JAERI**

1. Introduction

UV-B radiation can damage plants, decreasing growth and productivity[1]. Over a five-year period, we investigated the effects of supplementary UV-B radiation on the growth and yield of Japanese rice cultivars in the field in a cool rice-growing region of Japan[2]. The findings of that study indicated that supplementary UV-B radiation has inhibitory effects on the growth and grain development of rice. Furthermore, we investigated the sensitivity to UV-B radiation of rice cultivars of 5 Asian rice ecotypes, and found that (1) rice cultivars vary widely in UV-B sensitivity[3], (2) among the Japanese rice cultivars, Sasanishiki exhibited resistance to UV-B radiation, while Norin 1 was less resistant, although these cultivars are closelyrelated[4),5].

To date, we found that (1) two or more genes controlled the difference of sensitivity to UV-B between these rice cultivars[6], (2) putative quantitative trait loci (QTL) associated with the resistance to supplementary UV-B radiation in rice were detected on chromosomes 1, 3 and 10 at least[7], (3) Cyclobutane pyrimidine dimer (CPD), which is major DNA damages induced by UV-B, photolyase could be one of the main factors in determining the UV-B sensitivity in rice cultivars[8]. However, it is unclear the origin of the differences in UV-B sensitivity among rice cultivars.

The aim of our study is to clarify the molecular origin of the sensitivity to UV-B for improving UV-B resistance in plants by bioengineering or breeding programs. In order to make it, identifying rice mutants with increased or decreased UV-B resistance can help our study powerfully. Heavy ion beams, such as carbon ions, are more effective in plants for inducing mutations compared with electron beam (Shikazono et al. unpublished data). Novel mutants have been obtained by the carbon ion irradiation in several plant species[9].

The aim of this study is to isolate UV-B hyper-resistant or hyper-sensitive rice mutants induced by carbon ion irradiation.

2. Experimental procedure

2.1 Plant material and irradiation method

Dry rice seeds of Sasanishiki (*Oryza sativa* L.) were used. About 150 seeds were placed upward embryo on petri dish. The Irradiation Apparatus for Seed, connected to a vertical beam line of the AVF-cyclotron (JAERI, Takasaki), was used for the 320 MeV carbon-ion irradiation. We had found that the optimum radiation dosege for inducing mutations in rice "Sasanishiki" was 80 Gy[10]. Thus, the carbon-ion irradiation with the doses of 80 Gy was performed under atmospheric pressure within 3 min.

2.2 Mutant isolation

About 2,500 M1 seeds were grown to maturity and harvested. Twenty M2 seeds derived from each M1 plant were used for the first screening of root bending assay as follows. The root bending assay followed the method described by Britt et al.[11] Four-day-old seedlings vertically grown on 1.5% agar plate under visible radiation (350 μmol m^{-2} s^{-1}) were exposed to UVB radiation at a rate of 8.4 kJ m^{-2} (1.2 W m^{-2} for 2 h). After the exposure, the plate were rotated by 90° and incubated for 4 d under visible radiation. Then,

the length of new root growth after UVB exposure was measured. The eight candidates that showed the longer root length than that of wild type "Sasanishiki" and the ten candidates that showed the shorter root length than that of wild type were isolated from 50,000 M2 plants. These lines were further grown individually under normal conditions, self-pollinated and harvested to yield M3 families. Second and third screening was carried out using 10 to 20 seeds of the M3 or M4 progenies by the methods of long-term exposure assay (as follows) and root bending assay. Ten seeds of each candidate, soaked in water at 30°C for 2 d, were sown in pots containing fertilized soil in a large growth cabinet (Tabai Espec Ltd., Osaka, Japan)[12], with a 12/12 hr photoperiod, with temperatures at 27/17°C, irrespectively. Five seedlings were grown in each pot under visible light with or without supplementary UVB radiation for 30 days. The photosynthetic active radiation was adjusted to about 350 μmol m^{-2} s^{-1} at the top of the plants. Plants receiving UVB were subjected to the same photoperiod with visible radiation, and the UVB intensity at the plant level was 1.12 W m^{-2}. Growth analysis included the determination of the plant height, number of tillers and fresh weights of the aboveground parts of the plants.

2.3 ELISA

The induction and repair of CPD and (6-4) photoproducts ([6-4] pp) were analyzed by ELIZA. CPDs and (6-4) pp were detected by the specific antibodies TDM-2 and 64M-2, respectively. To induce CPD, the detached third fully expanded leaves were placed on wet filter paper and irradiated with unfiltered UVB radiation emitted from a UV-B-fluorescent tube (FL20SE; Toshiba, Tokyo, Japan) at a rate of 0 to 10 W m^{-2} for 15 min. For repair experiments, the detached leaves were exposed 4.5 kJ m^{-2} of UVB. Immediately after UVB exposure, the leaves were exposed to blue irradiation (60 μmol m^{-2} s^{-1}) from blue fluorescent tubes (20B-F, Toshiba, Tokyo, Japan) or kept in a light-tight box immediately after the UVB exposure. After exposure of UVB or blue radiation, the leaves were harvested immediately and stored in liquid nitrogen until being analyzed. All subsequent manipulations were carried out in red light to minimize uncontrolled photoreactivation. Rice DNA was extracted from each sample, fifty microliters of the extracted DNA was placed in each well. The DNA concentration was adjusted to 0.5μg ml^{-1} for TDM-2 and 3 μg ml^{-1} for 64 M-2. The ELISA procedure was described in detail elsewhere[13].

3. Results and Discussion

A total of 2,500 dry rice seeds were irradiated with a carbon ion beam and then germinated. After flowering, the plants were self-pollinated and the M2 seeds were harvested. The eight candidates that showed the longer (less than 20%) root length than that of wild type "Sasanishiki" (UV-resistant) and the ten candidates that showed the shorter (less than 20%) root length than that of wild type (UV-sensitive) were selected by root bending assay from about 50,000 M2 plants. To confirm genetic stability of UVB sensitivity, the candidates of the M2 through M4 generation were tested for UVB sensitivity by both a long-term exposure assay and root bending assay. Up to data, among them, one mutant line, named *UV sensitive* (*uvs*), was established to be UVB sensitive mutant (Figure 1).

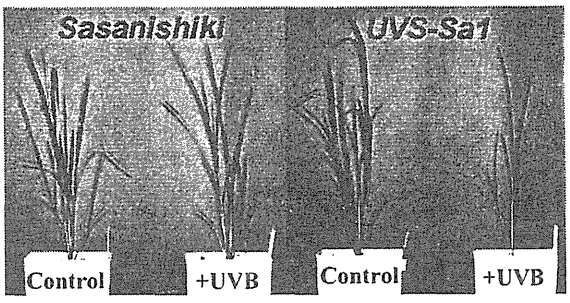

Figure 1. Effects of supplementary UVB radiation on the growth of wild-type "Sasanishiki" and UV-sensitive mutant "UVS-Sa1"

Under visible radiation alone, the mutation of *uvs-Sa1* did not affect the growth. In contrast,

when these strains were grown under supplementary UVB radiation, plant length, tiller number and fresh weight of the *uvs-Sa1* were markedly retarded in comparison with wild type "Sasanishiki".

We next examined to test whether the molecular origin of the *uvs-Sa1* is deficient of CPD or (6-4) pp photolyase activity, which is thought to play a role in coping with UVB-induced damages. To determine the susceptibility to CPD or (6-4) pp induction, the detached leaves were exposed to 0 to 10 kJ m^{-2} of challenge UVB radiation. UVB radiation produced similar levels of CPD or (6-4) pp in both strains. There was no difference in the susceptibility to CPD or (6-4) pp induction between both strains (data not shown). Our previous data showed that there was a significant correlation between the CPD levels induced by challenge UVB exposure and the amount of UV-absorbing compounds in rice leaves. Thus, mutation in *uvs-Sa1* could not affect the amount of UV-absorbing compounds. Furthermore, we found that there was no difference in the ability of photorepair of CPD or (6-4) pp between wild type and *uvs-Sa1* (Figure 2).

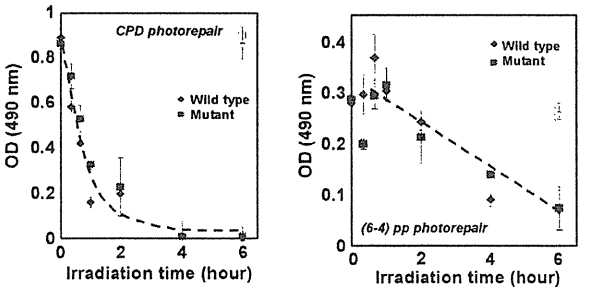

Figure 2 CPD and (6-4) photoproducts photorepair abilities in wild type (Sasanishiki) and UV-sensitive mutant (UVS-Sa1).

These results indicate that the mutation of unknown factor(s) for determining UVB sensitivity could lead to UVB sensitivity in *uvs-Sa1*. We are interested in what factors other than the CPD photolyase would effectively act to increase the UVB-sensitivity in rice, a question of which should be answered in the near future.

Acknowledgement

We thank Dr. T. Mori for providing the antibodies TDM-2 and 64M-2. This work was supported by Grants-in-Aid for Scientific Research from the Ministry of Education, Culture, Sports, Science and Technology, Japan (14704060 and 15201010).

References

1) A. Teramura, Physiologia Plantarum 58 (1983) 415-427.
2) T. Kumagai, J. Hidema, H. S. Kang and T. Sato, Agriculture, Ecosystems and Environment 83 (2001) 201-208.
3) T. Sato and T. Kumagai, Journal of Breeding 43 (1993) 61-68.
4) T. Kumagai and T. Sato, Journal of Breedng 42 (1992) 545-552.
5) J. Hidema, H-S. Kang and T. Kumagai, Plant and Cell Physiology 37 (1996) 742-747.
6) T. Sato, H. S. Kang and T. Kumagai, Physiologia Plantarum 91 (1994) 234-238.
7) T. Sato, T. Ueda, Y. Fukuta, T. Kumagai and M. Yano, Theoritical and Applied Genetics 107 (2003) 1003-1008.
8) J. Hidema, T. Kumagai and B. M. Sutherland, Plant Cell 12 (2000) 1569-1578.
9) Y. Hase, A. Tanaka, T. Baba and H. Watanabe, Plant Journal 24 (2000) 21-32.
10) J. Hidema, M. Yamamoto, Y. Hase, A. Sakamoto, A. Tanaka and T. Kumagai, JAERI-Review 2003-33, (2003) 85-87.
11) A.B. Britt, J.J. Chen, D. Wykoff and D. Mitchell, Science 261 (1993) 1571-1574.
12) J. Hidema, T. Kumagai, J. C. Sutherland and B. M. Sutherland, Plant Physiology 113 (1997) 39-44.
13) Y. Takeuchi, M. Murakami, N. Nakajima, N. Kondo and O. Nikaido, Plant and Cell Physiology 37 (1996) 181-187.

2.16 Mutation Induction in Melampodium and Petunia by Ion Beam Irradiation

M. Kato*, S.Kageyama*, T. Haketa*, M. Fukushima*,
Y. Hase** and A. Tanaka**
Takii Plant Breeding & Experiment Station*
Department of Ion-beam-applied Biology, JAERI**

1.Introduction

Ion beams have higher LET(linear energy transfer) and bring intensive RBE(relative biological effectiveness) than γ -rays and X-rays. By the irradiation with heavy ion beams, specific flower color, flower shape, and male sterile mutants were induced in several flowers.[1) 2) 3)]

In this study, we investigated the effect of ion beam irradiation on induction of mutants in Melampodium and Petunia.

2.Materials and Methods

2.1 Melampodium

Seeds of Melampodium 'Million Gold' were used in this study. Seeds were irradiated with 320MeV carbon(C) and 50MeV helium (He) ion at various doses (C-ion:20 to 120Gy, He-ion:50 to 300Gy).

After the irradiation, seeds were planted in a green house. Survival rate of the irradiated seeds was determined at 60 days after germination.

Plants that were irradiated the adequate dosages were cultivated farther and produced seeds by self-crossing. All the seeds produced (M_2 generation) were planted in field and allowed selection.

The selected plants produced seeds by self-crossing. The seeds produced (M_3 generation) were planted in greenhouse and investigated in several characters.

2.2 Petunia

The internodes where the diameters were less than 2mm of plant cultured on MS (Murashige and Skoog, 1962) solid medium were used.

The 7mm-length internodes which were laid on MS solid medium modified with 0.1mg/l NAA, 1.0mg/l BAP, and 30g/l sucrose were irradiated with 320 MeV C-ion beam at the doses of 2 to 50 Gy. After the irradiation, they were subcultured on the same medium.

The rate of producing of plantlets per internode was determined.

Plantlets that were irradiated the adequate dosages were acclimatized.

We selected some mutants from the group.

3.Results and Discussion

3.1 Melampodium

As an aspect of 50% lethal dose, the C-ions showed approximately 4 times greater than the He-ions effectively (Fig.1).

We adopted 40 and 100Gy as the adequate dosages for C-ion and He-ion to obtain mutants efficiently.

We selected 'pale flower' 'large flower' 'semi-double flower' 'cleft petal' 'dwarf' and 'large serration' mutants (Tab.1). 'Pale flower' 'large flower' 'cleft petal' 'dwarf' and 'large serration' mutants were observed both in the C-ion

and the He-ion irradiated plot. In other hand 'semi-double flower' mutant are observed only in the He-ion irradiated plot. The 'semi-double flower' mutant and one of the 'dwarf' mutants (all of them were induced by He-ion) were sterile.

The M_3 generations of 'dwarf' and 'large flower' mutants had significant difference to original variety at several characters contributed the selections (Tab.3 Tab.4).

The M_3 generations of 'large serration' mutant had significantly slender leaf compare to original variety at first node of lateral branch (Tab.5).

The M_3 generations of 'pale flower' mutant had it color flowers as M_2 plant.

The petal shape of the 'cleft petal' mutant's M_3 generations was not different from original variety.

The M_3 generations of 'pale flower' mutants and 'large serration' mutants had significantly short petals compare to original variety.

3.2 Petunia

We adopted 1.0Gy as the adequate dosages (Fig.2). We cultivated 0.5Gy, 1.0Gy, 1.5Gy irradiated plants 134, 424 and 604 respectively. We gained some mutants showing different flower color, dwarf and tiny flower and mottled leaf (Tab.2).

We propagated the mutants vegetatively and planted in field.

We are investigating these mutants farther.

References

1) M.Okamura, M.Ohtsuka N.Yasuno, T.Hirosawa, A.Tanaka, N.Shikazono, Y.Hase and M.Tanase, JAERI-Review 2001-039(2001) 52-53

2) K.Suzuki, Y.Yomo, T.Abe, Y.Katsumoto, K.Miyazaki, S.Yoshida and T.Kusumi, RIKEN Accel.Prog.Rep. 35,129(2002)

3) H.Yamaguchi, S.Nagatomi, A.Tanaka N.Shikazono,T.Morishita and K. Degi, Jaeri-Review 2000-24(2000) 41-42

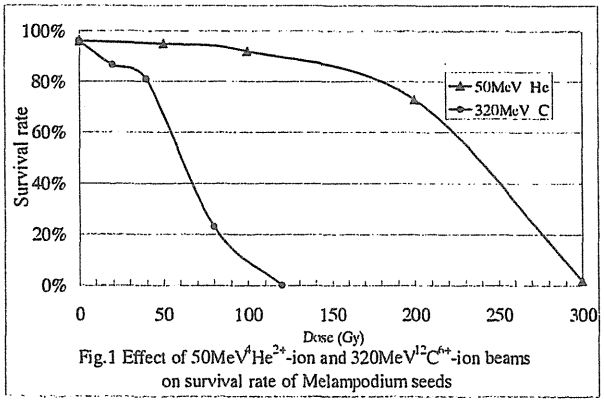

Fig.1 Effect of 50MeV$^4He^{2+}$-ion and 320MeV$^{12}C^{6+}$-ion beams on survival rate of Melampodium seeds

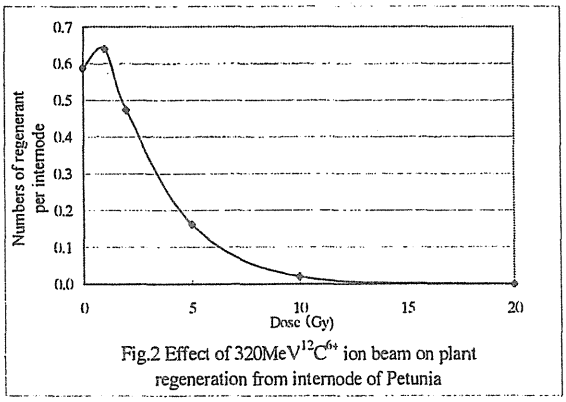

Fig.2 Effect of 320MeV$^{12}C^{6+}$ ion beam on plant regeneration from internode of Petunia

Tab.1 Number of selected Melampodium mutants induced by ion beam irradiation

Radiation and dose (Gy)	Numbers of tested M_2 lines	Selected character and numbers					
		Flower color	Large flower	Flower shape	Leaf shape	dwarf	total
320MeV$^{12}C^{6+}$ 40Gy	81	1	1	1	1	1	5
50MeV$^4He^{2+}$ 100Gy	92	1	2	2	1	2	8

Tab.2 Number of selected Petunia mutants induced by 320MeV $^{12}C^{6+}$ ion beam irradiation

Dose(Gy)	Tested plants	Selected character and numbers				
		Flower color	Mottled leaf	dwarf	Early flowering	total
0	398	0	0	0	0	0
0.5	134	0	1	0	0	1
1.0	424	2	0	1	0	3
1.5	604	0	0	0	1	1

Tab.3 The characters of Melampodium M_3 generation contribute to dwarf

Line No.	Radiation and dose	Character of selection	Node of first flower	Node's height of first flower(mm)	Length of peduncle (mm)	Height of first flower (mm)
Original			3.9± 0.3	50.4±11.1	46.4±18.0	96.9±24.0
No. 1	C 40Gy	dwarf	3.6± 0.5 *	42.3± 7.7 **	39.2±11.4	81.5±11.0 **
No. 2	C 40Gy	large serration	4.0± 0.2	52.4± 5.0	37.0± 8.1 *	89.5± 8.0
No. 3	C 40Gy	pale flower	3.8± 0.4	37.5± 5.7 **	40.6±13.6	78.1±13.8 *
No. 4	C 40Gy	large serration	3.6± 0.5 *	46.3±10.6	48.9±10.1	95.1±14.1
No. 5	C 40Gy	large flower	3.4± 0.5 **	46.3± 8.9	58.1±12.5 *	104.4± 6.7 **
No. 6	He 100Gy	pale flower	4.0± 0.2 *	48.0± 4.7	44.8± 8.5	92.8± 9.4
No. 7	He 100Gy	large flower	3.6± 0.5 *	52.0± 8.0	48.1±16.9	100.1±12.2
No. 8	He 100Gy	large flower	3.7± 0.5 *	46.1± 9.5	48.1±10.2	94.3± 6.5
No. 9	He 100Gy	cleft petal'	3.9± 0.3	51.4± 9.2	46.9±12.8	98.3±11.3
No.10	He 100Gy	dwarf	3.6± 0.5 **	51.5±10.8	50.5±17.4	102.0±12.6*
No.11	He 100Gy	large serration	3.6± 0.5	40.6± 5.4 *	46.4±20.8	87.0±24.9

* P<0.05 ** P<0.01

Tab.4 The characters of Melampodium M_3 generation contribute to flower size

Line No.	Radiation and dose	Character of selection	Diameter of flower(mm)	Length of ray floret(mm)	Diameter of inflorescence(mm)
Original			29.8± 4.0	11.7± 0.9	7.3± 0.8
No. 1	C 40Gy	dwarf	31.0± 2.2	11.8± 1.2	7.7± 1.0
No. 2	C 40Gy	large serration	31.1± 2.6	11.6± 1.0	7.9± 0.6 **
No. 3	C 40Gy	pale flower	27.8± 1.8	10.4± 1.0 **	7.1± 0.9
No. 4	C 40Gy	large serration	28.3± 1.8	10.1± 1.0 **	7.3± 0.9
No. 5	C 40Gy	large flower	32.0± 3.2	11.8± 1.2	8.2± 0.9 **
No. 6	He 100Gy	pale flower	30.4± 3.1	11.0± 1.3 *	7.6± 0.8
No. 7	He 100Gy	large flower	32.9± 2.1 **	12.3± 1.3	8.1± 0.7 **
No. 8	He 100Gy	large flower	31.6± 2.2	11.6± 1.1	8.4± 0.8 **
No. 9	He 100Gy	cleft petal'	33.1± 1.8 **	11.9± 0.9	8.1± 0.6 **
No.10	He 100Gy	dwarf	31.4± 2.3	11.4± 1.0	8.3± 0.8 **
No.11	He 100Gy	large serration	27.6± 1.6	10.0± 0.9 *	7.2± 0.4

* P<0.05 ** P<0.01

Tab.5 The characters of Melampodium M_3 generation contribute to leaf shape

Line No.	Radiation and dose	Character of selection	Width of leaf(mm)	Length of leaf(mm)	Ratio of length/width
Original			54.1± 8.2	87.4± 9.9	1.6± 0.2
No. 1	C 40Gy	dwarf	48.0± 3.8 **	77.0± 5.1 **	1.6± 0.1
No. 2	C 40Gy	large serration	46.8± 9.7 **	84.1± 5.5	2.4± 3.3
No. 3	C 40Gy	pale flower	48.8± 6.7	80.4± 7.1 *	1.7± 0.2
No. 4	C 40Gy	large serration	37.9± 9.2 **	78.8±11.9 **	2.2± 0.5 **
No. 5	C 40Gy	large flower	49.2± 6.6 *	83.7± 9.0	1.7± 0.2
No. 6	He 100Gy	pale flower	50.7± 5.8	86.5± 7.2	1.7± 0.2
No. 7	He 100Gy	large flower	52.4± 7.0	85.9± 8.2	1.6± 0.1
No. 8	He 100Gy	large flower	49.9± 6.4 *	82.3± 6.6 *	1.7± 0.2
No. 9	He 100Gy	cleft petal'	51.9± 8.5	87.0± 9.6	1.7± 0.3
No.10	He 100Gy	dwarf	46.0± 7.6 *	81.9± 9.3	1.8± 0.1 **
No.11	He 100Gy	large serration	38.5± 8.1 **	76.3± 9.5 **	2.0± 0.3 **

* P<0.05 ** P<0.01

2.17 Research on the Production of Mutants in *Cephaelis ipecacuanha* A. Richard which is a Source of the Expectorant as a First Aid

S. Isogai*, Y. Hase**, A. Tanaka** and K. Shimomura*
Graduate School of Life Sciences, Toyo University*
Department of Ion-Beam-applied Biology, JAERI**

1. Introduction

Cephaelis ipecacuanha A. Richard (Rubiaceae) is one of the important medicinal plants and its dried roots are commonly used as an expectorant, an emetic and an amoebacide. In recent years, ipecac syrup have been used as vomiting reagents for the first aid in Japan, therefore stable supply of ipecac is desired. The efficient methods of propagation through tissue culture have been studied such as shoot multiplication[1], adventitious shoot formation on the internodal segment[2] and adventitious root[3].

Since ipecac is a tropical plant, it is difficult to cultivate this plant in Japan except for the warm districts in winter[4]. Therefore, it is important to improve the characteristic of ipecac, showing good growth and proliferation under tropical condition, to cultivate it in the climate of Japan. We have started to produce the mutants, such as non-low temperature sensitive clone and high-alkaloid producing clone, by ion beam irradiation.

2. Experimental procedure

2.1 Plant material

Cephaelis ipecacanha shoots used for the experiment were maintained on phytohormone free (HF)-Gamborg B5[5] (B5) solid medium. In order to obtain sufficient shoot material for the experiment, the shoots were transferred onto B5 solid medium supplemented with 0.5 mg/L GA_3, and cultured at 25 °C under the dim light for 4 weeks.

2.2 Medium and culture condition

The media used for the experiments, proliferation of shoots and induction of adventitious buds, were adjusted to pH 5.7 before addition of 0.2 % Gelrite, and then was autoclaved at 121 °C for 15 minutes. The cultures were incubated at 25 °C under 14 h/day dim light (7~ 8 $\mu Em^{-2} S^{-1}$).

2.3 Induction of adventitious shoot formation and ion beam irradiation

Internodal segments (*ca.* 6 mm in length) of shoots cultured on B5 solid medium supplemented with or without 0.5 mg/L GA_3 were placed horizontally on WP solid medium supplemented with 0.01 mg/L N^6-benzyladenine (BA) and cultured at 25 °C under 14 h/day dim light.

After 3 weeks of culture, internodal segments were exposed to 320 MeV C ion beams of 0.5 to 200 Gy using the AVF cyclotron in TIARA. Before the irradiation, the plastic covers of the petri dishes were replaced with kapton film. Next day of the exposure, internodal segments exposed to ion beams were

transferred onto fresh medium and cultured. After 12 weeks of the exposure, adventitious shoots formed on the internodal segments were isolated and then cultured on HF-B5 solid medium at 25 °C under 14 h/day dim light. After 6 weeks of culture, all leaves developed were used for quantitative analysis of emetic alkaloids by HPLC.

2.4 Alkaloid extraction

Extraction method reported by Yoshimatsu and Shimomura[7] was slightly modified to quantify the emetic alkaloids by HPLC. Briefly, samples (*ca.* 5 mg) lyophilized individually were accurately weighed and crushed in the small test tube. The samples thus prepared was mixed with 100 μl of 10 % NH_4OH for 1 min then extracted with 3 ml of ether for 5 min using a voltex. The extract was filtrated with the cotton plug and concentrated under a N_2 gas stream, then further dried *in vacuo*.

2.5 HPLC analysis

The extract prepared as mentioned above was dissolved in 100 μl of MeOH and quantitatively analyzed by HPLC according to the method reported[7]. Analytical conditions were as follow, TSK gel ODS-120A (4.6 i.d. x 250 mm) with 10 mM1-heptanesulfonic acid sodium salt (adjusted to pH 4.0 with 2 % phosphoric acid)-CH_3CN (67: 33) as mobile phase, monitoring absorbance at 285 nm. The flow rate was 1.0 ml/min throughout the analysis.

3. Results and discussion

Ipecac shoots were propagated to obtain sufficient materials for excising internodal segments. Survival rate (Fig. 1A), adventitious shoot formation rate (Fig. 1B) and No. of adventitious shoots formed (Fig. 2) per internodal segment were examined. Internodal segments exposed to C ion beams of more than 50 Gy turned brown (Fig. 1A). Though both survival rate and adventitious shoot formation varied in the range of low doses (0.5~ 10 Gy), No. of adventitious shoots formed on the internodal segments decreased at dose 10 Gy, and in internodal segments exposed to C ion beams of more than 20 Gy, no adventitious shoots were

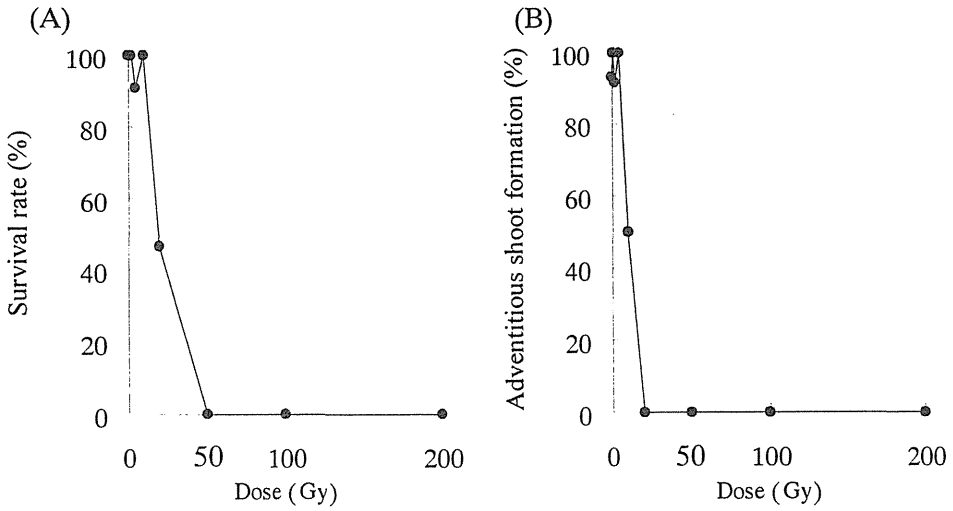

(Fig. 1) Survival rate and adventitious shoot formation on internodal segments exposed to different doses of C ion beam

formed (Fig. 1B and 2). Because decrease of adventitious shoot formation rate and No. of adventitious shoots per segment with 10 Gy exposure were observed. It was considered that this dose inhibited the adventitious shoot formation.

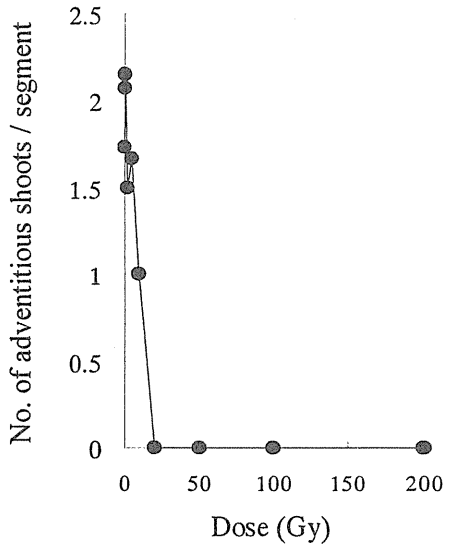

(Fig. 2) Adventitious shoot formation after exposure to C ion beam

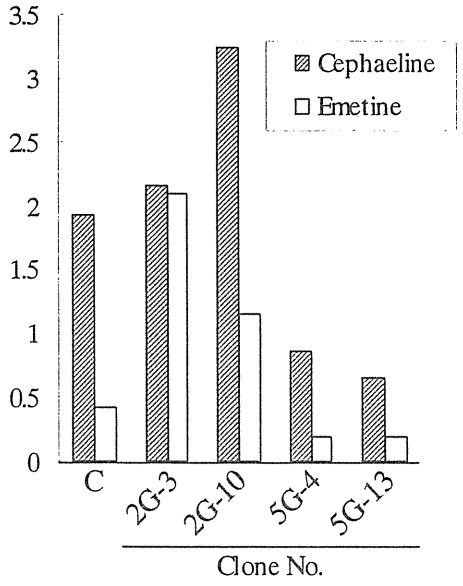

(Fig. 3) Alkaloid contents in regenerates from internodal segments exposed to C ion beam

Alkaloid contents of the regenerated shoots were analyzed by HPLC. Some shoots exhibited higher or lower alkaloid contents compared to the control. Among the clones examined, it is of interest that the clone showing high content of emetine compared to that of the control was found (Fig. 3).

When internodal segments were exposed to C ion beams of more than 2 Gy, the shoots which showed different alkaloid contents compared to the control were obtained.

It was considered that C ion beams of 5 to 10 Gy was suitable for inducing mutation. Investigation of the shoots having different feature is in progress.

References

1) K. Yoshimatsu and K. Shimomura, Plant Cell Reports, **7**: 288-291 (1998)
2) K. Yoshimatsu and K. Shimomura, Plant Cell Reports, **9**: 567-570 (1991)
3) K. Yoshimatsu and K. Shimomura, Plant cell Reports, **14**: 98-101 (1994)
4) K. Yoshimatsu, K. Aoi and K. Shimomura, J. Plant Physiol., **144**: 22-25 (1994)
5) O. L. Gamborg, R. A. Miller and K. Ojima, Exp. Cell Res., **50**: 151-158 (1968)
6) Lloyd, G. and McCown, B., Int. Plant Propag. Soc. Combd.Proc., **30**: 421-427 (1980)
7) K. Yoshimatsu and K. Shimomura, Phytochemical Analysis, **4**: 217-219 (1993)

2.18 Induction of Mutations by Ion Beam Irradiation on the *Saccharomyces cerevisiae*

Y. Matuo*, S. Nishijima*, T. Ishibashi**, Y. Hase***,
A. Sakamoto***, A. Tanaka*** and K. Shimizu****

Graduate School of Engineering, Osaka University*
Interdisciplinary Graduate School of Science and Engineering,
Kinki University**
Department of Ion-beam-applied Biology, JAERI***
Radioisotope Research Center, Osaka University****

1. Introduction

The ion beam is expected to increase the mutation frequency and wide spectrum, since it has the high linear energy transfer , and the breeding technology using the mutations induced by the ion beam has been greatly developed. However, the detailed molecula r mechanism has not been proven considerably. In this study, the budding yeast *Saccharomyces cerevisiae* was used as a model eukaryotic organism. This study is intended to elucidate the mechanism of the mutagenesis by ion beam at molecular level. At first, survival rate and mutation frequency for the ion beam were obtained using yeast S288C. N ext, mutation spectrum of mutants obtained by ion beam irradiation was measured by sequencing the mutation sites .

2.Materials and methods

2.1 Strains

S. cerevisiae strains used in this study are S288C(*RAD*$^+$), X36B-3C (*rad3*), JG-18(*rad18*), and G160/2b(*rad52*).

2.2 Sample preparation

Appropriate diluted yeast culture was filtrated through nitrocellulose membrane filter (HA, Millipore). The filter was put on petri dish (50 mm) and covered with kapton ® film (7.5 μm thick).

2.3 Irradiation methods

The yeast samples were irradiat ed with carbon ions ($^{12}C^{5+}$; 220 MeV) with the dose 10 to 300 Gy, and LET is 107 keV/μm. Carbon ion beam was generated from AVF cyclotron in JAERI. The angle scanning is carried out for the uniform irradiation. The samples were incubated at 30 °C for 2-3 days.

2.4 Measurement of cell survival and mutation frequency

The survival rates following irradiation were determined on the basis of colony -forming ability. The mutation frequencies on *URA3* locus were determined using 5 -FOA method [1]. Briefly, the yeast bearing *URA3*$^+$ gene cannot grow no the medium containing 5 -FOA, but when *URA3*$^+$ gene changes to *ura3*$^-$ by the mutation, the yeast can grown on it.

2.5 Sequence analysis of mutation sites

The mutation sites of *ura3* mutants were

determined by DNA sequencing. *URA3* regions of obtained *ura3* mutants were amplified by PCR and sequenced by primer extension using ABI model 3100.

3.Results and Discussion

3.1 The survival rates and mutation frequency

Fig.1 shows the survival rates of several strains exposed to $^{12}C^{5+}$ ion. Like X ray or γ ray, *rad52* strain showed high sensitivity to ion-beam. *RAD3* is involved in nucleotide excision repair. *RAD52* are defective in the repair of strand breaks in DNA. *RAD18* is gene in *RAD6* epistasis group, which is required for spontaneous mutagenesis [2].

Mutation frequencies are shown in Fig.2. This result indicates that the optimum dose for mutagenesis was 100 Gy, and at the dose, mutation occurred 168.5 times more than spontaneous mutation.

3.2 sequence analysis

We obtained the *URA3*→*ura3* mutants at a dose of 100 Gy, *URA3* gene region (800 bp) of *ura3* mutants were amplified by PCR method, and the sequ ence analysis was carried out.

The result shows that mutations caused with ion beam irradiation have remarkable features and hot spots (Table 1). Mutations of spontaneous generation tend to take the type of transition, and transversion is rare compared with transition. It was observed in this experiment that transversion was occurred by 5 times more than transition.

Moreover, the substitution of guanine (G) o f the base pair occupied 46.6%, and the substitution of cytosine (C) of the base pair occupied 42.7% within all substitutions. Additionally, we obtained single base deletion mutants not but multi bases deletion. The analysis of mutations in Arabidopsis sho wed that the deletion of large region and inversio n were predominant in mutations [3,4]. The budding yeast is more resistant to radiation than Arabidopsis, so such mutations caused by ion beam irrad iation may be almost repaired. To elucidate the ion beam eff ect on the budding yeast, we are going to analysis the *ura3* mutants obtained from *rad52* yeasts exposed to ion beam in the near future.

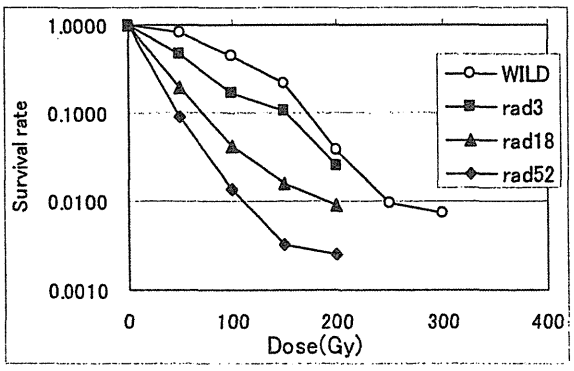

Fig.1. Survival rate of *S.cerevisiae* exposed to heavy ion beam

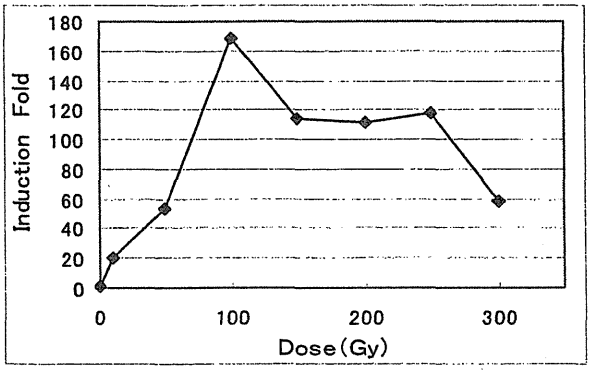

Fig.2. Mutation rate of *S.cerevisiae* exposed to heavy ion beam

Table 1. Nucleotide changes in *ura3* mutants.

Changed position	Nucleotide change (Amino acid change) [numbers]
	Total 39 mutations
+59	A-deletion [1]
+93	C-A (N-K) [6]
+98	G-T (C-F) [6]
+188	A-T (D-V) [1]
+221	T-G (V-G) [1]
+268	G-A (E-K) [4]
+315	C-A (Y-Stop) [2]
+344	G-C (W-S) [1]
+356	C-A (T-K) [4]
+465	C-A (C-Stop) [1]
+542	G-C (G-A) [6]
+561	C-deletion [5]
+764	G-A (G-D) [1]

References

1) D. Burke, et al., in 'Methods in Yeast Genetics' Cold Spring Harbor Laboratory Press (2000) pp7-15
2) E.C. Friedberg, et al., in 'The Molecular and Cellular Biology of the Yeast *Saccharomyces*' Cold Spring Harbor Laboratory Press (1991) pp147-192
3) N. Shikazono, et al., Genetics 163(2003) 1449-1455
4) S. Kitamura, et al., TIARA. Ann. Rep. 2002 (2003) 44-46

2.19 Improvement of Automatic Stage System for Heavy Ion Microbeam Irradiation on Cultured Cells

T. Funayama, S. Wada, T. Sakashita and Y. Kobayashi
Department of Ion-beam-applied Biology, JAERI

1. Introduction

Analyzing the biological effect of radiation of heavy charged-particle is very important when considering the risk of space radiation on astronauts and the cancer radiation therapy. Nevertheless, the fluctuation of the dose distribution by the conventional "broad-field" radiation of a high-LET heavy ion beam interferes with the analysis of biological effect.

Individual targeting of each cell with a single heavy ion is a good way to solve this issue. Thus, we established a method for irradiation of individual cell with a heavy ion microbeam apparatus at JAERI-Takasaki[1]. Using the established method, we found that the single hit of $^{40}Ar^{13+}$ ion on the cell nucleus of chinese hamster ovary cell resulted in strong growth inhibition[2].

1.1 Limitation of current irradiation system

Meanwhile, our microbeam system had a potential inaccuracy of cell targeting, so that system cannot avoid mistake in hitting. Therefore, we used to confirm the hitting position at all irradiated cells by etching CR-39-made cell dish to distinguish fail-to-hit cells, which was targeted but not hit with the delivered ions. This step limits the number of cells that can be irradiated within a beam time.

Nevertheless, the molecular biological analysis of irradiated cells requires a lot of number of cells. Thus, the improvement of the accuracy of cell targeting was required for carrying out molecular analysis of irradiated cells.

1.2 Factors lead to targeting errors

The procedure for irradiating mammalian cells with microbeams contains many steps: cell-image acquisition and processing, setting of fiducials, automatic stage movement, and irradiation with counted ions. The almost all steps mentioned above contain a potency that participates in the targeting errors.

Among these steps, the automatic stage movement is the most frequent action throughout whole irradiation process. Thus it was considered that the movement of automatic stage would affect greatly on the overall targeting accuracy.

Thus we replaced the automatic stages and measured the improvement of cell targeting accuracy. In this paper, we will report the improvement of the mechanical accuracy of automatic stages, object finding and retargeting accuracy using pseudo-cell sample, and accuracy of ion traversal on targeted cells.

2. Materials and Methods

2.1 Automatic microscope stages

We have replaced the automatic microscope stage AS3000 (Autoscan Pty., Ltd.), which had been used in our microbeam irradiation system, with BIOS-213T (SIGMA KOKI, Co,. Ltd.). These two different sets of automatic stages with different manufacturers were compared. The specifications of these stages were shown in Table 1.

2.2 Irradiation procedure using automatic stages

The stage system of our microbeam apparatus is designed to use two inverted optical microscopes (TMD300, Nikon). One

Table 1. Specifications of automatic stages for microbeam irradiation

	AS3000 (Old)	BIOS-213T (New)
Manufacturer	Autoscan Pty., Ltd.	SIGMA KOKI Co., Ltd.
Positional encoders	Rotary encoder	Optical microscale encoder
Positioning accuracy in design	± 1 μm	± 0.1 μm
Overall errors in automatic cell irradiation	± 5-20 μm	± 1-2 μm

microscope (off-line microscope) is used for automatic searching of target cells before microbeam irradiation in preparation room. The other microscope (on-line microscope) is for targeting and irradiation of the registered objects[3].

For the targeting irradiation of cultured cells, we had been adopted two type of experimental procedure concerning in the use of automatic stage: two-stage procedure and one-stage procedure.

The two-stage procedure is the procedure that was designed at first to be adopted in our system, which uses two automatic stages with same specification. The stages were installed on both off-line and on-line microscope, and the sample was transferred from off-line microscope to on-line and vice versa.

On the contrary the one-stage procedure uses only one automatic stage. The stage itself was transferred between two microscopes with the sample anticipating that the use of only one stage eliminates the effect of individual difference between two stages. This procedure was designed as a last resort, because our system had not exhibit enough accuracy for targeting small object like cultured cells with two AS3000 stages.

2.3 Evaluation of errors of automatic stages using pseudo-cell sample

Etched ion-pits on CR-39 film were used as a pseudo-cell sample for measuring targeting accuracy of automatic stages.

The sample was set on the off-line stage, then the positions of each etch-pit were automatically obtained and stored in positional database by Autoscope software. Thereafter, the etch-pits were sequentially revisited according to the data in positional database, and their photographs were taken by digital camera. For every obtained etch-pit positions, 5 revisit experiments were carried out. The experiment was carried out with both one-stage and two-stage procedures.

The coordinate data of etch-pit in each digital photograph was measured and the average of the coordinates of 5 repetitive experiments was used as an expected value of actual coordinates of revisited etch-pit. The distance of individual coordinate from expected coordinate was calculated, and the mean of them was evaluated as errors of stage movement in single revisiting action of each automatic stages.

In addition, the mean of coordinate data in a sequential revisit of the position of all etch-pit in object database was calculated and used as an expected value of actual position of screen origin, where the micoraperture was arranged at the microbeam irradiation. The distance from the origin was calculated in each coordinates of the etch-pit, then the mean of them was evaluated as a error in the overall action of automatic stage in microbeam irradiation.

2.4 Measurement of distribution of the numbers of ion-hit on mammalian cells

CHO-K1 cells were kept in an exponential growth phase with a culture medium (F12, Invitrogen Life Technologies) containing 10% FBS. Before cell inoculation into the sample holder, the cytoplasms of the cells were stained with a fluorescent dye (CellTracker Orange, Molecular Probe). Thereafter, the cells were trypsinized and inoculated in the sample holder. Approximately 50 cells were inoculated within an area of 5 mm x 5 mm at the center of the sample holder, whose bottom was made with thin CR-39 film (100 μm thick).

Before microbeam irradiation, positional data of the individual cells were obtained by fluorescent microscopic searching with off-line microscope. Images of the cells were taken by a high sensitivity CCD camera (MC681SPD, Texas Instruments), and the cell image was applied to position-detecting the Autoscope software for obtaining coordinate of inoculated cells.

Just before irradiation, the medium was removed to make ions penetrate both the cells and the bottom of the sample holder. During the irradiation procedure, the cells were covered with an 8 μm-thick polyimide film (Kapton, Toray Industries). The number of ions having traversed the sample was counted with a constant fraction discriminator coupled to a preset counter/timer. A pulse-chopper in the injection-line of the cyclotron was used as a fast beam switch. All cells found in the sample holder were irradiated with 5 count of $^{40}Ar^{13+}$ beam with the diameter of 5 μm.

Immediately after irradiation, the sample holder was refilled with the medium, then the bottom was etched from the opposite side of the

cells with an alkaline-ethanol solution[4] at 37 °C for 15 minutes. Thereafter, we took photographs of both the cell and the etched pit by a digital camera at the same field of view with different focus planes, then immediately overlaid these two images with the custom-made computer software, 'PitMarker'. From the overlaid images, the number of ions hit on the each cells were scored.

3. Results and Discussions

3.1 Reduced Errors of stage movements

The mean value of errors in single stage action and errors in overall procedure of irradiation were shown in Table 2 and Table 3, respectively.

The error in overall procedure of object targeting was about 10 times larger than that of single movement of automatic stage. This result indicated that the small error in single action is enhanced by overall procedure of cell irradiation because of repeat of stage actions. Thus, the accuracy of stage movement is very important to improve overall cell irradiation accuracy.

The larger differences of error were observed with the revisiting experiments with AS3000 stages. However, there were no differences in overall error between one-stage and two-stage procedure of BIOS-213T.

The difference of errors between two procedures with AS3000 stage came from the characteristics of the encoder for detecting stage movements. Since BIOS-213T stages adopted the optical microscale encoder for obtaining the absolute distance of stage movement, the cause of difference of two automatic stages was limited only to the manufacturing error of the microscales. On the contrary, the detection of stage movement by rotary encoder coupled to the driving motor of automatic stage potentially includes the errors from the allowance of whole driving mechanism. Since the difference in allowance of driving machinery is difficult to avoid, it was considered that the enhancement of individual difference was occurred between two AS3000 stages.

3.2 Targeting accuracy of irradiation of the cultured cells

The targeting accuracy to the cultured cell was compared between one-stage procedure with AS3000 stage, which we had been applied for experiment of cell irradiation, and two-stage procedure with BIOS-213T stage. The cells were irradiated with 5 count of $^{40}Ar^{13+}$ ions.

The samples irradiated using AS3000 stage included more than 25% of fail-to-hit cells. On the contrary, the distribution of ion-hits with BIOS-213T stage indicated that 70% of cells were irradiated with 3-5 ions and less than 5% of cells were failed to hit.

This result indicated that the use of BIOS-213T stage enable us to irradiate mammalian cultured cells with two-stage procedure with higher accuracy in object targeting. The increasing accuracy will make it possible to carry out molecular biological analysis of the cells irradiated with heavy ion microbeams.

Table 2. Stage errors in single action

	AS3000	BIOS-213T
Off-line stage	0.52 μm	0.12 μm
On-line stage	2.16 μm	0.17 μm

Table3. Stage errors in overall targeting procedure

	AS3000	BIOS-213T
One-stage procedure	6.22 μm	1.60 μm
Two-stage procedure	11.47 μm	1.39 μm

References

1) Y. Kobayashi, T. Funayama, M. Taguchi, S. Wada, M. Tanaka, T. Kamiya, W. Yokota, H. Watanabe, K. Yamamoto, JAERI-Review 2001-039, TIARA Annual Report 2000 (2001) 73-75.
2) Y. Kobayashi, T. Funayama, S. Wada, M. Taguchi, H. Watanabe, Nucl. Instr. and Meth. in Phys. Res. B, 210 (2003) 308-311.
3) T. Kamiya, W. Yokota, Y. Kobayashi, M. Cholewa, M. S. Krochmal, G. Laken, I. D. Larsen, F. Fiddes, G. Parkhill, K. Dowsey, Nucl. Instr. and Meth. in Phys. Res. B, 181 (2001) 27-31.
4) G. Somogyi, I. Hunyadi, Proceeding of the Xth International Conference on Solid State Nuclear Track Detector (1980) 443-452.

2.20 Effects of Heavy-ion Beams on the Larval Epidermis of the Silkworm, *Bombyx mori*: Prevention of Scale Differentiation

K. Kiguchi*, K. Fukamoto*, K. Shirai*, R. Kanekatsu*, Y. Kobayashi**, T. Funayama**, T. Sakashita** and H. Watanabe**
Department of Applied Biology, Faculty of Textile Science and Technology, Shinshu University*
Department of Ion-beam-applied Biology, JAERI**

1. Introduction

Epidermis (epidermal cell) is one of the most intriguing research targets in the study of cell differentiation, since they secrete larval, pupal or adult cuticle in each stage of the life cycle, accompanying morphologically drastic changes of the surface structure. Adults of lepidpoteran insects, such as silkworm, are covered with a dense array of scales. It is known that each scale develops from a single specialized cell (scale cell) derived from the larval epidermis[1]. However, precise process of scale cell differentiation has not been fully understood yet.

In the previous paper, we showed that heavy-ion beams are extremely useful for radio-surgery to study bio-function and differentiation of various tissues and organs[2, 3]. For example, locally targeted irradiation of heavy-ion beams to the silkworm larvae has no serious effects on the survival, but inflicts severe functional disruption in the irradiated tissues or organs. When larval epidermis is locally irradiated with heavy-ions, the irradiated area of the resultant moth loses their scales depending on the irradiation doses[2].

In this paper, we have investigated the effects of heavy-ion irradiation to the larval epidermis in hopes of searching a clue to clarify the mechanism of scale differentiation in the silkworm.

2. Experimental procedure

Insects

A laboratory colony of the *pnd* mutant strain of the silkworm, *Bombyx mori*, was used for experiments. The larvae were routinely reared on an artificial diet at 25 °C under a 16-hr light and 8-hr dark photocycle. Fifth instar day 1 larvae were exposed to heavy-ion beams.

Ion beam irradiation

We used carbon ion beams ($^{12}C^{5+}$, 220 MeV, 18.3 MeV/u, range in water=1.2 mm) provided from the AVF-cyclotron in TIARA. As described in the previous paper[2], we made several holes (4 mm in diameter) on an acrylic resin plate (2 mm in thickness) for irradiation, and through the holes larval integuments (left side of the 5th segment) were selectively subjected to heavy ion beam irradiation. Right side of the integument was used as control.

Morphological observations

After irradiation, larvae were reared on an artifical diet and the larval or adult integuments were cut and fixed in Carnoy's fixative at desired stages for light microscopic observation. For scanning electron microscopy, adult integuments were cut off and processed through a series of procedures including cuticle point drying and coating with gold, they were observed using SEM(HITACHI S-2380N).

3. Results and Discussion

We first examined the dose response of carbon ions inducing complete deletion of scales in the adult moths. The larval integument consists of a single layer of epidermal cells, overlaying cuticle and basement membrane. The thickness of the epidermis of 5th instar day 1 larva is the maximum within 0.3 mm[3]. Taking account of the range of carbon-ions (1.2 mm in water), larvae were irradiated with beams through 4sheets of miller-firm (100 . m in thickness) to avoid ion-penetration to inner tissues such as intestine. Judging from the result, 350 Gy seemed to be optimal. A typical result of scale deletion induced was shown in Fig.1. Scanning electron microscopic observation revealed that surface structure of the irradiated area is quite different from the control. Many socket structures were observed in the control. By contrast, only few deformed sockets were recognizable in the irradiated area (Fig.2, a).

Next, we prepared paraffin sections of the larval integuments to see the effects of irradiation. It is well known that hemocytes are involved in phagocytosis of the disintegrated injured cells. However, few hemocytes were observed at the site of irradiated integuments (Fig.3, a, b, c). In addition, the larval epidermal cells seemed to be normal unexpectedly at least under light microscopical observation. The epidermal cells of the resultant adult moth also looked normal, although the number of sockets drastically decreased (Fig.3, d). These results suggest that the larval epidermis is considerably resistant against ion-beam irradiation, and that deletion of scales is not brought about by apoptotic elimination of the irradiated cells, but by prevention of scale differentiation.

Reference

1) H. F. Nijhout, The Development and Evolution of Butterfly Wing Patterns, Smithonian Institution Press, Washington and London (1991).
2) Z-L. Tu, S. Yamasaki, K. Shirai, R. Kanekatsu, K. Kiguchi, Y. Kobayashi, M. Taguchi and H. Watanabe, Journal of Sericulture Science Japan. 68 (1999) 443-453.
3) E. Ling, K. Fukamoto, S. Xu, K. Shirai, R. Kanekatsu, Y. Kobayashi, Z-L. Tu. T. Funayama, H. Watanabe and K. Kiguchi, Journal of Insect Biotechnology and Sericology. 72 (2003) 95-100.

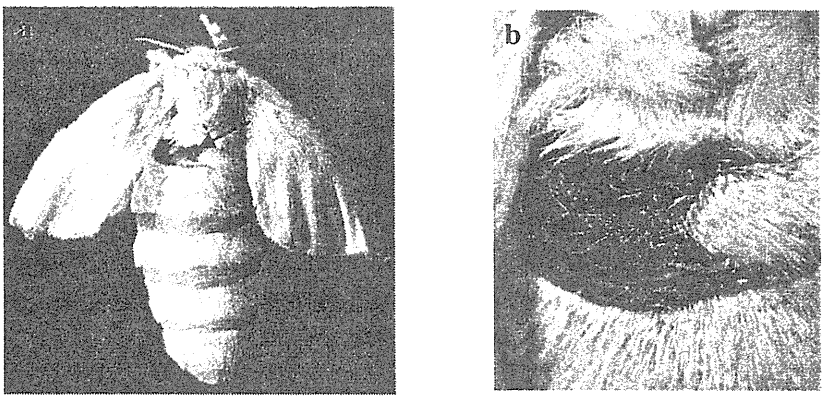

Fig.1 Deletion of scales induced by local irradiation of heavy-ion beams(350 Gy).
a: left half of the segment lost the scales(arrow),
b: an enlarged picture of the segment.

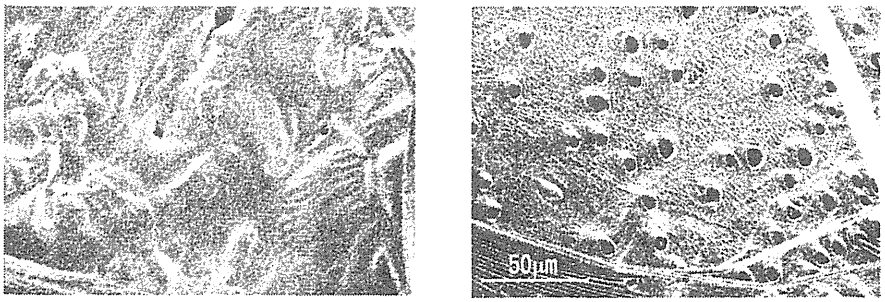

Fig.2 Scanning electron micrographs of the adult cuticle derived from the individual irradiated at the larval stage.

a: an irradiated region which lacks scales,

b: the control region from which scale-hairs were pull out to see the basal socket structure.

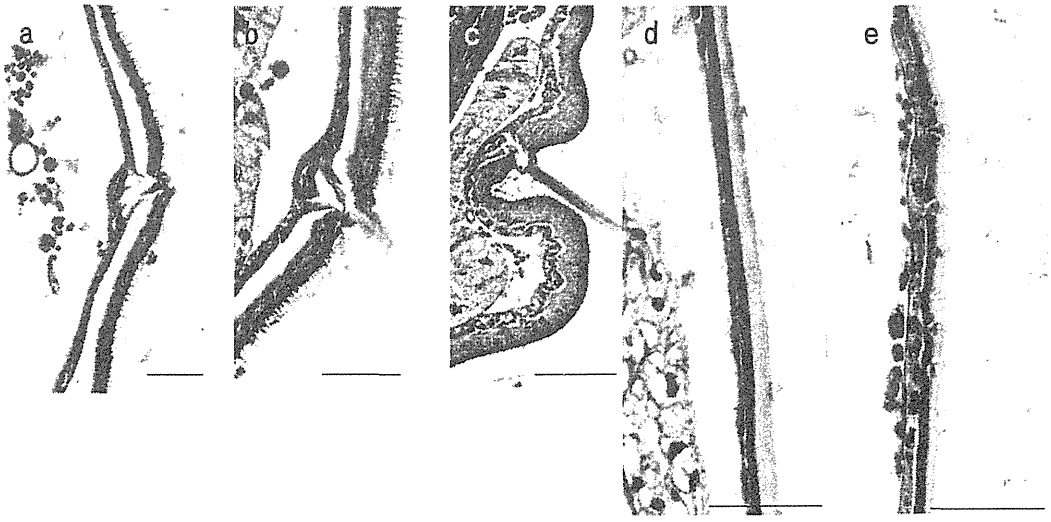

Fig. 3 Cross sections of the integuments irradiated with carbon ions(350 Gy) on day 0 of the 5th instar.

a, b, c: 24 hrs, 48 hrs and 96 hrs after irradiation, respectively,

d: irradiated region of the resultant moth,

e: the control region of d.

2.21 Development of Irradiation Procedure to Detect Distance the Signal Transfer of GJIC Bystander Effect

Y. Furusawa*, M. Aoki*, C. Shao*,***, Y. Kobayashi**, T. Funayama**, T. Sakashita** and S. Wada**
Heavy-Ion Radiobiology Research Group, NIRS*,
Department of Ion-beam-applied Biology, JAERI**,
Gray Cancer Institute, UK***

1. Introduction

It has been thought for many years that the heritable biological effects of radiation requires an interaction of the radiation with DNA either by direct ionization or by the production of hydroxyl radicals in water molecules close to the DNA. Presumably, no effect would be expected in cells that received no direct radiation exposure. Recently, evidence has been presented demonstrating that low doses of alpha particles lead to the formation of sister chromatid exchanges (SCE) in 30% of the cell population even though only 1% of the cells' nuclei have been traversed by an alpha particle[1]. This phenomenon has been called the "bystander effect," through which cells in the vicinity of directly targeted cells can respond to the radiation. By the use of several experimental approaches such as very low dose alpha particle where not every cell nuclear is traversed, microbeam irradiation of selected few cells in a population, and transfer of medium harvested from irradiated cells to cultures of non-irradiated cells, reports of the bystander effect have appeared with multiple biological end-points, including cell killing, inductions of micronucleus, mutation, genomic instability, and so on.

Although the gap junctional intercellular communication (GJIC) is an important pathway for the production of bystander responses[2, 3], but it is not always required. By irradiating nonconfluent human fibroblast cells with a precise number of particles, the findings that targeting of a single cell led to additional 10s of cells being damaged[4] give direct evidence of non-GJIC involved but the likelihood of medium mediated bystander responses. These responses are thought to be relative to the genotype of irradiated cells. It has been found that some signaling factors including reactive oxygen species (ROS), and transforming growth factors can be produced from the irradiated cells and play important roles in the medium-mediated bystander effect. Furthermore, the accumulation of inducible nitric oxide synthase (iNOS) and the activity of constitutive NOS have been known to be an early signaling event induced by irradiation so that nitric oxide (NO) becomes an important bystander signaling factor[5-8].

To clarify the mechanisms of transduction of bystander signal through the GJIC, an irradiation method to obtain a distance distribution in induction of micronuclei in no irradiated cells from irradiated cells was preliminary established.

2. Development

2.1 Design of irradiation dish

To measure the distance distribution of the bystander effect from the hit cells, we have designed a special made irradiation dish. Briefly, a 25 mm diameter cell culture coverslip (NUNC 174985) was attached on a 60 mm plastic dish (Falcon 351006) with 13 mm through hole in

the middle of the bottom the dish with white Vaseline. In the middle of the cover slip, a scratch line was made, and 1-2 mm width of adhesive tape was put on the surface of the cover slip with rectangular coordinates as a landmark line on the bottom and to prevent cells will attach in the clear zone as shown in figure 1.

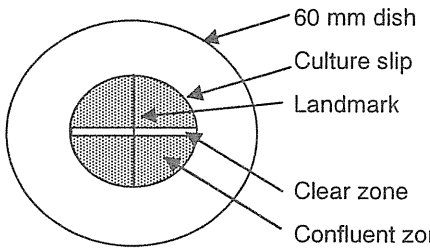

Fig.1. Schematic image of irradiation dish. Cells are seeded only in the gray area, and a part of cells on the landmark in one side of the clear zone was irradiated by neon microbeams.

Micronicle (MN) only can be seen in growing cells, i.e. in a binucliated (BN) cells. Cells can only be grown from confluent zone to clear zone, because cells were cultured to be confluent in confluent zone indicated in gray zone in figure 2. This means MN cells can be seen on the border of the clear zone and the confluent zone. Distribution of the distance to reach the bystander effects from irradiated cell that placed on the landmark line may possible to obtain by measurement of the distance between the landmark line and the position of MN cells in the border of the clear zone in the irradiated side. When there are still medium mediated bystander effects, even if we used and suppressed by inhibitors, we can observe the effect in the opposite side of the irradiated side.

2.2 Cell culture and treatments

AG1522 normal human skin fibroblasts purchased from Coriell Cell Repositories were cultured at 37°C in humidified atmosphere of 95% air and 5% CO_2 with Eagle's minimum essential medium (Sigma M5650) supplemented with 2 mM L-glutamine and 18% fetal bovine serum (Lenexa) plus streptomycin and penicillin. Cells destined for heavy-ion irradiation were seeded in the specially made dish at a density of $1.4x10^5$ cells per dish 4 days before irradiation. The medium was changed at day 2 so that at the time of irradiation the cells were in full confluence.

Just before irradiation, a thin Kapton film was floated on the medium surface and the medium was removed and covered cell surface by the film. This process kept the cells fully hydrated during irradiation, which was 30 min. After the irradiation, by adding new medium in the dish, the film was floated in the medium surface again and could remove the film safely without gives any damage to the cells. After a post incubation to transfer bystander signals, adhesive tape to prevent clear zone was removed. While the tape was stay on the clear zone, no cells grown on the tape, and following incubation, cells could grown to the clear zome after removind the tape (Fig.2).

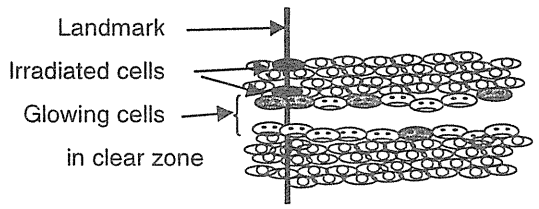

Fig.2. Microscopic image at the central area of the dish after culture. Adhesive tape on the clear zone was removed after irradiation, and cells are grown to the clear zone. Binucliated cells can be found in this area.

2.3 Irradiation method

A charged particle microbeam apparatus installed below a vertical beam line of the cyclotron at TIARA was used to deliver precise

number of heavy ions of 260 MeV ^{20}Ne with calculated LET values of 380 keV/um for cell irradiation. Particles traversing through horizontal cover slip, Kapton film and cells were detected by photomultiplier tube (PMT) with plastic scintillator.

Fifty cells in the confluent culture on the landmark line in a one side of the clear zone were irradiated. After the irradiation, 2 ml medium was immediately supplied to each dish and cells were subsequently cultivated for 15 h until adhesive tape were removed for the MN assay to start growing. During this process, with respect to PMA pretreated culture, PMA with a reduced concentration of 0.5 nM in case of any toxic effect was added in the medium to maintain the inhibition level of GJIC. No irradiated control dishes were treated with the same protocol except for irradiation. Chemical treatment of PMA did not show a significant toxic effect on cells.

2.4 MN assay

The formation of MN was assayed by using the cytokinesis block technique. The cells were incubated in the presence of 2.5 g/ml cytochalasin-B. After 48 h, the cells were treated with a 75 mM KCl hypotonic solution at 37°C for 10 min, and fixed by methanol at –30°C overnight. The fixed cells were stained with 10 mg/ml acridine orange for 5 min. After this cytochalasin-B treatment, 20% of cells became binucleated (BN) cells when the cells were sub-cultured in a new Petri dish.

The cover slip was removed from the special made irradiation dish, and Vaseline was wiped. The cover slip was placed on a slide grass by inversed way and MN in BN cells was checked by fluorescence microscopy and morphologically identified by the criteria method. Distance of MN cells in BN cells from the landmark could be measured with a scale equipped to the microscope sample stage.

References

1) H. Nagasawa, and B. J. Little, Cancer Research 52 (1992) 6394-6396.
2) C. Shao, Y. Furusawa, Y. Kobayashi, T. Funayama, and S. Wada, FASEB Journal 17 (2003) 1422-1427.
3) C. Shao, Y. Furusawa, M. Aoki, and K. Ando, Radiat Res 160 (2003) 64-69.
4) C. Shao, V. Stewart, M. Folkard, B. D. Michael, and K. M. Prise, Cancer Research 63 (2003) 8437-8442.
5) H. Matsumoto, S. Hayashi, M. Hatashita, H. Shioura, T. Ohtsubo, R. Kitai, T. Ohnishi, O. Yukawa, Y. Furusawa, and E. Kano, (2000) International Journal of Radiation Biology **76** (2000) 1649–1657.
6) C. Shao, M. Aoki, and Y Furusawa, Journal of Radiation Research **42** (2001) 305–316.
7) C. Shao, Y. Furusawa, M. Aoki, H. Matsumoto, and K. Ando, International Journal of Radiation Research 78 (2002) 837-844.
8) C. Shao, M. Aoki, Y. Furusawa, Journal of Radiation Research 45 (2004) 97-104.

2.22 Effect to Mammalian Nucleus Irradiation with Heavy-ion Beams

S. Wada[*], T. Funayama[*], Y. Kobayashi[*]
N. Ito[**], M. Natsuhori[**], T. Kakizaki[**] and T. Sano[**]

Department of Ion-Beam-Applied Biology, JAERI[*]
Department of Veterinary Medicine, Kitasato University[**]

1.Introduction

Radiation of high linear energy transfer (LET) has greater biological effectiveness than the same absorbed dose of low LET radiation, the relative biological effectiveness (RBE) increases with LET, reaching a maximum at around 100 keV/μm in mammalian cells. Thus, LET is used to describe radiation quality. However, It is considered that the different particles with the same LET induce different biological effects and the difference in the biological effects is caused by a difference in track structures. Because the different particles with the same LET differ in their pattern of energy deposition in the target materials, it is considered that the different biological damage was produced.

For mammalian cells exposed to high LET heavy charged particles, DNA double strand breaks (DSB) have an important role in the biological effects. The quantitative analysis of every approach relies on the assumption that ions hit randomly to the cells and DNA damage induced by high LET heavy charged particles were evaluated with the absorbed dose. To analyze the track structures in detail, the biological effects should be evaluated not with the absorbed dose but the number of the hit ions.

Recently we established a method of simultaneous detection of ions traversing the cellular nuclei and DNA damage in the individual cells[1]. By the method the induction of DNA damage per a particle for different ion with the same LET was different[2].

In this study we investigated the biological effects of the track structure of the ion beams for different particles with the same LET value by visualization of DNA damage site induced by hit-ions.

2.Materials and methods

CHO-K1 cells were grown in Ham's F12 medium supplemented with 10% serum and 0.1 mg/ml kanamaycin in 10-cm diameter culture dishes. Cells were incubated at 37°C in humidified atmosphere of 5% carbon dioxide and 95% air.

Accelerated heavy ions of 17.3 MeV/u $^{12}C^{5+}$ and 10.4 MeV/u $^{20}Ne^{7+}$ were provided by the AVF cyclotron at TIARA JAERI-Takasaki. The energy of C ion beam was reduced by nickel plates.

Cells were attached on the CR-39 plate that is particle track detector. To evaluate DNA damage, immunohistochemistry was applied. DNA single strand breaks (SSB) and DSB were detected through the use of exonuclease III (exo III) and terminal deoxynucleotidyl ransferase (tdt). Immediately After irradiation the cells were

fixed by 1% paraformalehyde in PBS. The cells were incubated with exo III (2 unit/μm) in humidified chamber at 37℃ for 3 hr, following washes in PBS. DNA fragment generated by exo III were labeled with dig-dUTP using tdt (2.5 unit/μl) at 37℃ for 2 hr. after washing PBS, the cells were incubated the antibody against dig-dUTP-FITC at room temperature for 1 hr.

DSB introduced into mammalian cells by ionizing radiation results in specific phoshorylation of histon H2AX on serine residue 139, yielding a specific modified form named .H2AX. Using a fluorescent specific antibody for .H2AX, we detected discrete nuclear foci at the site of DSB. At 30 min after irradiation, cells were fixed 1% paraformalehyde in PBS. The cells were incubated with anti-.H2AX for 1 hr at the room temperature. And the cells were washed in PBS and incubated with fluorescent secondary antibody Alexa 568 goat anti-rabbit IgG for 1 hr at room temperature.

The cells on the CR-39 were stained with DAPI and the opposite side of the CR-39 plate was etched with KOH-ethanol solution at 37°C. Using a fluorescence microscope we examined about the cell image at 400 magnification. The cell images were stored using CCD camera. Then the microscope was focused on the image of pits etched on the CR-39 plate, and the image was also stored using CCD camera. By merging both images, hit-ions and the fluorescent signal were simultaneously detected. The relation between the location of hit-ion and the area of DNA damage was investigated, and difference of the area of DNA damage was compared due to difference of ion track structure.

3.Result and discussion

Cells attached on the CR-39 were exposed to C ion and Ne ion with the same LET (about 437 keV/μm), and when DNA strand breaks and .H2AX were detected by immunochemistry, the fluorescent signal was observed in nuclei. When the focus was adjusted on the CR-39 form a site of the fluorescent signal, the site of the fluorescent signal and the sites of etched pit were coincident. This indicate that this fluorescent signal show DNA damage induced by hit-ion and the area of fluorescent signal show the area of DNA damage. So, to evaluate the area of DNA damage, the diameter of this area of fluorescent signal was measured.

The area of fluorescent signal of DNA strand breaks induced by exposure to C ion and Ne ion were not significantly different. While the area of fluorescent signal of DNA strand breaks and .H2AX induced by exposure to C ion were not significantly different, the area of fluorescent signal of DNA strand breaks was three times larger than that of .H2AX for exposure to Ne ion.

It was considered that both ions induce DSB around ion trajectory and Ne ion induces SSB relatively at larger area than C ion. This indicates that the difference of ion track structure influence the pattern of induction of DNA damage.

Reference

1) S. Wada et al., Journal of Radiation Research, 43: (2002) S153-156
2) S. Wada et al., TIARA Annual Report, 2002: (2003) 99-101

2.23 Isolation of Human Cell Mutants in HIV-1 Sensitivity and of Human Retroviruses Mutants in Cell Tropisms

H. Hoshino*, T. Ohtsuki*, N. Shimizu*, A. Tanaka*, M. Shinagawa*,
S. Wada**, T. Funayama** and Y. Kobayashi**
Department of Virology and Preventive Medicine, Gunma University Graduate School of Medicine*
Department of Ion-beam-applied Biology, JAERI**

1. Introduction

In order to analyze effects of heavy ion-beam irradiation on cellular and viral genes, we tried to establish irradiation target cells that could easily be characterized molecular biologically as shown schematically in Fig. 1. For this, human immunodeficiency virus type 1(HIV-1) was selected to be used in this experiment. Thus, we transduced NP-2 cells, which are resistant to HIV-1 infection, with a few genes that determine HIV-1 susceptibility. In addition, we tried to transduce this cell line with many other HIV-1 co-receptor genes for us to be able to examine HIV-1 strains with different cell tropisms. The aim of this study was isolation of cell mutants in HIV-1susceptibility to identify cellular genes necessary for HIV-1 infection and replication. We also aimed at clarifying effects of heavy ion-beam irradiation on viral genes.

Effects of irradiation with heavy ions ($^{4}He^{2+}$, $^{12}C^{5+}$ and $^{20}Ne^{8+}$) on human cellular genes have rarely been reported using methods to analyze quantitatively. Therefore, we used a cell line system, in which gene mutation was expected to be relatively easily analyzed, and tried to clarify effects of He, C or Ne ion irradiation on induction of mutation of cellular genes. For this, we had established a cell line, NP-2/CD4/EcoR/CCR5/GFP two years ago. Namely, a human glioma cell line, NP-2, was transduced with genes for human CD4, ecotropic murine leukemia virus (MuLV) receptor EcoR, and human chemokine receptor gene CCR5. Further, another vector that carried the green fluorescent protein (GFP) downstream of the HIV-1 RNA transcription control region in its long terminal repeat (LTR) and nuclear localization signal (NL) for proteins was transfected into this cell line. In this study, we thus made cell systems carrying HIV-1 co-receptor genes other than CCR5 to be used for this analysis.

For analyses of effects of heavy ion-beam irradiation, it will be relatively easy if vectors carrying known genes or viruses are used, because target gene sizes are small and details of their genetic structures are known. HIV-1 is a virus that should be handled with care, because it is a biohazardous organism. Therefore, before analysis of effects of heavy ion irradiation on HIV-1, we examined irradiation conditions and its characteristics that will be applicable for irradiation of HIV-1.

2. Experimental procedures,

2-1 Establishment of target cells for irradiations

NP-2/CD4/EcoR/CCR5/GFP cells had been transduced with CD4 using a neomycin resistance gene as an indicator of transduction. Furthermore, the cells transduced with the ecotropic MuLV receptor gene EcoR and the human chemokine receptor gene CCR5 had been estimated by their resistance to hygromycin and puromycin, respectively. The cells transduced with a GFP-expressing plasmid under control of HIV-1 LTR were selected by detection of fluorscence in the nuclei of cells infected with HIV-1. We used the expressions vectors for CD4, EcoR and CCR5 that would simultaneously induce the

expression the genes for resistance to neomycin, hygromycin and puromycin, respectively. As a GFP-expressing plasmid, pHIV-1-LTR-NL-GFP, in which GFP gene and nuclear localization (NL) signal sequence were placed downstream of the region for HIV-1 RNA transcription regulation was used, and cells that were negative for GFP before infection, but became positive for GFP in the nuclei after cells had been infected with HIV-1.

We have expected that cells would not become positive for GFP after HIV-1 infection when either one of CD4, CCR5, or GFP or one of cellular factors necessary for HIV-1 replication was inactivated. To increase the number of HIV-1 strains used for this analysis, we tried to isolate cells expressing another co-receptor, CXCR4. In addition, isolation of cells expressing both CCR5 and CXCR4 were also tried.

2-2 Detection and isolation of cell mutants in their susceptibilities to HIV-1

HIV-1-susceptible cell lines were irradiated with heavy ion-beam, and we examined effects of irradiation on expression of the transduced genes. Mutant cells were mainly detected according to their change in HIV-1 susceptibility. That is, we should determine change ratios in the following properties of the irradiated cells: (1) HIV-1 susceptibility, (2) neomycin resistance, (3) hygromycin resistance, (4) puromycin resistance and (5) inhibition of GFP expression.

3. Results and Discussion

3-1 Establishment of NP-2/CD4/CXCR4/GFP and NP-2/CD4/CCR5/CXCR4/GFP cells

We could isolate a clonal cell line, NP-2/CD4/CXCR4/GFP, as we had succeeded previously. After transduction of CXCR4 into NP-2/CD4/CCR5/GFP cells, we also isolated NP-2/CD4/CCR5/CXCR4/GFP cells that became GFP-positive after infection with X4 HIV-1 strains.

3-2 Trial to isolate HIV-1 susceptibility mutant cells after heavy ion-beam irradiation

Cell lines described above were irradiated with heavy ion $^{4}He^{2+}$ (50 MeV), $^{12}C^{5+}$ (220 MeV) or $^{20}Ne^{8+}$ (350 MeV). Then we tried to isolate cells resistant to HIV-1. We could isolate many cell clones that did not become positive for GFP after HIV-1 infection. In these cells, many syncytia were usually observed, indicating that they were, in contrary to our expectation, susceptible to HIV-1.

Then we examined their resistance to neomycin and puromycin to further estimate the presence of CD4 or CCR5 gene in these cells. These cell clones of NP-2/CD4/CCR5/GFP cells lacking in GFP expression after HIV-1 infection were susceptible to either antibiotics. Although these clones were apparently susceptible to HIV-1 infection, CD4 and CCR5 were again, against our expectation, below a detection limit of flow cytometry using anti-CD4 or anti-CCR5 monoclonal antibody.

These cell clones should still express a small amount of CD4 and CCR5, since they were apparently susceptible to HIV-1. The expression of CD4 and CCR5 were confirmed to be detected in the parental NP-2/CD4/CCR5 cells upon flow cytometry, indicting that our assay conditions worked well.

3-3 Effects of heavy ion-beam irradiation on cell growth

Our preliminary experiments suggested that there was a difference in cell death taken place soon after irradiation between NP-2/CD4/CCR5/GFP and NP-2/CD4/CXCR4/GFP cells. Therefore, we irradiated cells with $^{4}He^{2+}$ (50 MeV), $^{12}C^{5+}$ (220 MeV) or $^{20}Ne^{8+}$ (350 MeV). On the following day, the cells were detached, counted, and seeded into wells of 96-well plates at different cell concentrations.

Numbers of wells containing growing cells were counted after 1-2 months of cultivation.

Irradiation with $^{4}He^{2+}$ or $^{12}C^{5+}$ did not give a difference in colony-forming efficiencies between these two cells. There seemed to be not a clear correlation between the colony-forming efficiencies and irradiation doses of $^{20}Ne^{8+}$. This observation were noticed repeatedly. As for $^{20}Ne^{8+}$ irradiation, we considered that Ne ions could not hit cells because of the presence of culture medium and short flying distance of Ne ion.

3-4 Effects on HIV-1 infection

We examined susceptibilities of cell clones, derived from heavy ion-irradiated cells, to HIV-1 after prolonged cultivation for 1-2 months. Parental cell lines became GFP positive in their nuclei after HIV-1 infection, while cell clones showing different phenotypes from them were frequently isolated. The major population of these cell clones did not become GFP-positive, although these clones were positive for HIV-1-induced syncytia formation, suggesting that the abnormal expression of GFP took place easily among the genes transduced by the MuLV vectors , i.e. CD4, CCR5 or GFP.

For isolation of cell mutants resistant to HIV-1 infection, we should develop a system, by which targets, cells in suspension culture or viruses in culture supernatants, are surely irradiated with ion beams. This system will permit us to use a wider range of experimental materials as irradiation targets. Further, it will also be necessary for us to develop a system to select HIV-1-resistant cells easily. Although NP-2 cells persistently infected with HIV-1 are viable, these cells can be killed if infecting HIV-1 carries a gene like thymidine kinase. Then HIV-1 resistant cells will be isolated more easily.

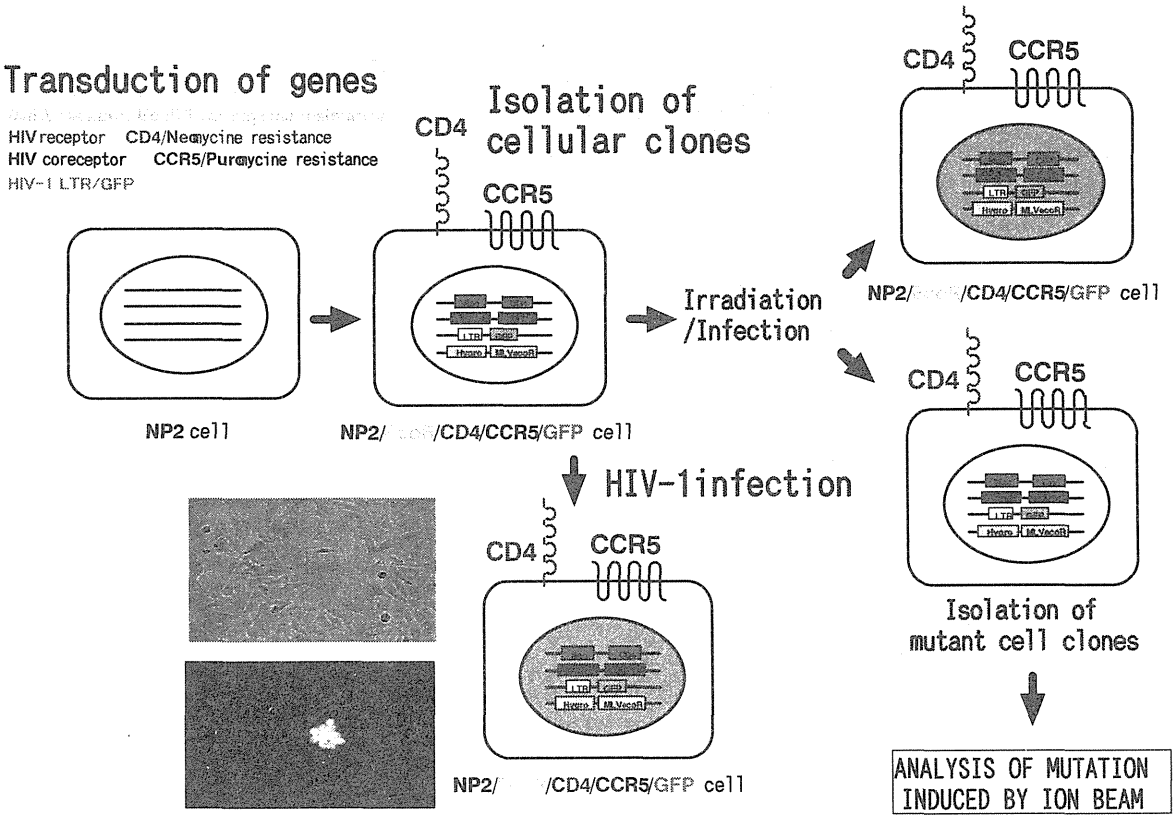

Fig. 1 Isolation of human cell mutants in HIV-1 susceptibility

2.24 Ion Beam Irradiation has Different Influences on the Ciliary Body among ^{20}Ne, ^{4}He, ^{12}C, and ^{1}H

K. Akeo*, T. Funayama**, A. Ogawa*** and Y. Kobayashi**
Department of Ophthalmology, Takasaki National Hospital*
Department of Ion-Beam-Applied Biology, JAERI**
Department of Research and Examination, Takasaki National Hospital****

Outline

Active secretion of sodium and potassium was shown to primarily occur in non-pigmented epithelium (NPE) by Okisaka[1] and associates and NPE is responsible for the maintenance of aqueous humor formation. NPE in the ciliary processes might have high metabolic functions, i.e. the secretive function, because the ciliary processes are rich in the capillary vessels. The gamma ray (^{60}Co) causes ionization uniformly in the whole irradiated tissue. We reported last year that high dose of gamma irradiation prevented programmed cell death regulated by p53 and bcl-2 genes in the ciliary body dissected from living body, and was useful for preservation of organ after culture by the protective influence of inflammatory reaction. The ion beam is an ionization particle that is induced by acceleration of the ionizing atom of ^{20}Ne, ^{12}C, ^{4}He, ^{1}H, and so on, but has a characteristic to lose energy and stop at the constant depth of tissue. The reaching depth to the tissue depends on the ion species and the acceleration energy. The reaching depth in water is 1.64 mm in $^{4}He^{2+}$(50MeV), 1.08 mm in $^{12}C^{5+}$(220MeV), 0.57 mm in $^{20}Ne^{8+}$(350MeV), and 4.02 mm in $^{1}H^{+}$(20MeV). If ion beam can selectively irradiate NPE in the ciliary body where hyper-secretion of aqueous humor happens, we might be able to cure ocular hypertension and glaucoma instead of surgery. Gamma ray penetrates into the tissue, but an ion beam has the strongest energy and a maximum influence at a point inside the tissue. Moreover, the ion beam is supposed to have a bystander effect around the irradiated tissue. We investigate which part of the ciliary body the ion beam influences, and we compared the effects among the species of the ion. As for as we know, this is the first report concerned with morphological changes in ciliary body cultured after the ion beam irradiation. We are now submitting materials and methods, results, and discussion to an article.

Morphology of the tissue should be damaged due to necrosis by the cease of blood flow after dissection from living body. If the radiation induced preventive reaction into the cells and quit the destruction of the living tissue by necrosis, the long-time preservation of the internal organs and the living tissue would be possible and leaping contributed to the medical field.

Especially, the labyrinth of the blood vessel in the ciliary processes does not make the blood supply spread entirely because of the more complicated structure than the ciliary folds. It is necessary to know which part of the ciliary

body is damaged at the initial phase by the cease of blood. We thought that the ciliary body was most useful to investigate the inflammatory reaction by gamma radiation because of the complicated vascular structure. Gamma radiation of blood products is considered the mainstay of transfusion-associated graft-versus-host disease prevention. Recently it is reported that there is evidence of cellular variability with production of cytokines at different storage time which could be related with irradiation activity and cellular damage repair but not lymphocyte inhibition rate in blood components just one time after irradiation, and the cytokines had a central role in the stimulation of cellular and inflammatory reactions[1].

References

1) Okisaka S, Kuwabara R, Rapoport SI. Science 1974;184:1298E.

2.25 The Resistance of *Euglena gracilis* to γ-rays and Ion Beam Radiation as a Simulated Cosmic Ray and its Light-dependency to Ionizing Radiation

H. Hayashi*, M. Furuta*, K. Uehara*, T. Funayama**, S. Wada**, I. Narumi**, Y. Kobayashi** and H. Watanabe**

Research Institute for Advanced Science and Technology, Osaka Prefecture University*

Department of Ion-beam-applied Biology, JAERI **

1. Introduction

More than 100 kinds of *Euglena* have been found thus far on the earth. Among these, *Euglena gracilis* has the highest photosynthesis activity and nutritional value. In the near future, humankind may be forced to live in a space station equipped with a closed ecological life support system for the long-term. Given the high photosynthetic efficiency and nutritional quality of *E. gracilis*, it has been proposed to be valuable as a good biological component for use in such a closed system. In order to use *E. gracilis* in space, the radiation damage caused by cosmic rays that includes high LET particles will be problematic. Therefore, as the first step to solve this problem, we assessed the radiation effect of heavy ion beams on *E. gracilis*. Each survival curve was characterized by a "shoulder" [1], suggesting DNA repair activity after irradiation, followed by a subsequent exponential slope as shown in Fig.1. In this study, we assessed the DNA repair of light-grown and dark-grown *Euglena* cells using strains Z (wild type) and SM-ZK (chloroplast deficient mutant strain) after γ-irradiation giving the largest "shoulder" in their survival curves.

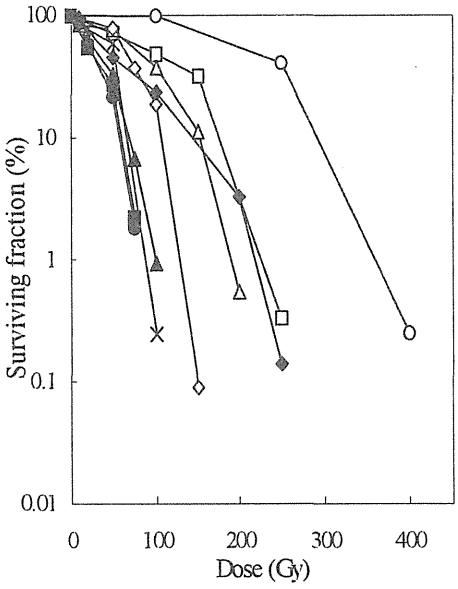

Fig. 1. Survival of *E.gracilis* strain Z exposed to heavy ion beam at different doses. ○ :γ-ray, □ :H^+, △ : He^{2+}, ◇ :C^{6+}, × :C^{5+} (108 keV/μm), ● : C^{5+} (196 keV/μm).

2. Experimental procedure

2.1 Organism and Cultivation Conditions

E. gracilis strain Z (wild type) and strain SM-ZK (chloroplast deficiency mutant) were used. The cells were grown at 25°C in 150 ml of Koren-Hutner (KH) medium in a 500-ml Sakaguchi flask to stationary growth phase (for 5 days) with agitation under the illumination of fluorescent light (5,000 lx) or dark condition.

2.2 Irradiation conditions

Irradiation of γ-rays was carried out by using ^{60}Co γ-ray source at JAERI Takasaki (dose rates: 100 to 500 Gy/h). Light-grown and dark-grown cells of *E. gracilis* strains Z and SM-ZK were harvested by centrifugation, washed, and resuspended in a fresh KH medium or 0.1 M phosphate buffer (pH 6.8). The aliquots (1 ml) from the cell suspension (2×10^7 cells/ml) were dispensed into glass test tubes, and irradiated at room temperature with ^{60}Co γ-rays at the dose rates of 0.25 to 1.5 kGy/h.

2.3 Measurement of Cell Survival

The survival rates of *E. gracilis* following irradiation were determined on the basis of colony-forming ability. The irradiated cells were grown on KH agar medium at 28°C under the illumination of fluorescent light (5,000 lx) for 7 to 10 days.

2.4 Assessment of DNA repair

Comet assay[2] was applied to assess DNA double strand breaks repair ability. Fifteen ml of the cells cultured to stationary phase was washed and resuspended in 15 ml of fresh KH medium. One ml of the suspension was dispensed to a 15-cm test tube. After 750 Gy of γ-ray irradiation, the cells were harvested and resuspended in 15 ml of fresh KH medium.

The suspension was moved to a Sakaguchi flask containing KH medium and agitated under the illumination of fluorescent light. The cells were withdrawn from the culture at constant times (0, 3, 6, and 12 h), embed with 1% low-melting agarose gel and cytolysised with Proteinase K. Then electrophoresis was conducted under neutral conditions (pH 8) . Using a fluorescence microscopy equipped, about 50 cells per slide were examined. The dsb rejoining fraction at 12 h after irradiation were calculated by the equation of (1- tail moment at 12 h after γ-irradiation / tail moment at 0 h after γ-irradiation) × 100.

3. Results and discussion

The survival curves of γ- irradiated light-grown and dark-grown cells of strains Z and SM-ZK are shown in Fig.2. The curves have a large "shoulder" in which the survival rates decrease slowly within smaller doses until the dose of 750 Gy, and the values do not show significant differences. However, at doses of 750 Gy and 1000 Gy, the values for light-grown cells are significantly higher than those for dark-grown cells, strongly suggesting that the light-grown cells are more radiation-resistant. We estimated the LD_{90} (90 % lethal dose) of light- and dark-grown cells from the curves. For the strain Z, the LD_{90} of light- and dark-grown cells were 776 Gy and 596 Gy, respectively. The LD_{90} values of light- and dark-grown cells of strain SM-ZK were 664 Gy and 479 Gy, respectively.

The difference in radiation resistance between light- and dark-grown cells was also observed in strain SM-ZK, a chloroplast-deficient mutant. The changes in tail moment in light- and dark-grown cells of strains Z and SM-ZK were investigated. The decrease rate of the tail moment for strain Z was higher than that of other cells at 12 h after irradiation,

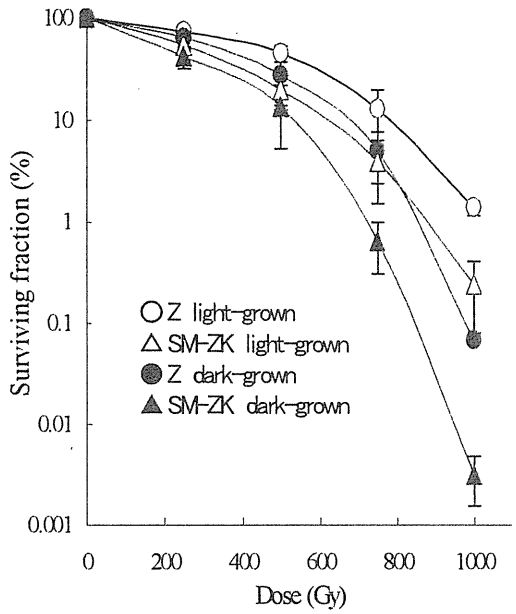

Fig.2 Survival of Euglena gracilis strains Z and SM-ZK exposed to γ-rays at different doses.

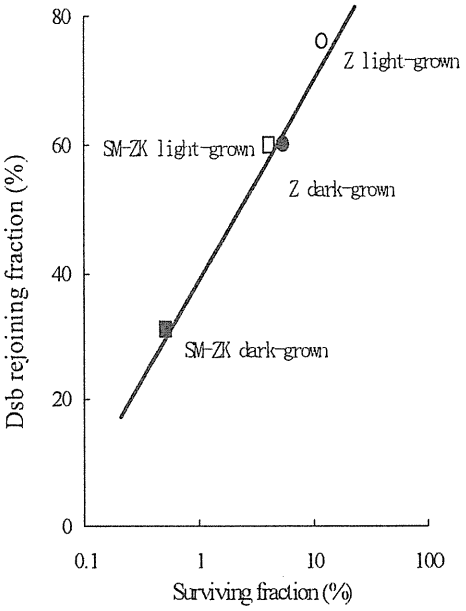

Fig.3 The relationship between surviving fracti and dsb rejoining ability in *E. gracilis* followi γ-irradiation (750 Gy).

dark-grown cells of strain Z and light-grown cells of SM-ZK showed intermediate values. The respective values for light- and dark-grown cells of strain Z were 76 % and 60 % and for light- and dark-grown cells of strain SM-ZK 60 % and 31 %. Fig. 3 shows the relationship between surviving fractions and the calculated dsb rejoining fractions. The ability of dsb rejoining was correlated with the surviving fraction, suggesting that the difference in radiation resistance reflect the ability of dsb rejoining of irradiated cells. In this study, the ability of dsb rejoining was shown to be higher in light-grown cells irrespective of the strain used, strongly suggesting that a light-inducible dsb repair system. It is a novel finding that a repair enzyme for DNA double-strand breaks is induced by visible light prior to γ-irradiation in *Euglena*.

References

1) H.Hayashi, S. Wada, T. Funayama, I. Narumi, Y. Kobayashi, H. Watanabe, M. Furuta, M. Furuta, *J. Eukaryot. Microbiol.*, 51:321 (2004)

2) S.Wada, H.Kurahashi, Y. Kobayashi, T. Funayama, K. Yamamoto, M. Natsuhori, N. Ito, *J. Vet. Med. Sci.*, 65:471 (2003)

2.26 Molecular Mechanisms for Radiation-induced Bystander Effects

H. Matsumoto*, M. Hatashita*, A. Takahashi**, Y. Kobayashi***,
T. Funayama***, S. Wada*** and T. Sakashita***
Department of Experimental Radiology and Health Physics, Faculty of Medical Science, University of Fukui*
Department of Biology, Nara Medical University**
Department of Ion-beam-applied Biology, JAERI***

1. Introduction

Estimates of the various damage types at sub-cellular, cellular and supra-cellular level induced by low doses, where no experimental data are available, are generally based on linear back-extrapolations from data at higher doses. However, a large amount of data produced during the last decade seem to indicate higher damage yields than expected, possibly due to the so-called "bystander effect (BE)" (i.e. the induction of damage in cells that were not directly hit by radiation). One of the most intriguing aspects of these experiments relies in that bystander damage is observed even at very low doses, down to the mGy level. No clear-cut conclusions can be drawn on the mechanisms underlying bystander effect observations. Different pathways may be involved, depending on the specific conditions. In any case the various forms of cellular communication seem to play a key role, since damage in non directly hit cells may represent a response to signals coming from cells that were directly hit by radiation.

On the other hand, it is well known that an adaptive response (AR) is induced by the priming low-dose or low-dose rate irradiation. The expression "AR" is used by different investigators to indicate different effects also including hormesis, defined as a "stimulatory effect caused by low levels of toxic agents" [1], and increased radioresistance, i.e. sub-linear response at low doses. Strictly speaking, the term AR applies to protection provided by low-dose irradiation with respect to subsequent (higher-dose) irradiation[2]. Although the mechanisms underlying this effect are largely unknown, several similarities between AR and bystander effects can be found. In the framework of low-dose effect estimates, it has been inferred that AR might lead to a sub-linearity in cancer risk at low doses (e.g. [3]). If so, AR should be considered as a possible competing phenomenon with respect to bystander effects.

2. Materials and Methods

2.1. Cells

Human non-small cell lung cancer H1299 cells were kept in an exponential growth phase with a culture medium (Dulbecco's modified Eagle medium, Sigma) containing 10% FBS and 20 mM HEPES. Two days before irradiation, cells were spotted to make nine colonies (1000 cells per spot) into the sample holder, 32 mm dish in diameter with bottom made with 100 μm CR-39 in thickness and then cells were cultured under the conventional conditions.

2.2. Irradiation with $^{20}Ne^{7+}$ beams

Just before irradiation, the medium was removed to make ions penetrate both the cells and the bottom of the sample holder. During irradiation, cells were covered with an 8

μm-thick polyimide film (Kapton, Toray Industries). The number of ions having traversed the sample was counted with a constant fraction discriminator coupled to a preset counter/timer. A pulse-chopper in the injection-line of the cyclotron was used as a fast beam switch. A cell of the center colony was irradiated with 5 ~ 10 count of $^{20}Ne^{7+}$ beams.

Immediately after irradiation, the sample holder was refilled with the medium, then cells were cultured under the conventional conditions.

2.3. Detection of phosphorylated H2A.X (γH2A.X) by immunochemical fluorescence staining

Cells were fixed for 5 min in a 1:1 methanol:acetone solution prior incubation with anti-phosphorylated H2A.X monoclonal antibodies (clone JBW301, Upstate, NY, USA) for 60 min at room temperature. Alexa Fluor 488-conjugated goat anti-mouse IgG (A-11029, Molecular Probes, OR, USA) was used as secondary antibodies. Cells were counter stained with 4',6-diamidino-2-phenyl-indole (DAPI) for 15 sec, mounted, and viewed with a Nikon ECLIPSE E600 fluorescence microscope using a 40× objective. Images were processed using Adobe Photoshop and Microsoft PowerPoint software.

3. Results and Discussion

3.1. Detection of γH2A.X by immunochemical fluorescence staining

The formation of γH2A.X foci was examined by immunochemical fluorescence staining. Thirty minutes after irradiation with 10 counts of $^{20}Ne^{7+}$ beams, the foci of γH2A.X were found in the irradiated cell in the target center colony. The foci of γH2A.X were also found in the unirradiated cells in the target center colony. Six hours after irradiation with $^{20}Ne^{7+}$ beams, the foci of γH2A.X were found in the unirradiated cells in the bystander colonies. These findings indicate that the soluble bystander factors excreted from the irradiated cells in the target colony affect the unirradiated cells in the target and bystander colonies to form the foci of γH2A.X, suggesting that the soluble bystander factors can induce single and double strand breaks of DNA.

We have previously reported that nitric oxide excreted from the irradiated cells with X-rays or Carbon beams is an initiator and mediator of the radiation-induced bystander effect [4,5]. Further, we must elucidate the bystander factors induced by microbeams of $^{20}Ne^{7+}$ in the present study.

References

1) Stebbing, A.R.D.: A theory for growth hormesis. BELLE Newslett., 6: 1-11, 1997.
2) Cai, L.: Research of the adaptive response induced by low-dose radiation: where have we been and where should we go? Hum. Exp. Toxicol., 18: 419-425, 1999.
3) Ikushima, T.: Radioadaptive response: responses to the five questions. Hum. Exp. Toxicol., 18: 433-455, 1999.
4) Matsumoto, H., Hayashi S., Hatashita M., Shioura H., Ohtsubo T., Kitai R., Ohnishi T., Yukawa O., Furusawa Y., Kano E.: Induction of radioresistance to accelerated carbon-ion beams in recipient cells by nitric oxide excreted from irradiated cells of human glioblastoma. Int. J. Radiat. Biol., 76: 1649-1657, 2000.
5) Matsumoto H., Hayashi S., Hatashita M., Ohnishi K., Shioura H., Ohtsubo T., Kitai R., Ohnishi T., Kano E.: Induction of radio-resistance by nitric oxide-mediated bystander effect. Radiat. Res., 155: 387-396, 2001.

2.27 Effect of High-energy Ion Irradiation on Larval Development and Metamorphosis in Larvae of a Cryptobiotic Chironomid, *Polypedilum vanderplanki* and Non-cryptobiotic Chironomids, *P. nubifer* and *Chironomus yoshimatsui*

M. Watanabe*, T. Okuda*, A. Fujita*, T. Kikawada* ,T. Sakashita**, S. Wada**, T. Funayama** and Y. Kobayashi**

Department of Physiology and Genetic Regulation, National Institute of Agrobiological Sciences*

Department of Ion-beam-applied Biology, JAERI**

1. Introduction

Cryptobiosis (anhydrobiosis) is the state in which an organism can tolerate complete desiccation without ill effects and can survive for an extended period [1]. The sleeping chironomid, *Polypedilum vanderplanki*, is the highest and largest multicellular animal entering cryptobiotic state. The cryptobiotic larva can tolerate exposure to extreme temperatures such as –270 to 103 °C and prolonged dry preservation for 17 years [2), 3)].

In our preliminary experiments, we found that desiccated larvae of *P. vanderplanki* survived after ^{60}Co gamma-rays irradiation at the dose of 7 kGy, whereas wet larvae died at 3 kGy. Biological influence by irradiation is mainly divided into two types based on the process of DNA break; the one is the direct action that ionizing radiation absorbed directly into DNA causes and the other is the indirect action that various reactive species such as OH radicals generated from water by irradiation cause. It is, however, not clear how high-LET heavy-ion beams that the rate of biological influence by direct action is thought to be higher than gamma rays affect biological activity in dry and wet larvae of *P. vanderplanki*.

In the present study, we compared effects of high-energy ion-beams irradiation on larval survival and metamorphosis between dry and wet larvae of *P. vanderplanki* and between wet larvae of *P. vanderplanki* and non-cryptobiotic chironomids, *P. nubifer* and *Chironomus yoshimatsui*, which do not have tolerance to desiccation.

2. Experimental procedure

2.1 Insect rearing and preparation for irradiation

Three species of chironomids were reared for successive generations under controlled light (13 h light: 11 h dark) and temperature (27 °C). The detail methods for rearing were described in Watanabe et al. (2002) [4]. Last instar larvae were used for irradiation experiments in each species.

Wet larvae of each three species were placed in a group on a moistened filter paper (diameter, 4.7 cm) in a plastic Petri dish (diameter 5 cm, height 1cm). The dish containing larvae was covered by a polyimide film (7 μm in thickness, Kapton ®, Dupont-Toray, Tokyo). Dry larvae of *P. vanderplanki* were put between two pieces of polyimide film and covered on a Petri dish. These dishes were sealed with a Parafilm (American National Can, IL 60631).

2.2 high-energy helium ion irradiation

Chironomid larvae of each species were exposed to 50 MeV $^{4}He^{2+}$ ion-beams from AVF cyclotron accelerator at the TIARA of

JAERI-Takasaki at the dose ranging from 1 Gy to 5 kGy.

2.3 Larval survival and metamorphosis

Irradiated wet-larvae were returned in distilled water soon, and examined their survival at 48h after irradiation. Irradiated dry-larvae were put in distilled water within 8 hours after irradiation, and checked their survival at 48 h after rehydration. Surviving larvae were reared with milk (2%)-agar (1%) in a glass container (ca. 600 ml), and examined whether they pupated and emerged as adults or not.

2.4 Measurements for water and trehalose

Larvae were individually or in a group (20 larvae) heated at 100 °C for 1 day. Water content was calculated from the difference in mass before and after the heat treatment. Larval trehalose content were measured as described in Watanabe et al. (2002)[4].

3. Results and Discussion

Table 1 shows values of ID50 (50% of inhibitory dose) of $^{4}He^{2+}$ irradiation on larval survival and metamorphosis in three species of chironomids. Both dry and wet larva of P. *vanderplanki* survived at 48 h after irradiation at the dose of 2 kGy, but the rate of survival drastically decreased at each phase of metamorphosis such as pupation and adult emergence. This indicates that there is some high radiation-sensitive process in metamorphosis.

Table 1 ID50 of $^{4}He^{2+}$ irradiation on larval survival at 48h, pupation and adult emergence in larvae of three species of chironomids

		ID50(Gy) a		
Species b	State	Larval survival	Pupation	Adult emergence
P. van	Dry	2556	993	98
P. van	Wet	2017	102	16
P. nub	Wet	1045	34	12
C. yos	Wet	1124	16	6

a: 50% inhibitory dose; b: *P.van - P. vanderplnaki*, *P. nub- P. nubifer, C. yos- C. yoshimatsui*

Dry larvae of *P. vanderplanki* had higher tolerance against high-energy helium ions irradiation than wet ones, especially in pupation and adult emergence (Table 1). The value of ID50 in the dry larvae of *P. van* was 10 times higher in pupation than that of wet ones and 6 times higher in adult emergence than that of wet ones, suggesting that the radiation-induced damage on the process of metamorphosis was reduced by entering cryptobiosis.

Dry larvae of *P. vanderplanki* had only a small amount of water (2.9%), but accumulated quite a large amount of trehalose, a kind of disaccharide (Table 2). On the other hand, wet larvae of *P. vanderplanki* contained much water (81.6%) and less trehalose (1.5%) than the dry ones. Irradiation of water frequently produces OH radicals that cause DNA breaks, while trehalose protects DNA from radiation-induced damage [5]. Higher radiation tolerance in dry larvae may be caused by lack of water and/or accumulation of trehalose. This could be partly elucidated by of the degree of DNA damage among dry larvae containing different amounts of trehalose.

Table 2 Contents of water and trehalose in larvae of three species of chironomids

Species b	State	Water content (%) a,b	Trehalose content (% dry body weight) a,b
P. van	Dry	2.9±0.2A	19.4±0.6A
P. van	Wet	81.6±0.4B	1.5±0.1B
P. nub	Wet	84.0±0.3C	1.1±0.2B
C. yos	Wet	83.6±0.5C	1.1±0.1B

a: mean±SE. b: the different capital letters after SE indic: a significant difference in mean at 5% level of Mann-Whitney*U* test.

Even wet larvae of *P. vanderplanki* had higher tolerance against helium ions irradiation than wet ones of non-cryptobiotic species, *P. nubifer* and *C. yoshimatsui*; the value of ID50 in the wet larvae of *P. vanderplanki* is more than

twice in larval survival and more than 3 times in pupation than those of other chironomids (Table 1). There was only a small or no difference between *P. vanderplanki* and the other chiromonids on contents of water and trehalose (Table 2). High ability to tolerate irradiation even in wet larvae of *P. vanderplanki* may be caused by some physiological reason(s) except for water and trehalose.

References

1) Clegg, J. S., Comp. Biochem. Physiol. B. 128 (2001) 613-624.
2) Hinton, H. E., J. Insect Physiol. 5 (1960) 286-300.
3) Adams, S., Antenna 8 (1985) 58-61.
4) Watanabe, M., T. Kikawada, N. Minagawa, F. Yukuhiro, T. Okuda, J. Exp. Biol. 205 (2002) 2799-2802.
5) Yoshinaga K., H. Yoshioka, H. Kurosaki, M. Hirasawa, M. Uriytani, K. Hassegawa, Biosci. Biothech. Biochem. 61 (1997) 160-161.

2.28 Measurement of p53 Transcription Activity in Mouse Fibroblast Cells Irradiated by Heavy Ion-microbeam: Establishment of Detection System

M. Saitou*, T. Sugihara*, K. Tanaka*, T. Matsumoto*, T. Funayama**, S. Wada**, T. Sakashita** and Y. Kobayashi**
Department of Radiobiology, Institute for Environmental Sciences*
Department of Ion-beam-applied Biology, JAERI**

1. Introduction

The experiment of microbeam irradiation targeting individual cells will be necessary to verify biological effects induced by low dose rate radiation. Prior to investigate change of gene expression in mouse-cultured cells by the microbeam, we established irradiation procedures and detection system for gene transcription activity. As preliminary experiment, the confluent cells were irradiated by soft X-rays or by ion microbeam and the response levels of p53 in irradiated cells were examined. The soft X-ray-irradiation was performed to confirm in advance the increase of p53 levels of the cells used.

2. Experimental procedure

2.1 Cell line

A mouse fibroblast cultured cell line, NIH3T3/pG13 Luc, was used. This is a transformant of NIH3T3 cells and has luciferase gene-introduced plasmid DNA (pG13 Luc). The plasmid DNA can be emitted chemiluminescent light by a treatment after cell-lysis when luciferase gene is expressed by transcription activity of p53 protein.

2.2 Confirmation of confluent state of cells

Confluent state present in cells growing at stationary phase was confirmed association of gap junction intercellular communication (GJIC). Cells (1 ml, 8.5 x 10^5 cells/ml) are seeded into 24-well plate wells (21.5 mm in diameter) with the density of 2.3 x 10^3 cells/mm^2 at 2 days before irradiation. A 1 ml of 1 nM PMA (Sigma) in 14 mM DMSO was added for inhibition of GJIC, followed incubation at 37°C for 1h and then, the cell layer on a well bottom was scraped by a blade. A 1 ml of 0.05% lucifer yellow dye (Sigma) was added to stain the cell layer at 37°C, 3 min. The fluorescence image was obtained by a confocal laser microscope (Fluoview FV300, Olympus).

2.3 Soft X-ray irradiation

Cells (0.24 ml, 1.2 x 10^5 cells/ml) are seeded onto a sample area (8 mm in diameter) in a specially made 35mm dish with a 7.5 μm-thick replaceable Kapton polyimide film at the bottom with a density of 2.3 x 10^3 cells/mm^2 for 2 days before irradiation. Then, D-MEM medium solution between confluent cells and Kapton film was removed just before irradiation. Cells were irradiated by soft X-rays (140 kVp, 6 mA) for 1, 2, 4 and 8 Gy with the dose rate of 0.56 Gy/min using a soft X-ray irradiator (M-150WE, Softex). After irradiation cells were incubated in 0.24 ml D-MEM at 37°C for 4h to measure p53 protein activity.

2.4 Heavy ion microbeam irradiation

Microbeam and "broad-field" irradiation were performed by using 260 MeV $^{20}Ne^{7+}$ ion beam from TIARA AVF cyclotron. Cells (0.24 ml, 1.2

x 10^5 cells/ml) were seeded onto a sample area under the same conditions mentioned at previous section. In broad ion beam irradiation, three samples were used for each irradiation. The particle fluence was about one ion/(10 μm)^2, which is correspondent to the averaged number of one ion per cell. In microbeam irradiation, the exact number of ions were irradiated at each cross point of orthogonal lattice of irradiation area of 3 x 3 mm. Cells (0.24 ml, 1.2 x 10^5 cells/ml) were seeded in the same conditions as above mentioned. The number of irradiation points were 1 x 1, 1 x 4, 2 x 4, and 4 x 4 points in a area of 3 x 3 mm with the interval of 1 mm to measure ion number dependent transcription activity, and 1 x 1, 4 x 4, 8 x 8 and 11 x 11 points on the same area with the interval of 1, 1, 0.429 and 0.300 mm, respectively, for the experiment to measure point density dependent transcription activity. In both experiments of broad beam and microbeam, D-MEM medium solution between cells and Kapton film was removed just before irradiation. After irradiation cells were incubated in D-MEM at 37°C for 4h to measure p53 activity.

2.5 Measurement of chemiluminescence and amount of total protein

After irradiation, a cell samples was treated by 100 μl of 0.25% trypsin-EDTA (GIBCO) and suspended by 500 μl of D-MEM medium solution. The sample was treated by 100 μl of passive lysis buffer (Promega). The all lysate (10 μl) was poured into a well of a 96-well white plate for fluorescent measurement and then, 10 μl of pure water and 50 μl of luciferase assay reagent (Promega) were added into the well. Chemiluminescence light from the sample was measured by a plate-reader. A 20 μl of identical sample was poured into a well and then, 80 μl of 1/5 x protein assay dye reagent (Bio-Rad) was added into each well for quantification of total protein. The absorbance of the sample was analyzed at 595 nm by a plate-reader.

3. Results and Discussion

The formation of GJIC in stationary cell stage was confirmed by dye staining and observation with confocal laser microscope. Permeation of dye with the strong intensity of fluorescence from the end of the scratch into inside cell layer was observed in only scraping-treated group. The intensity of dye fluorescence in cell layer was decreased down to near level of control in 1 nM PMA-treated group.

The p53 transcription activities of confluent cells increased with the soft X-ray dose, but activities at 4 Gy were lower than that at 2 Gy (Fig. 1). It was probably due to insufficient cell dissolution or insufficient separation of protein from cell debris. Exposure with soft X-rays elevated the p53 transcription activity in irradiated cells. The p53 transcription activity of confluent cells irradiated by broad beam of 260 MeV Ne ion (about 0.7 Gy) was induced 2-fold of control (Fig. 2). The p53 transcription activity in the confluent cells irradiated by microbeam of 260 MeV Ne ion had a tendency of decrease with the irradiation points increased from 1 to 16 (Fig. 3). And then, the p53 transcription activity also decreased with the number of irradiation point of Ne ion per sample lattice area (Fig. 4). These results that microbeam irradiation induced reduction of the p53 transcription activities in irradiated cells were differed from those obtained by irradiation with broad beam. Otherwise, it may be influenced by the drying up of cell layers proceeded in a very low humidity during irradiation. The irradiation procedures and detection system for p53 transcription activity were established. The protection of the drying up will be re-examined hereafter.

This study was financially supported by Aomori Prefecture, Japan.

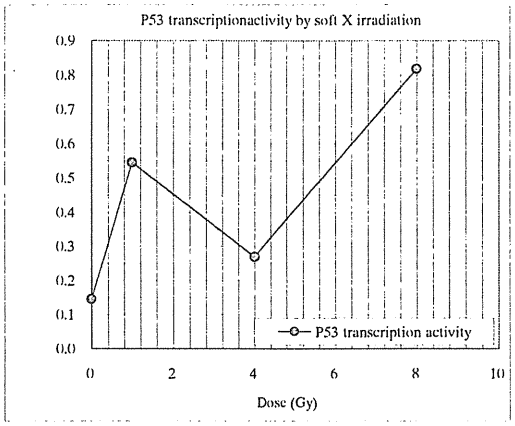

Fig. 1 p53 protein-transcription activities of cells irradiated by soft X-rays. An each ordinate is chemiluminescence intensity normalized by amount of protein.

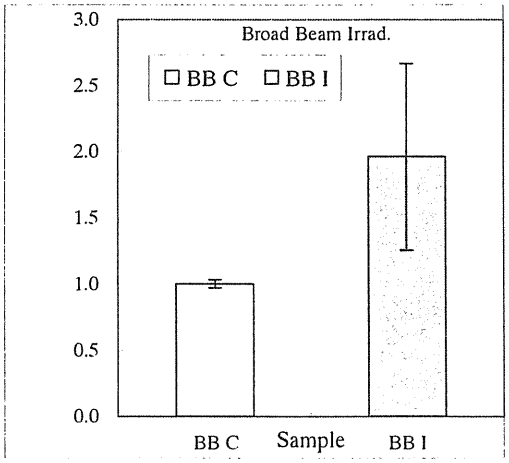

Fig. 2 p53 protein transcription activities of cells irradiated by broad beam of Ne ion. BBI: broad beam irradiation, BBC: control.

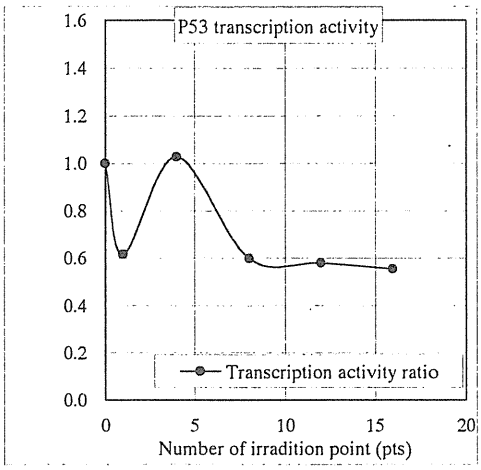

Fig. 3 p53 protein transcription activities of cells irradiated by microbeam of Ne ion. An each abscissa shows the number of irradiation point.

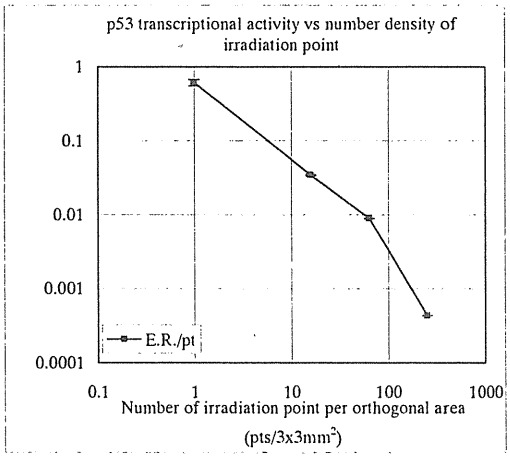

Fig. 4 p53 protein transcription activities of cells irradiated by microbeam of Ne ion. An each abscissa shows the number of irradiation point per sample lattice area of 3 x 3 mm.

2.29 The Translocation and Distribution of the Products of Photosynthesis in Hemp

K. Sakamoto*, S. Fujimaki*,**, N. S. Ishioka*, S. Watanabe*,
K. Arakawa* and S. Matsuhashi*

Department of Ion-beam-applied Biology, JAERI*
Theoretical Analysis Group for Radiation Application, JAERI**

1. Introduction

Plants produce organic matter in the form of sugar from carbon dioxide and water by photosynthesis. The photosynthates produced in a leaf (source) accumulate in various plant organs (sink) after they are transported through sieve tubes. The relationship between a source and sink is influenced by environment and growth step of a plant. The photosynthates required for vegetative growth are transported mainly to the root and stem, while those required for reproductive growth are transported to the fruit and seeds. It is thought that a drastic change occurs for the transportation of carbon source in transitionary phase from vegetative growth to growth in reproductive phase. However, no studies have analyzed the translocation and distribution of captured photosynthates between vegetative growth and reproductive growth.

In order to elucidate the drastic transition of carbon source from vegetative growth to reproductive growth, we firstly analyze the behavior of photosynthates in an extending stem for vegetative growth using a positron-emitting tracer imaging system (PETIS). Hemp (*Cannabis sativa* L.) was used as a best suitable plant material in this experiment because it grows very rapidly. We report a degree about the translocation and distribution of photosynthetic product in hemp for vegetative.

2. Experimental procedure

2. 1 Plant material

Seeds of *Cannabis sativa* L. var. sativa (CBDA strain) were obtained from an inbred population. The plants were cultivated at 25.C with 16 h of light and 8 h of darkness daily. The plant of about 25-30 cm height was used for this experiment.

2. 2 Production of $^{11}CO_2$

The gas-target system was performed as described by Ishioka *et al.* (1999)[1]. Using the gas target system, $^{11}CO_2$ was produced by the $^{14}N(p,\alpha)^{11}C$ reaction on nitrogen (99.9999% purity, under 5 kg/cm^2 pressure). After irradiation, the $^{11}CO_2$ was collected in a stainless steel trap immersed in liquid nitrogen. The collected $^{11}CO_2$ was applied to experiments on translocation of photosynthesis products.

2. 3 Measurement with PETIS

The positron emitting tracer imaging system consists of two planer detectors, each of which is a $Bi_4Ge_3O_{12}$-scintillators array coupled to a position sensitive photomultiplier tube. The two detectors are placed facing each other with a sample plant between to detect annihilation γ-rays from the plant. Although the detection area

is limited to 19 cm x 21 cm and the resolution in space is as large as 2 mm, the great advantage of the system is that the sample plant can be fed and watered, receiving light, as it is alive. Two dimensional counting data are accumulated in a certain period of time and transferred to the computer memory.

2. 4 PETIS experiment

$^{11}CO_2$ was supplied to the largest expanded leaf or the third leaf in hemp for 5 min, and ^{11}C-tracer movement to the shoot was monitored using PETIS for 120 min. The experiment condition as followed: Temperature at 25.C, Humidity 50-60%, Light intensity at 500 μmol Photon m^{-2} s^{-1}(Fig. 1).

3. Results and Discussion

After supplying the largest expanded leaf with $^{11}CO_2$, the ^{11}C-tracer accumulated rapidly in most parts of the growing stem below that leaf and at the shoot apex (Fig. 2). When $^{11}CO_2$ was supplied to a lower leaf, the photosynthetic products were transported via the stem to the root supplying the lower leaf (Fig. 3). The sink for the largest expanded leaf was the stem below that leaf and the shoot apex, while it was clear that the sink for the lower leaf was the root and stem feeding the lower leaf. From this study, we demonstrated the transportation and distribution of captured photosynthates in vegetative growth.

In order to examine the relationship between the translocation of photosynthates and the extending stem in hemp, PETIS is very effective means. This study and further investigations of the behavior of photosynthates should contribute to the elucidation of the drastic transition from vegetative growth to reproductive growth.

Reference

1) N. S. Ishioka, H. Matsuoka, S. Watanabe, A. Osa, M. Koizumi, T. Kume, S. Matsuhasi, T. Fujimura, A. Tsuji, H. Uchida and T. Sekine: Production of positron · emitters and application of their labeled compounds to studies. J. Radioanal. Nucl. Chem. 239(2): 417-421 (1999)

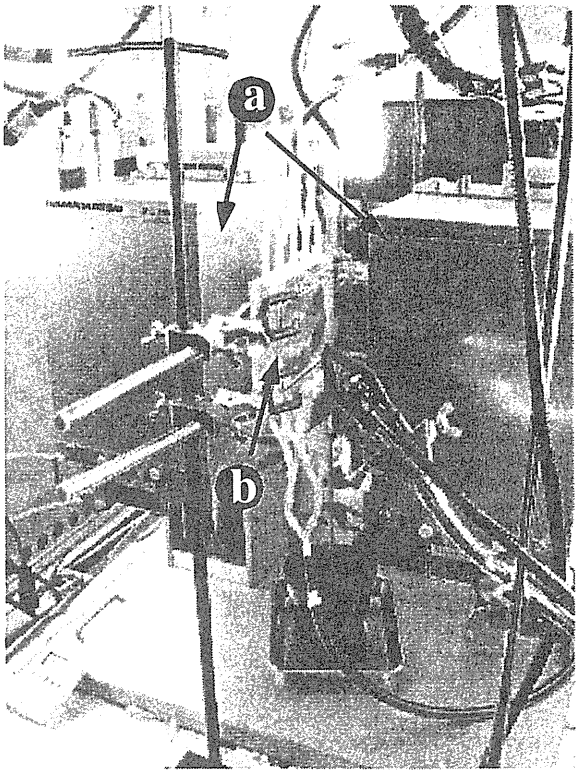

Fig. 1 Setting of PETIS experiment.

a: One pair of planer detectors

b: $^{11}CO_2$ feeding cell.

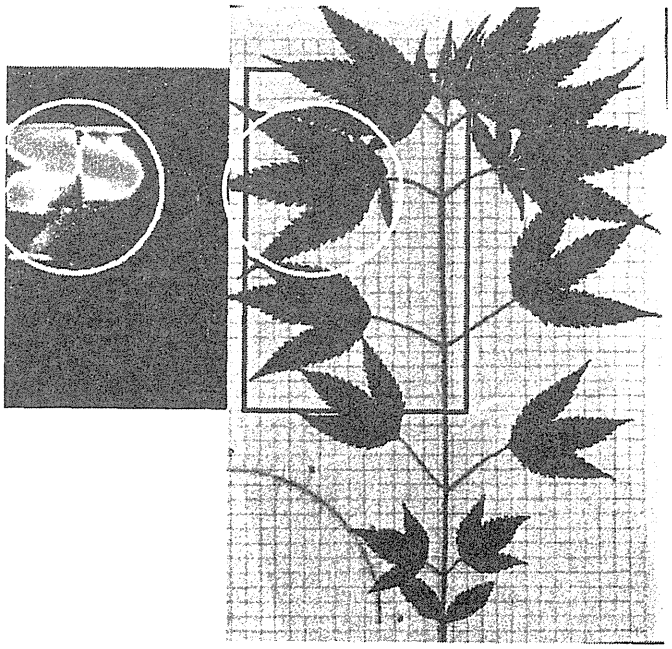

Fig. 2 The multiplication imaging and morphological features of hemp in the case of supplying the largest expanded leaf with $^{11}CO_2$. The white circles indicate same leaf supplied with $^{11}CO_2$. The black box indicates detection area (19 cm x 21 cm).

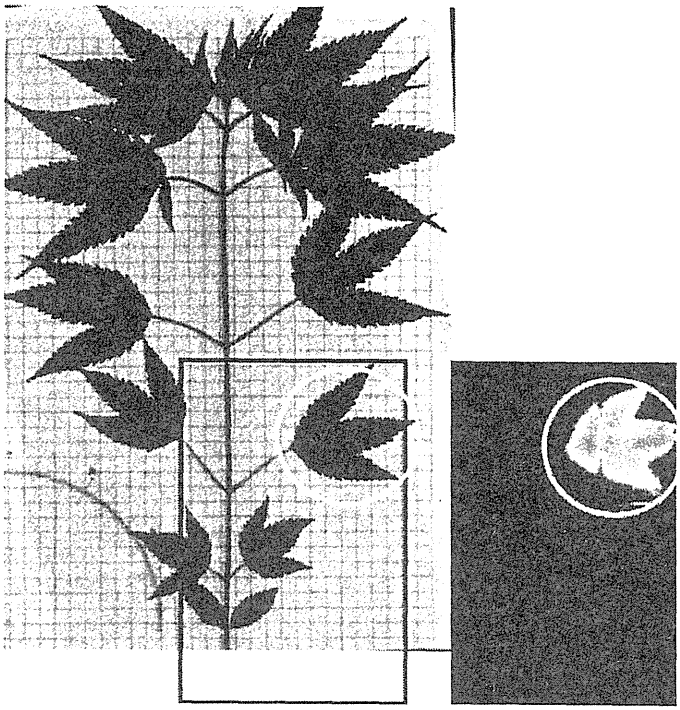

Fig. 3 The multiplication imaging and morphological features of hemp in the case of supplying the third leaf with $^{11}CO_2$. The white circles indicate the same leaf supplied with $^{11}CO_2$. The black box indicates detection area (19 cm x 21 cm).

2.30 Inhibition Mechanisms of Soybean Root Nodule Growth and Nitrogen Fixation by Nitrate

A. Yamazaki*, T. Ohyama*, K. Sueyoshi*, N. Ohtake*, S. Ito*,
S. Matsuhashi**, S. Fujimaki**, K. Sakamoto**, N. S. Ishioka**,
S. Watanabe**, K. Arakawa** and T. Kume**
Faculty of Agriculture, Niigata University*
Department of Radiation Research for Environment and Resources, JAERI**

1. Introduction

Soil bacteria belonging to the genera *Rhizobium* and *Bradyrizobium* are able to invade the roots of their leguminous host plants and trigger the formation of new organ, the root nodule. In rhizobium-legume symbioses, considerable metabolic energy is invested by the plant to produce nitrogen fixing nodules and to maintain nitrogen fixation.

High nitrate levels suppress the symbiosis, as shown by decreased nodule mass as well as decreased nitrogenase activity. Recently Fujikake et al. [1] reported that carbon distribution in root was enhanced by nitrate supply using split root system. Nitrate reductase is the first enzyme in the pathway of nitrate assimilation and well known as a nitrate-inducible enzyme in most of the higher plants. Absorption and reduction of one nitrate molecule required 2ATP, one NAD(P)H and 6 ferredoxin in addition to carbon skeleton. The nitrate inhibition mechanism was possibly due to decreased carbohydrate availability resulting from nitrate reduction and assimilation.

Tungsten is a non-essential element for plant growth, which exerts harmful effects on plants. When tungstate is applied to the planting medium, it competes with molybdate and inhibits some enzymes, which have a Mo cofactor in the active site such as nitrate reductase and nitrogenase. In this report, we evaluated how tungstate effect nodule growth and nitrogen fixation co-existence nitrate in the point of nitrate and carbon translocation and accumulation.

2. Experimental Procedure

Soybean (cv. Williams) seeds were inoculated with *Bradyrizobium japonicum* strain USDA 110 and they were cultivated hydroponically with N free medium. One hundred μM tungstate with or without 1mM nitrate treatment was started at 14 days after sowing. For estimation of nodule grows, photographs of the nodules on the primary root were taken every 12 hours during 3 days by using a computer microscope (Intel Play QX3 Computer Microscope, Japan) through the bottle with 10 X magnification.

The positron emitting radioisotope ^{11}C atoms were produced by a ^{14}N (p, .) ^{11}C nuclear reaction by bombarding a target nitrogen gas with 10 MeV protons at a current of 1 μA using the TIARA (Takasaki Ion Accelerators for Advanced Radiation Application) AVF cyclotron. The $^{11}CO_2$ was produced from the ^{11}C atoms and the oxygen present in the target chamber. Nitrate labeled with ^{13}N (a positron emitter with a half life of 10 minutes) was produced from $^{16}O(p,.)^{13}N$ reaction, bombarding 6ml of target water with 1. A of 20MeV H^+ particles from the AVF cyclotron of TIARA. The solution of $^{13}NO_3^-$ was purified by passing it through a cation exchange column.

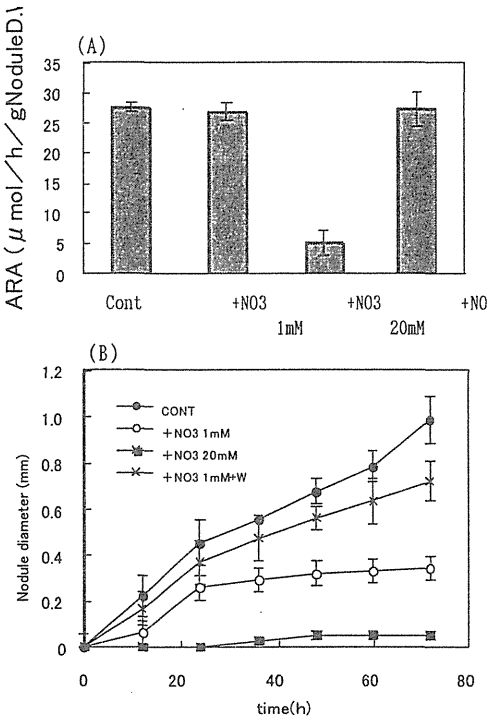

Fig. 1 Tungustate and nitrate effects on the (A) nitrogen fixation activity and (B)nodule growth.

Three days after treatments, $^{11}CO_2$ was supplied to the first trifoliolate leaves for 10 min, and ^{11}C movement to the root was monitored using a PETIS for 90 min. Alternatively $^{13}NO_3^-$ was supplied to the root and the radioactivity was monitored at shoot for 40 min using PETIS. After analysis by PETIS, the radioactivity of a whole plant was observed with a Bio-imaging analyser (BAS-1500, Fuji Film, Japan).

3. Results and Discussions

100μM tungstate treatment did not cause visible damage in plant and also not inhibit nodule growth. When 1mM nitrate were supplied to the culture solution, individual nodule growth was immediately suppressed, but did not effect on the nitrogen fixation activity (Fig. 1 A). 20mM nitrate application inhibited both nitrogen fixation and nodule. The nitrate inhibition effect to the nodule growth was canceled applied by 100μM tungstate to the culture medium (Fig.1 B).

To investigate how tungstate canceling nitrate inhibition, $^{13}NO_3^-$ and $^{11}CO_2$ translocation and distribution were analyzed. The fixed carbon was immediately transported to the root in the control plants. Application on 1, 5 and 20mM nitrate enhanced ^{11}C accumulation at the root position (Fig. 2 A). Solo tungstate application reduced ^{11}C accumulation in the root position. When 1 and 5mM nitrate with tungstate enhanced ^{11}C accumulation in the root. The highest accumulation of ^{11}C was showed in the 1mM nitrate with 100μM tungstate. Tungstate with 20 mM nitrate showed lowest ^{11}C accumulation in the root comparing treatments (Fig 2 A). This result suggested that high accumulation of nitrate in the root inhibit carbohydrate transport.

At shoot position, $^{13}NO_3^-$ was accumulated irrespective nitrate concentrations in the medium. Tungstate treatment strongly depressed ^{13}N accumulation at the shoot position in all nitrate treatments. The distribution visualized by BAS showed that the accumulation of ^{13}N in the root position was scarcely effected on the tungstate treatment. This result indicated that 100μM tungstate effect on the nitrate transport in addition to inhibit nitrate absorption the absorption.

The results obtained here suggested that tungstate decreased the nitrate trasport to the shoot, while the canceling of the nodule growth inhibition by nitrate was mainly due to enhanced carbon transport to the root, and nodules possibly through the inhibitory effect on nitrate absorption and reduction.

Reference

1) Fujikake H., Yamazaki A., Ohtake N., Sueyoshi K., Matsuhashi S., Ito T., Mizuniwa C., Kume T., Hashimoto S., Ishioka N-S., Watanabe S, Osa A., Sekine T., Uchida H., Tsuji A. and Ohyama T. Journal of Experimental Botany, 54, 1379-1388,

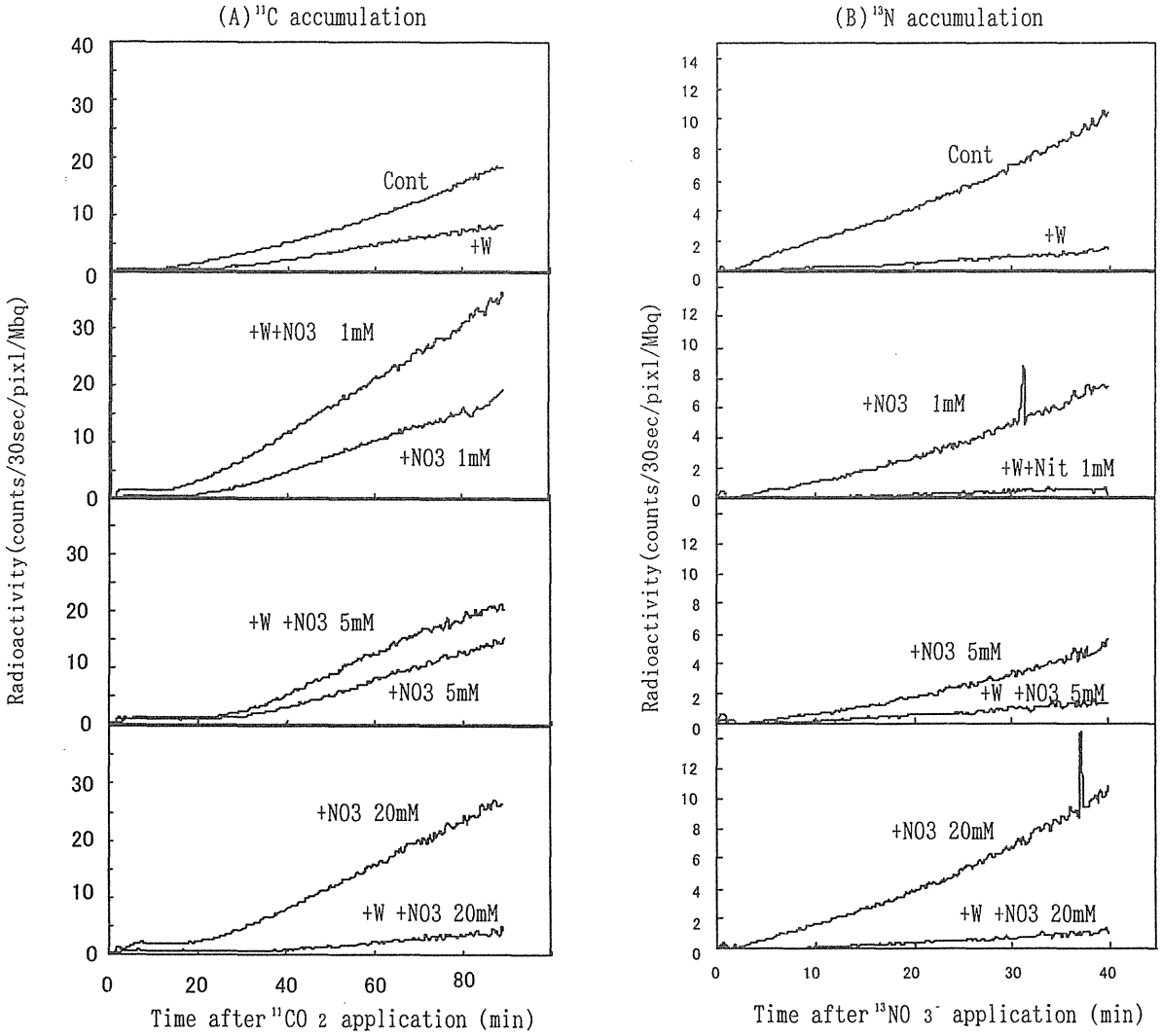

Fig. 2 Tungstate and nitrate effects on the (A) ^{11}C accumulation at root position and (B) ^{13}N accumulation at the shoot position.

2.31 Diagnosis of Salt Stress by Monitoring ^{11}C Translocation in Tomato Plants by using PETIS

R.Suwa*, S.Fujimaki**, K.Sakamoto**, S.Matsuhashi**, R.E.A. Morghaieb*, N.T.Nguyen*, T.Tsukamoto**, K.Arakawa**, T.Kume**, and K.Fujita*
Graduate School of Biosphere Sciences, Hiroshima University*
Department of Ion-beam-applied Biology, JAERI**

1. Introduction

Agricultural productivity is severely affected by soil salinity, and the damaging effect of salt accumulation on agricultural soils have influenced ancient and modern civilizations. The detrimental effect of salt on plants is a consequence of both a water dificit derived from osmotic stress[1] and the effect of excess sodium ions[2] on key biochemical processes. However the effect in terms of translocation especially at early times after treatment initiation has not yet well studied.

This experiment mainly focused on the fast responses of ^{11}C translocation using Positron Emitting Tracer Imaging System (PETIS), as ^{11}C emits positrons, here we visualized the real time ^{11}C translocation in tomato plants by PETIS under salt stress.

2. Experimental procedure

2.1 Plant materials

Tomato seeds were germinated on soil in 12 cm diameter pot containing granite regosol : perlits 1:1 in a growth chamber with a 14-h light(25°C)/10-h dark(25°C) regime and photon flux of 300. mol $m^{-2}s^{-1}$. For salt treatment plant was applied to 150 mM NaCl under complete nutrient solution. ^{11}C administration experiments were performed after two month of germination.

2.2 Production of ^{11}C

^{11}C was produced in the $^{14}N(\gamma,\alpha)^{11}C$ reaction by bombarding a N_2 gas with a 20 MeV proton beam from the TIARA AVF cyclotron. Using a beam current of 5pμA for 2 min, about 100 MBq of ^{11}C was produced. $^{11}CO_2$ gas was immediately solidified by using N_2 gas after made, and when before applying $^{11}CO_2$ for plant, it was made as gas again.

2.3 Experimental set up for ^{11}C translocation in the plant

One tomato plant was set up for respective 2 growth chambers equipped with PETIS. The plant was fixed in the middle between a pair of PETIS detectors. ^{11}C was added to leaf as a CO_2 gas. The data was automatically collected using 20 min as the half-life of ^{11}C.

3. Results

In all the Tomato plants ^{11}C administered to leaf translocated into root part through the stem. Fig.1,2,3 showed that ^{11}C translocation in control plant was not changed inspite of difference in ^{11}C feeding time at 7 h interval. For example, ^{11}C activity was initially detected at ROI5 feeding 15 min from ^{11}C feeding (Fig2.a,b). On the other hands, under salt

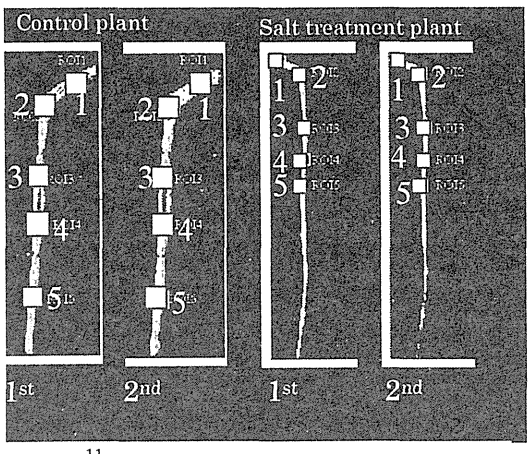

Fig.1 ^{11}C distribution of all treatment plant

treatment, time of ^{11}C detection at ROI5 before and after 7h of salt treatment was 18 and 22 min respectively. respectively.(Fig3.a,b).

Our results show that 7 h of salt treatment affects ^{11}C translocation in tomato plants. In addition, a separate experiment using the same species shows that 6-8h of salt treatment had no effect in photosynthetic activity in tomato leaf.

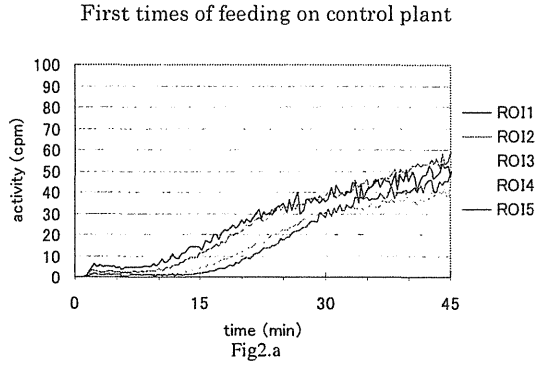

Fig2.a

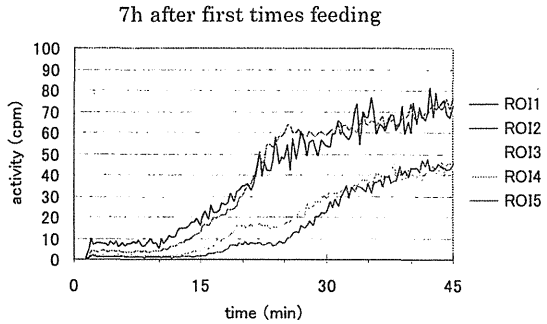

Fig.2 a,b time-course study of the translocation of ^{11}C from leaf to stem on control plant.
(ROI 1 is petiole, 2,3,4,5 is stem)

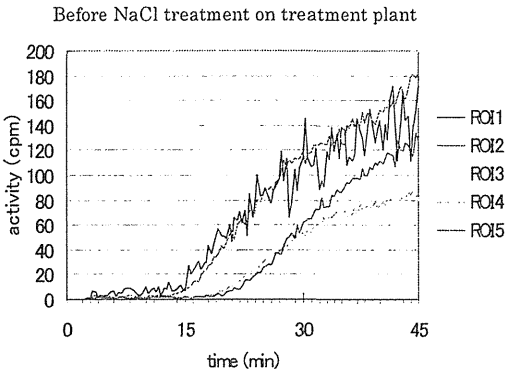

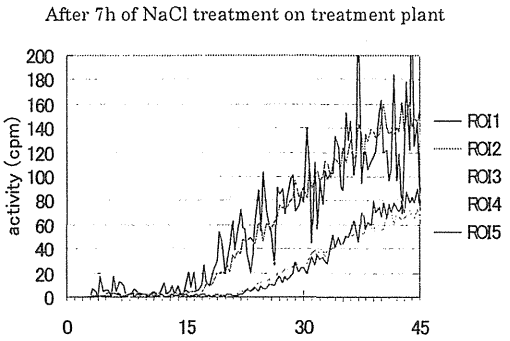

Fig.3 a,b Time-course study of the translocation of ^{11}C from leaf to stem on before and 7 h of salt treated plant.

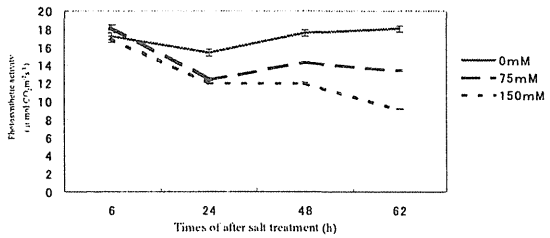

Fig.4 change of photosynthesis on each times of salt treatment.

Through the present study, we have faced some problems like an abnormal reaction of after 7 hours of second times ^{11}C translocation 20min after ^{11}C feeding in control plant. It might be due to bending of some parts of petiole by overload of chamber weight or ventilation effect.

4.Conclution

These results suggest that salt adversely affects photosynthate translocation from leaf at 7h after the treatment initiation, however at the identical time, its affection on photosynthesis does not appear. This result may show that salt directly affect for sink activity such as root part.

Reference

1) Ourry A, Mesle S, Boucaud J, New Phytol 120:275-280
2) Suleyman I. Allakheverdiev, Atsushi sakamoto, Yoshitaka Nishiyama, Masami Inaba, and Norio Murata, Plant physiol (2000) 1047-1056